Characterisation of two short QT syndrome potassium channel mutations

By Andrew Butler

Supervised by Professor Jules Hancox

and Dr Christopher Dempsey

A dissertation submitted to the University of Bristol in accordance with the requirements for award of the degree of MSc by Research in Physiology and Pharmacology in the Faculty of Life Sciences and the school of School of Physiology, Pharmacology and Neuroscience (September 2018).

Word count: 20, 686

Abstract

The hERG potassium channel, which mediates the rapid delayed rectifier current I_{Kr}, is critical in determining the duration of cardiac action potentials (APs) and therefore the length of the QT interval. Within the last 15 years, gain-of-function hERG mutations have been identified clinically and these have been shown to abbreviate repolarisation, causing variant 1 of the short QT syndrome (SQT1), with symptoms including atrial fibrillation, syncope and sudden cardiac death. Recently, two new mutations have been associated with SQT1. The first of these, I560T, was published alongside electrophysiological data which showed the mutation to modestly affect hERG inactivation, but a more detailed characterisation of channel properties has not been undertaken. The second mutation, S631A, has been studied *in vitro* since 1996, when it was shown to cause signification attenuation of inactivation across physiological voltages.

Now that both mutations have been identified clinically, this study aimed to characterise fully the kinetics of I560T-hERG; to investigate the effect of both mutations on hERG current (I_{hERG}) during physiological APs; and to evaluate mutant channels' affinity for anti-arrhythmic drugs. Using whole-cell patch clamp recordings of wildtype and mutant I_{hERG} in HEK cells, this work shows the I560T mutation to increase I_{hERG} density and attenuate channel inactivation whilst also affecting wider channel properties. These changes lead to augmentation of I_{hERG} during APs and can be expected to increase susceptibility to arrhythmia. Similarly, the attenuation of inactivation caused by the S631A mutation was shown to shift I_{hERG} timing to significantly earlier during repolarisation which can be predicted clinically to abbreviate repolarisation and increase propensity for arrhythmia. Application of quinidine to cells expressing I560T or S631A-hERG showed that the channels' affinity for the drug was only modestly affected by the mutation, whilst sotalol also retained effectiveness in blocking I560T-hERG, thus suggesting therapeutic options for the identified patients.

Dedication and Acknowledgements

Firstly, I'd like to thank Jules Hancox for everything he's done for me over the past year. Not only has he given me a great opportunity to develop my abilities as a researcher and offered continued support and guidance throughout the course of my degree, he has gone beyond the role of a master's supervisor by helping me secure a position on a PhD programme. For all of this, I could not be more grateful. I would also like to thank Yihong Zhang for her endless patience, support and willingness to share her knowledge. She has taught me all the practical and analytical skills I've needed, and whilst these have been critical in the work produced here, they will also continue to serve me throughout my developing career and so I feel indebted to her for all the help she has offered.

I'd like to thank Chris Dempsey for both the insights offered throughout my degree and the provision of structural data for this thesis and for the papers we have submitted. Without these, a huge gap in my own knowledge, in this thesis, and in the work we have submitted would exist and so I certainly would not be able to consider this year a success without his input. Additionally, I'd like to thank Neil Marrion and Beck Richardson for their time and feedback throughout year.

Finally, I'd like to thank everybody else who I've had the pleasure of working with daily. In addition to those mentioned above, Rachel Caves, Matthew Helliwell, Chunyun Du, Aziza El Harchi, Stephanie Choisy and Adam McCartan have all made me as welcome as possible and been more than happy to offer support as needed. I've thoroughly enjoyed being a part of the laboratory over the past year and am very much looking forward to continuing working with everybody throughout my PhD.

Author’s declaration

I declare that the work in this dissertation was carried out in accordance with the requirements of the University's *Regulations and Code of Practice for Research Degree Programmes* and that it has not been submitted for any other academic award. Except where indicated by specific reference in the text, the work is the candidate's own work. Work done in collaboration with, or with the assistance of, others, is indicated as such. Any views expressed in the dissertation are those of the author.

SIGNED: ..... DATE: .....

Table of contents

List of figures

List of tables

List of abbreviations

AF	Atrial fibrillation
AP	Action potential
APD	Action potential duration
CA	Catheter ablation
ECG	Electrocardiogram
EM	Electron microscopy
E_{rev}	Reversal potential
ERP	Effective refractory period
HEK	Human embryonic kidney
hERG	Human ether-à-go-go-related gene
ICD	Implantable cardioverter-defibrillator
I_{hERG}	hERG current
iPSC	Induced pluripotent stem cell
Kv channels	Voltage-gated potassium channels
mERG	Mouse ether-a-go-go-related gene
PF	Purkinje fibre
QTc	Rate-corrected QT
rEAG	Rat ether-à-go-go protein
SCD	Sudden cardiac death
SF	Selectivity filter
TEA	Tetraethylammonium
$V_{0.5}$	Half maximal voltage
VF	Ventricular fibrillation
VS	Voltage sensor
VSD	Voltage-sensing domain
WT	Wildtype

Chapter 1 Introduction

1.1 Cardiac function

Normal cardiac function is dependent upon the propagation of electrical impulses from pacemaking cells in the sinoatrial node, through the specialized conduction system and working myocardium. This co-ordinated activity triggers orderly contraction of the atria and ventricles, pushing deoxygenated blood to the pulmonary circulatory system and oxygenated blood to the remaining muscles and organs as required (Nerbonne and Kass, 2005, Hoshi and Armstrong, 2013). Excitation and contraction is followed by an electrical refractory period, which allows the relaxed heart to fill with blood while re-establishing a negative membrane potential within cells (Courneya and Parker, 2011).

The period required for myocardial depolarisation and repolarisation is termed the action potential duration (APD) and can be measured noninvasively via the electrocardiogram (ECG). As shown schematically in Figure 1, the surface ECG reflects the action potentials (APs) triggered by cardiac excitation, with atrial (PR interval) and ventricular (QT interval) APs each showing a distinct morphology. The diversity of AP waveforms across different tissues are a consequence of the changes in ion channel expression between the cell types (Nerbonne and Kass, 2005). For example, Kir2.1 (which contributes to the inwardly rectifying K^+ current, I_{K1}) is expressed more highly in the ventricles, Kir3.1 (which mediates the acetyl-choline activated K^+ current, $I_{K,Ach}$) is expressed more highly in the atria and hERG (I_{kr}) expression is similar across all cardiac tissues (Schram et al., 2002, Gaborit et al., 2007). Variations in expression of a number of other channel types including ultrarapid delayed rectifiers ($K_v1.5$; I_{Kur}) voltage-dependent calcium channels ($Ca_v1.2$; $I_{Ca,L}$) and G-protein-gated K+ channels (Kir3.4, $I_{K,Ach}$) all combine to produce the described AP alterations (Gaborit et al., 2007). Furthermore, as show schematically in Figure 2, APD is also dependent upon the activation and inactivation profiles of different channel types instigated by the change in voltage experienced during an AP.

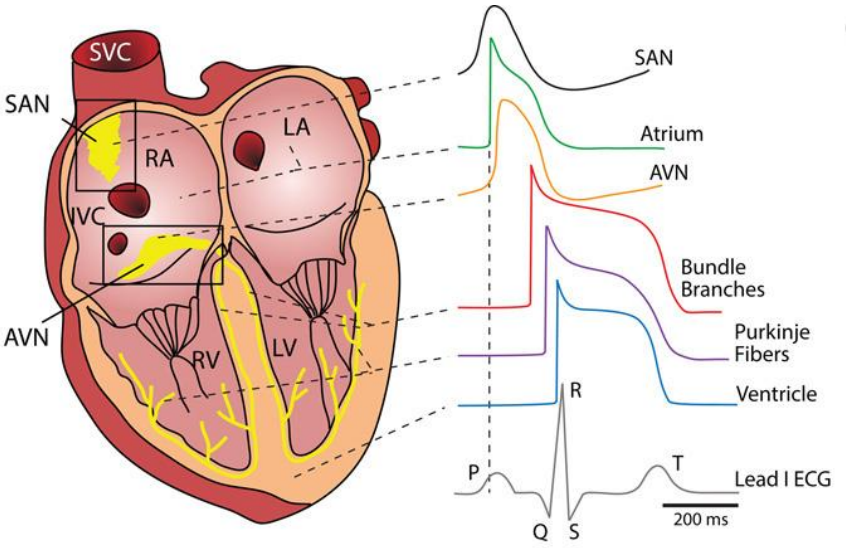

Figure 1: Human action potential waveforms. The different regions of the human heart annotated with the AP waveform seen in specific tissue types. Waveforms are aligned with an ECG trace for identification of different intervals, with the QT interval clearly aligning with the ventricular action potential. Modified from Bartos et al. (2015). RA and LA denote right and left atria respectively, whilst RV and LV denote right and left ventricles. SAN and AVN denote the sinoatrial and atrioventricular node respectively and SVC denotes the superior vena cava.

The human ventricular action potential (Figure 2) is typically split into five separate phases with each representing a distinct pattern of ion permeability (Huang et al., 2017). In the atrial and ventricular myocardium, during phase 4 the membrane is held at a resting potential of ~-80mV by inwardly rectifying K^+ current (I_{K1}), with cells depolarising once the incoming wave of electrical excitation drives the membrane potential past the AP threshold of ~-60mV. At this voltage an influx of sodium ions via fast sodium channel current (I_{Na}) drives the membrane potential to +60mV (phase 0) before fast inactivation of the channel and activation of $I_{to,fast}$ (transient outward current) forms the AP notch (phase 1). Subsequently phase 2, the plateau phase, begins as the membrane potential is kept relatively constant by a balance of L-type Ca current ($I_{Ca\text{-}L}$) and composite delayed rectifier K^+ current, which is comprised of the rapid and slow delayed rectifiers (I_{Kr} and I_{Ks}) (Charpentier et al., 2010). I_{Kr} increasingly contributes to the membrane potential and eventually begins cellular repolarisation (phase 3) before it is deactivated by the negative resting potential and I_{K1}

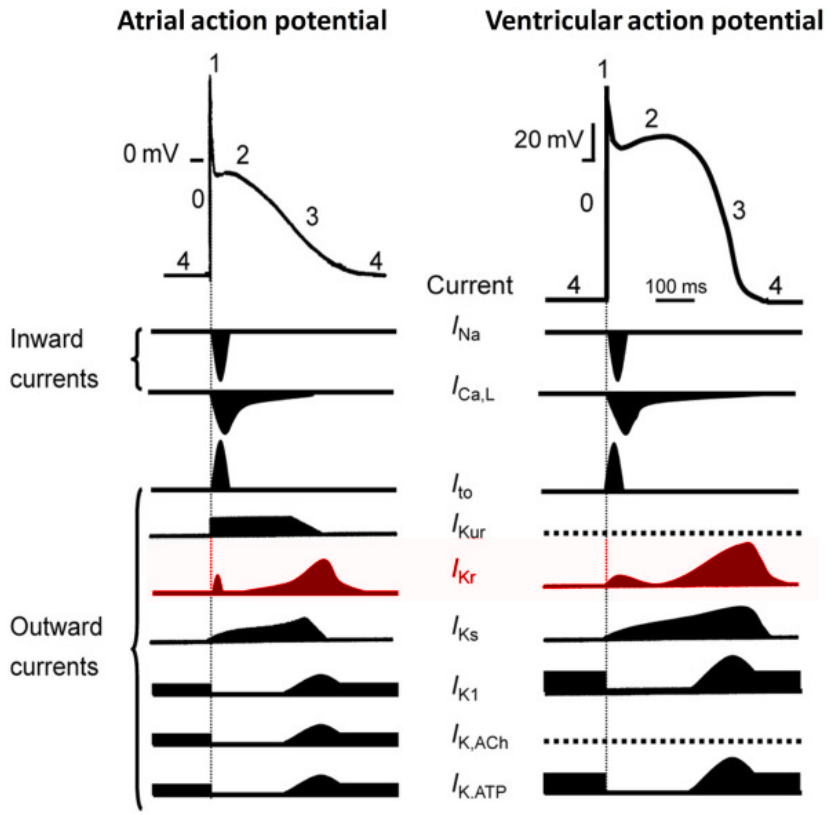

Figure 2: Human cardiac currents. Ionic currents involved in the different phases of atrial and ventricular action potentials. Modified from (Moreno et al., 2012).

again becomes the dominant current. In atrial, but not ventricular cells in the human heart an additional current, the ultrarapid delayed rectifier (I_{Kur}) also contributes to repolarization (Figure 2; Moreno et al, 2012).

1.2 Role of hERG

1.2.1 Characterisation of I_{kr} and hERG

Understanding contribution of I_{Kr} to cardiac action potentials initially began when seminal work by Noble and Tsien (1969) revealed two distinct components to cardiac delayed outward K^+ current (I_K) following depolarisation. These two components, then termed I_{x1} and I_{x2} due to the possible conductance of other ions in addition to potassium, were distinguishable from one another due to the much more rapid activation and inward rectification of I_{x1} (Noble and Tsien, 1969). Further classification of these two components,

however, was made possible in 1990 through use of the novel pharmacological compound E-4031 (Sanguinetti and Jurkiewicz, 1990).

E-4031 was shown to prolong the action potential duration of guinea pig ventricular myocytes by reducing I_K and inhibiting only the rapidly activating I_{x1}, then termed I_{Kr} (rapidly activating delayed rectifier current) and hence distinguish it pharmacologically from the slowly activating I_{x2} (redefined as I_{Ks}) (Sanguinetti and Jurkiewicz, 1990). Consequently, E-4031 was used to show the drug-sensitive I_{Kr} as a current with inward rectification across the positive voltage range and with a maximal current which saturated at ~10mV. This was in contrast to I_{Ks} which continued to increase across the positive voltage range. Differences in the voltage dependence of activation and K^+ selectivity were also shown (Sanguinetti and Jurkiewicz, 1990).

Subsequent to this work, mutations in the recently discovered K^+ channel gene, *hERG* (*human Ether-à-go-go-Related Gene*; alternative nomenclature *KCNH2*), were also shown to be linked to prolongation of the QT interval and the hERG protein was shown to be highly expressed in the heart (Warmke and Ganetzky, 1994, Curran et al., 1995). Consequently, the channel was experimentally expressed in oocytes in order to define its physiological role (Sanguinetti et al., 1995, Trudeau et al., 1995). This work showed that hERG current (I_{hERG}) to reach its peak outward current at a voltage of ~10mV and to decline at positive voltages, properties similar to those previously reported for I_{Kr} (Sanguinetti and Jurkiewicz, 1990, Sanguinetti et al., 1995, Trudeau et al., 1995). Furthermore, this rectification was also shown to be due to rapid inactivation, as previously suggested for the rectification of I_{Kr} (Shibasaki, 1987); the dual components of deactivation identified matched those reported for I_{Kr} (Yang et al., 1994); and modulation of current by extracellular K^+ was similar to that of I_{Kr} (Sanguinetti and Jurkiewicz, 1992). Many of these properties are distinct from any other characterised cardiac currents, and so the study provided ample evidence that channels mediating I_{Kr} involve the hERG protein.

Despite this evidence, the kinetics of the I_{hERG} did not match those of I_{Kr} exactly, and so the identification of an alternate *hERG* transcript specifically expressed in the heart was of great interest to the field (Lees-Miller et al., 1997, London et al., 1997). The two papers, published simultaneously from different laboratories, identified mouse ERG (mERG) 1a and 1b as alternate transcripts. Whilst mERG 1a shares >99% identity with that of the protein previously characterised as hERG, mERG 1b was shown to have an N-terminus ~340bp shorter and capped with a unique sequence of 36 amino acids (Lees-Miller et al., 1997, London et al., 1997). Subsequently, mERG 1b was shown to co-assemble with mERG 1a in oocytes and its more rapid deactivation (compared with that of mERG 1a) caused the resulting heteromer to possess kinetics which more closely resembled that of I_{Kr} (London et al., 1997). Although initial studies suggested that ERG 1b proteins were not expressed in cardiac tissues (Pond et al., 2000, Finley et al., 2002), improvements in antibodies in subsequent years demonstrated the expression of both isoforms in rat, canine and human hearts (Jones et al., 2004) and more recent work on human induced pluripotent stem cell (iPSC) derived cardiomyocytes provides evidence that currents mediating native I_{Kr} are sensitive to knockdown of hERG1b (Jones et al., 2014), suggestive that human I_{Kr} involves hERG 1b in addition to hERG 1a.

The two hERG isoforms preferentially form heteromers, with direct N-termini interactions masking an ER retention signal present in hERG 1b which prevents homomeric 1b channels from forming in humans (Phartiyal et al., 2007, Phartiyal et al., 2008, McNally et al., 2017). These make up the alpha, pore-forming subunits of tetrameric hERG channels, with each monomer consisting of six transmembrane segments (S1-S6) (Vandenberg et al., 2012, Wang and MacKinnon, 2017). As shown in Figure 3A and 3B, S5 and S6 from each monomer contribute to the pore-forming domain of the channel, with the amino acid loop which connects them containing the pore helix and selectivity filter. The cytoplasmic S4-5 linker connects the voltage-sensing domain (VSD; comprised of S1-S4) to the pore-forming helices and the movement of the VSD in response to changes in membrane potential are

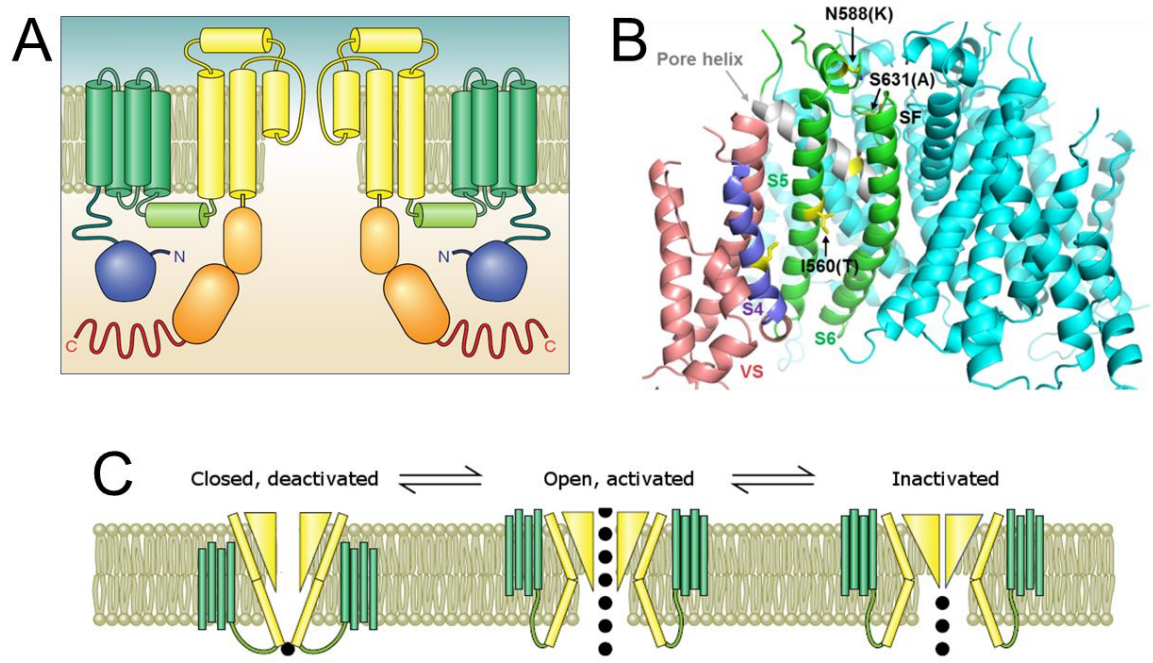

Figure 3: Structure and gating of hERG channels. **(A)** Simplified representation of opposing hERG monomers with N-terminus (blue), VSD (green), pore-forming domain (yellow) and C-terminus (orange) indicated (adapted from Vandenberg et al. (2012)). **(B)** hERG membrane domain based on the recent cryo-EM structure (Wang and MacKinnon, 2017), with voltage sensor (VS), selectivity filter (SF) and pore helix highlighted alongside selected residues. Provided by Dr Christopher Dempsey (University of Bristol). **(C)** The different kinetic states of hERG. Modified from Vandenberg et al. (2012)).

coupled with the gating of both activation and inactivation (Wang and MacKinnon, 2017, Helliwell et al., 2018). Each monomer also has a cytoplasmic C- and N-terminus, the latter of which contains the PAS domain (in hERG 1a only) which characterises the *ERG* subfamily of voltage-gated potassium channels (Vandenberg et al., 2012).

In addition to the major pore-forming subunit, potential roles for the KCNE1 (MinK) and KCNE2 (MiRP1; encoded by *KCNE1* and *KCNE2* respectively) as β-subunits in I_{Kr} have been suggested in the literature, but the exact nature of the relationship is still debated (Anantharam and Abbott, 2005, Hancox et al., 2008, Vandenberg et al., 2012). KCNE1 is well documented to associate with KCNQ1 α-subunits to mediate the I_{Ks} current (Barhanin et al., 1996, Sanguinetti et al., 1996), but it's co-expression with hERG has also been shown to

increase current density but without altering gating kinetics, and mutations to KCNE1 reduce this effect (McDonald et al., 1997, Bianchi et al., 1999). Importantly, the A8V mutation in KCNE1 has been shown to cause arrhythmia and a prolonged QT interval *in vivo*, whilst co-expression of A8V- KCNE1 and KCNQ1 *in vitro* caused little change to current properties and co-expression of A8V- KCNE1 and hERG significantly reduced hERG current density (Ohno et al., 2007). The study therefore, demonstrates a significant effect on hERG can be caused directly by the KCNE1 protein (Ohno et al., 2007). In addition to this, imaging work has shown hERG to be more likely to associate with KCNE1 than KCNE2 in recombinant channel expression experiments (Um and McDonald, 2007).

In contrast to KCNE1, KCNE2 has been shown to decrease hERG current density and increase the rate of deactivation, whilst also possibly having an effect on the voltage dependence of activation (Mazhari et al., 2001, Weerapura et al., 2002b). Further work has also shown KCNE2 to facilitate hERG degradation, which may contribute to the alterations seen in current density but cannot account for changes in kinetic properties (Zhang et al., 2012); and mutations to KCNE2 to affect hERG block by some pharmacological agents (Abbott et al., 1999, Sesti et al., 2000). Although such interactions are clearly evident in expression systems, *in vivo* KCNE2 has been shown to only be express at very low levels outside the conduction system and so it is unlikely that such interactions are critical for hERG function (Lundquist et al., 2005, Sanguinetti and Tristani-Firouzi, 2006). Overall, current literature suggests ability of KCNE1 and KCNE2 to interact with hERG in expression systems, but more work is required regarding their roles in the native current. The hERG 1a protein is central to the current, with hERG1b potentially also playing a role.

1.2.2 Rapid inactivation

The predominant contribution of I_{Kr} to repolarization during the late phase of the ventricular action potential is a result of hERG's unusual voltage-dependent activation and inactivation gating (Sanguinetti et al., 1995, Trudeau et al., 1995, Spector et al., 1996). While most

voltage-gated potassium channels (Kv channels) can transition between the closed, activated and inactivated states (Figure 3C), the speed at which hERG transitions between these are part of what makes it unique (Spector et al., 1996, Cheng and Claydon, 2012). Although activation time-course of hERG is fast in comparison that of I_{Ks}, it is slow when compared to its own inactivation. Macroscopic I_{hERG} activation occurs over hundreds of milliseconds in hERG, whereas transitioning from the open to the inactivated state is much more rapid, taking under 10ms. Consequently, at more positive voltages the channel is instantaneously inactivated, leading to the rectification of current described above. (Charpentier et al., 2010, Cheng and Claydon, 2012).

This C-type inactivation was first described in 1996 in work by both Schonherr et al. and Smith et al. In the first of these, the K^+ channel blocker tetraethylammonium (TEA) was applied both intra- and extracellularly and shown to only affect rate of inactivation when applied to the extracellular surface, indicative of C-type inactivation (Smith et al., 1996). This was further supported when the S631A mutation, corresponding to a residue which is critical for C-type inactivation in other Kv channels (Hoshi et al., 1991), was induced into hERG and shown to remove this inactivation under the experimental conditions (Schonherr and Heinemann, 1996).

Typical Kv channels display voltage-dependent inactivation with a significantly longer time-course and although the exact mechanisms underlying the rapidity of hERG inactivation are not clear, a number of studies have helped identify differences between S6 and the selectivity filter of hERG compared with other channels with shared homology. Using a chimera of the non-inactivating mEAG channel and hERG, it has been shown that mutation of a small S6-Pore region (residues 613-650) was able to confer rapid, voltage-dependent inactivation (Herzberg et al., 1998) to mEAG. In addition to this, five key residues shown as pivotal for stabilising hydrogen bonds in the selectivity filter of the well-characterised bacterial Kv channel KcsA, are not conserved in hERG, possibly enabling it to change state at a much faster rate (Fan et al., 1999). These five residues include Phe627, which more

recently has been shown to be uniquely positioned when compared to both EAG and KcsA in a cryo-electron microscopy structure (Wang and MacKinnon, 2017), further supporting a distinctive hERG pore structure which may contribute to its rapid collapse.

1.2.3 Experimental demonstration of hERG properties

The properties of I_{hERG} can be demonstrated experimentally using whole-cell patch clamp and conventional 'step' voltage protocols to control the membrane potential, as can be seen in Figure 4A. Following depolarization to +20mV, the relatively slow activation occurs and current begins to flow but is limited in size by rapid inactivation (portion of trace shown in red). Once the voltage is repolarised to -40mV, inactivation is rapidly removed, resulting in a resurgent 'tail' current with a rapid increase in current amplitude which then declines as the slower deactivation occurs and channels return to their resting state (portion of trace coloured in green).

As shown in Figure 4B, in which a ventricular AP was applied to a hERG-expressing cell using whole-cell patch clamp techniques (see Sections 3.2.2.1 and 4.2.1.2), this slow activation and rapid, voltage-dependant inactivation mean that during phase 4 hERG channels deactivate and phases 0 and 1 see slow activation but rapid inactivation which limits current size. During phase 2, further activation occurs and as the plateau begins to lower, the decrease in membrane potential removes inactivation. Consequently, phase 3 sees the highest level of I_{Kr} as channels are fully open and inactivation progressively reduces as membrane potential falls. *In vitro*, the fully activated channel has been observed to drive membrane repolarisation, forcing the channels back in to the closed state (Hancox et al., 1998a, Zhou et al., 1998, Sanguinetti and Tristani-Firouzi, 2006, Vandenberg et al., 2012).

Additionally, this slow deactivation confers a protective effect against arrhythmias triggered by prematurely occurring APs as it leaves a proportion of the channels in the open state during the later phases of the AP (Lu et al., 2001, McPate et al., 2009a, Melgari et al., 2014). Consequently, as shown in Figure 4C, if a second, overlapping AP occurs, a large transient current is passed. This current is limited in duration by rapid inactivation but is large enough

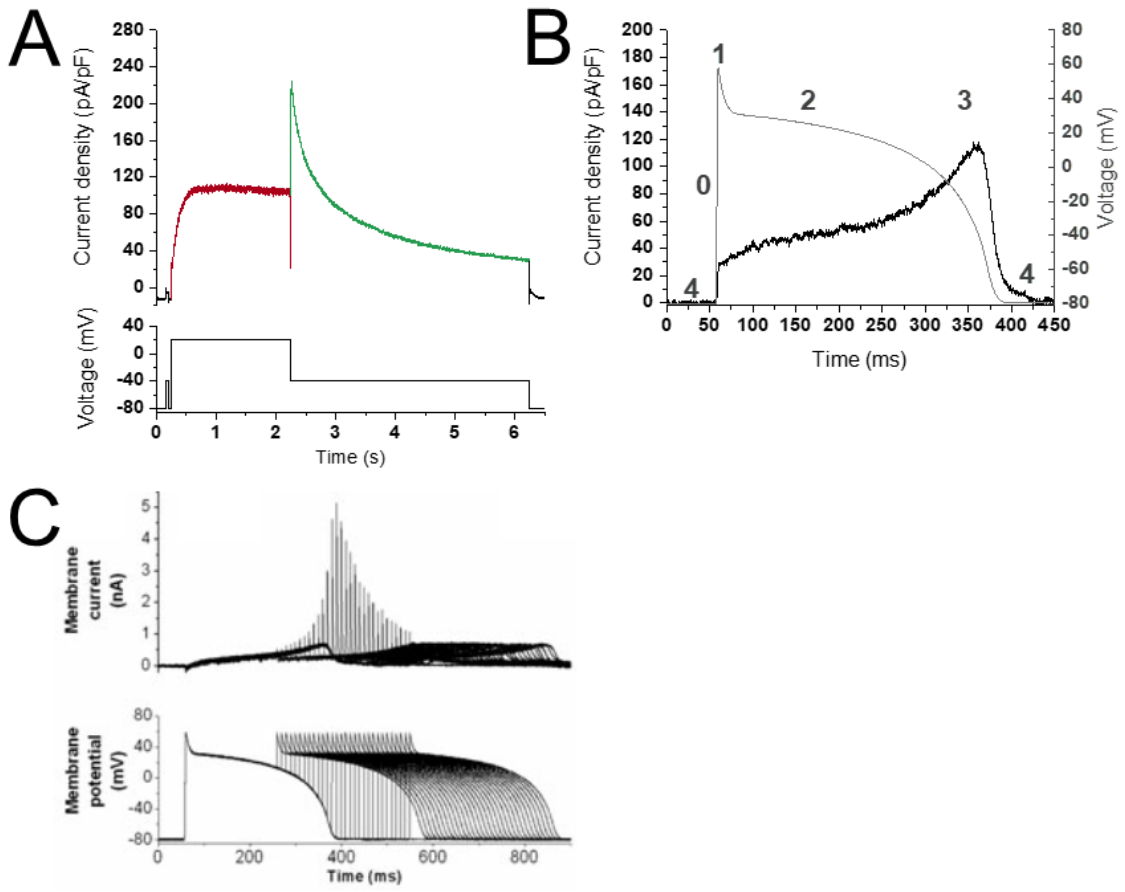

Figure 4: Experimental demonstration of hERG properties. **(A)** Typical trace of WT I_{hERG} with corresponding voltage protocol. Coloured sections represent I_{hERG} following channel activation in the presence of rapid inactivation (red), and slow hERG deactivation following the removal of inactivation (green). **(B)** Typical profile of WT I_{hERG} (shown in black) during a ventricular action potential (shown in grey). Numerical annotations represent the phase of the AP. For (A, B) I_{hERG} recordings were made by myself from HEK293 cells expressing hERG using whole-cell patch clamp at 37°C. All presented data is in line with widely published data (Hancox et al., 1998a, Lu et al., 2001, McPate et al., 2005, McPate et al., 2009a, Zhang et al., 2011) **(C)** Effect of premature ventricular AP stimuli on I_{hERG} (upper panel), using the paired AP protocol shown in the lower panel (Taken from Du et al. (2010)).

supress sodium channel (I_{Na}) activation; oppose the premature depolarisation; drive normal repolarisation; and prevent the activation of L-type Ca^{2+} which are associated with further arrhythmogenesis (Lu et al., 2001).

1.3 Alterations in QT interval

1.3.1 The long and short QT syndromes

The patients in whom Curran et al. (1995) first identified *KCNH2* mutations were suffering from a prolongation of the QT interval which caused seizures, syncope and aborted sudden death, and often had a family history of sudden cardiac death (SCD). This occurs as loss-of-function mutations reduce hERG's ability to terminate the plateau phase of the action potential and drive repolarisation (Witchel and Hancox, 2000, Sanguinetti and Tristani-Firouzi, 2006, Charpentier et al., 2010). In addition to *KCNH2*, mutations in *SCN5A* and *KCNQ1*, encoding $Na_V1.5$ (I_{Na}) and $K_V7.1$ (I_{Ks}) respectively have been shown to cause LQTS. These three genes contribute to >90% of cases of congenital LQTS, with hERG mutations accounting for ~40% of these (Vandenberg et al., 2012). Furthermore, off-target pharmacological inhibition of hERG channel current (I_{hERG}) and/or trafficking is also responsible for the majority of acquired LQTS incidents (Hancox et al., 2008). LQTS is most commonly diagnosed according to the Schwartz criteria, which accounts for family history of cardiac symptoms and the patients' own clinical history in addition to ECG characteristics. A rate-corrected QT (QTc) interval of >450ms is seen as an LQTS risk factor whilst those with a QTc of ≥480ms are at the highest risk (Schwartz and Ackerman, 2013, Baskar and Aziz, 2015). This prolongation of the QT interval can lead to early afterdepolarizations through the re-activation of Ca^{2+} or Na^{+} channels and cause severe ventricular tachycardia, torsades de pointes and syncope or SCD (Yap and Camm, 2003, McPate et al., 2008, Chen et al., 2016).

Similarly, a reduction in QT interval can cause ventricular or atrial fibrillation, polymorphic ventricular tachycardia, syncope and SCD (Maury et al., 2008, Harrell et al., 2015, Chen et al., 2016). This occurs as either a heightened outward repolarizing current or a reduced

inward depolarizing causes a decrease in APD and in the effective refractory period which can promote a uni-directional block in electrical current, leading to a substrate for re-entrant arrhythmia (Bjerregaard et al., 2006, Tse et al., 2017, Hancox et al., 2018). Current clinical guidelines recommend a QTc interval of ≤340ms to be diagnostic of SQTS, although this can be expanded to ≤360ms in the presence of a pathogenic mutation; family history of SQTS or SCD; or survival of episodes of ventricular tachycardia or fibrillation in the absence of heart disease (Priori et al., 2015). The adjustment of these guidelines over time (Ackerman et al., 2011, Gollob et al., 2011, Priori et al., 2013, Priori et al., 2015) mean that large population studies aiming to quantify the prevalence of SQTS have used different reference ranges for their research. A very short QTc interval of ≤320ms has been found with a prevalence of 0.1% (Anttonen et al., 2007, Dhutia et al., 2016), QTc interval of ≤330ms at 0.2% (Dhutia et al., 2016) and, most clinically relevant, QTc interval of ≤340ms has been shown to be prevalent in 0.05-0.4% of the population (Anttonen et al., 2007, Guerrier et al., 2015), whilst a male predominance for the syndrome has been consistently highlighted (Anttonen et al., 2007, Miyamoto et al., 2012, Guerrier et al., 2015, Dhutia et al., 2016). Despite this prevalence of an accelerated QT interval, clinical diagnoses of SQTS remain rare (Mazzanti et al., 2017b, Hancox et al., 2018). Increased understanding of the disorder, however, has further reaching implications, with knowledge of how variations in ionic conductance contribute to arrhythmogenic wavebreak formation; stabilisation of rotors; and post-repolarisation refractoriness being key for a better understanding of other idiopathic arrythmias including atrial and ventricular fibrillation (Cerrone et al., 2006).

1.3.2 Identification of SQTS

SQTS as a distinct congenital entity is a relatively new disorder with the first discussion in the literature occurring within the last twenty years (Gussak et al., 2000). Then an idiopathic condition, Gussak et al's study described three subjects from the same family presenting with a shortened QT interval alongside spontaneous atrial fibrillation and other unreported

rhythmic abnormalities. A fourth, unrelated patient with syncope and subsequent SCD following the identification of a dramatically shortened QT interval was also presented.

A genetic cause of SQTS was first recognised in 2004 with the clinical identification of missense mutations to the *KCNH2* gene leading to an asparagine to lysine substitution (N588K) in the S5-Pore linker region of the hERG channel protein (Brugada et al., 2004). Using TSA201 cells transiently transfected with WT or N588K hERG, the authors showed this mutation to disrupt inactivation, resulting in reduced current rectification at positive voltages and augmented activation during a ventricular AP which could physiologically abbreviate the QT interval (Brugada et al., 2004). Subsequent work further supported these findings, showing a positive shift in rectification caused by a ~60mV shift in half-maximal inactivation; and I_{hERG} density and timing to be altered during ventricular, atrial and Purkinje fibre APs (McPate et al., 2005, McPate et al., 2009a). As the first gene to be directly linked with SQTS, mutations to *KCNH2* gene make up the genotypic group of SQT1. Subsequently, the SQT1 mutation T618I, located within the pore-loop region of the hERG channel, has been established as the most commonly occurring SQTS mutation, although the exact mechanisms underlying abbreviation of the QT interval remain unclear (Sun et al., 2011, El Harchi et al., 2012, Hu et al., 2017, Hancox et al., 2018); and mutations to the N- and C-termini of hERG channels (E50D and R1135H) have been reported to slow the rate of channel deactivation in further SQT1 patients, which could in turn contribute to an abbreviation of repolarisation (Itoh et al., 2009, Hu et al., 2017).

As summarised in Table 1, gain- and loss-of-function mutations which drive repolarisation and reduce then QT interval have since been identified across 7 further genes, the most recent of which occurred just last year (Thorsen et al., 2017). Whereas most genomic analysis of SQTS patients involves the screening of candidate genes, this SQT8-identifying work used whole exome sequencing to, for the first time, recognise a mutation in an anion transporter with two potential mechanisms of abbreviating repolarisation (reduced intracellular Cl^- and increased intracellular pH) (Thorsen et al., 2017). Despite the huge

increase in understanding of SQTS since its relatively recent discovery, this successful use of whole exome sequencing contrasted with the knowledge that only ~25% of SQTS diagnoses have been successfully genotyped highlights there is still much work to be done to fully characterise the disease (Thorsen et al., 2017, Hancox et al., 2018).

Gene	Effect of mutation	SQTS type
KCNH2	↑ I_{Kr}	SQT1
KCNQ1	↑ I_{Ks}	SQT2
KCNJ1	↑ I_{K1}	SQT3
CACNA1C	↓ $I_{L,Ca}$	SQT4
CACNB2	↓ $I_{L,Ca}$	SQT5
CACNA2D1	↓ $I_{L,Ca}$	SQT6
SCN5A	↓ I_{Na}	SQT7
SLC4A3	↓ I_{Cl}, ↑pH_i	SQT8

Table 1: Genes associated with SQTS. Three potassium channels, three calcium channels, a sodium channel and one anion exchanger have been shown as the causes of the 8 identified variants of SQTS. Adapted from Rudic et al. (2014), Perez Riera et al. (2013), Hancox et al. (2018).

1.3.3 Treatment of SQTS

SQTS patients are at high risk of SCD, with prevalence of cardiac arrest at 4% in the first year of life, 1.3% per year between 20 and 40 years, and 41% by 40 years of age (Mazzanti et al., 2014). Implantable cardioverter-defibrillators (ICDs) currently offer a reliable preventative measure and are consequently commonly used in patients (Schimpf et al., 2007). Adjunctive or alternative pharmacological agents however are important as ICDs can trigger inappropriately due to the large T waves seen in some SQTS patients (Giustetto et al., 2011, Mondoly et al., 2016); and ICD implantation can present technical difficulties, especially in paediatric populations (Carro et al., 2017, Hancox et al., 2018). One long-term

follow-up study of SQTS patients reported 58% of patients to have complications associated with ICDs (Giustetto et al., 2011). In order to increase the likelihood of these therapeutic interventions having the desired effects, an understanding of specific SQT1 mechanisms is required as hERG mutations have been shown to affect drug binding in varying ways.

For example, a large number high affinity drugs bind to the inactivated state of hERG much more strongly than they bind the open, activated state (McPate et al., 2008, Perrin et al., 2008), and as a consequence mutations which attenuate hERG inactivation, such as the N588K mutation, can reduce the affinity of pharmacological agents. This was demonstrated experimentally when N588K was shown to be associated with a 20-fold reduction in affinity for the I_{Kr} blocking Class III antiarrhythmic drug D-sotalol (Wolpert et al., 2005). Residues Y652 and F656 (S6 domain) as well as T623, S624 and V625 (pore helix), have been shown as key binding sites for class 1a antiarrhythmics such as disopyramide and quinidine (Mitcheson et al., 2000, Helliwell et al., 2018). For these drugs, the perturbing of inactivation had little to no effect on hERG blockage while the mutation of key residues caused a profound reduction in channel block (Lees-Miller et al., 2000a, Paul et al., 2001, McPate et al., 2006). Such findings have been taken into a small clinical trial supporting the effectiveness of disopyramide in SQT1 patients with the N588K mutation, and so it is clear that *in vitro* study of *KCNH2* mutations can help produce, and potentially predict, more optimal treatment for patients (Schimpf et al., 2007).

1.4 Recently identified SQT1 mutations

In the last three years, two new mutations have for the first time been found to cause SQT1 in patients. Firstly in 2015, a novel heterozygous hERG mutation was identified in a 64-year-old male presenting with palpitations, near syncope, paroxysmal atrial fibrillation and a QT interval of 319ms. There was also a family history of SCD. This c.1679T>C missense mutation caused an isoleucine to threonine substitution at the highly conserved position 560 (I560T) in S5 of hERG (Figure 3B) (Harrell et al., 2015). The authors then used whole-cell patch clamp measurements and computer simulations to determine that this mutation altered

QT interval by modifying the inactivation properties of the channel. Although electrophysiological characterisation of voltage-dependence of activation and inactivation of the channel was performed, there was no analysis of the time-dependence of activation, deactivation, inactivation or the recovery from inactivation; and the reported voltage of half maximal inactivation in the WT was positively shifted in comparison with previously reported data from this and other laboratories (Vandenberg et al., 2006, Sun et al., 2011, Zhang et al., 2011, El Harchi et al., 2012). Furthermore, no work has yet been undertaken to establish the response of the channel to physiologically relevant AP waveforms and no work has been conducted to evaluate any changes in antiarrhythmic drug affinity caused by the mutation. Such information may be of particular value both due to the location of the residue relative to the pore region that contains the canonical binding site (Mitcheson et al., 2000, Harrell et al., 2015, Helliwell et al., 2018); and also because the index patient declined ICD implantation (Harrell et al., 2015).

In a separate study, a 6-year-old female is described who was initially screened following the sudden death of a cousin aged 17. At the time, she presented with a QTc interval of <320ms but she remained asymptomatic until the onset of arrhythmic syncope during exercise at 16 years of age, at which point she was fitted with an ICD. Most recently, at the age of 18, an ECG revealed a QTc interval of 323ms, but she has remained asymptomatic since implantation. Next generation sequencing was used and the authors determined the heterozygous hERG missense mutation c.1891T>G to be the cause of shortened QTc. This mutation leads to a serine to alanine substitution at position 631 (S631A) in the pore region of the hERG channel (Figure 3B) (Akdis et al., 2017). The S631A mutation has been previously engineered for use in experimental work to aid the understanding of both hERG inactivation and drug binding (Schonherr and Heinemann, 1996, Hancox et al., 1998b, Lees-Miller et al., 2000a, McPate et al., 2008), and consequently there is a strong body of work describing the biophysical properties of S631A-hERG. Now that the mutation has been described clinically however, there is clear need to investigate the response of the channel

to cardiac APs and confirm the retention of the channel's ability to bind antiarrhythmic agents.

1.5 Objectives

It can be seen from the background described that correct ion channel operation is vital for maintenance of normal cardiac function and the normal features of hERG activation and inactivation are key in the prevention of arrhythmogenesis. Specific point mutations which affect the hERG protein that mediates I_{Kr} must be characterised to aid clinical responses as well as to increase understanding of both SQTS and wider arrhythmia. Following the clinical identification of the I560T and S631A mutations, the aims established for my current master's project are to:

1) Fully characterise the I560T-hERG mutation's effects on I_{hERG} amplitude and kinetics, in order to identify the way in which the change can cause a shortening of the QT interval.
2) Investigate the impact of the I560T mutation on pharmacological properties of hERG using clinically relevant antiarrhythmic drugs that inhibit wild-type (WT) I_{hERG}.
3) Supplement the existing information, generated from conventional voltage clamp, by characterising the effect of the S631A mutation on I_{hERG} during AP waveforms and on binding of a class I antiarrhythmic agent used against other forms of SQTS.

Chapter 2 Materials and methods

2.1 Mutagenesis

The hERG channel containing the I560T mutation was generated externally by Mutagenex Inc (Suwanee, GA 30024, USA) from a WT construct in modified pcDNA3. DH5*α* *Escherichia coli* (Invitrogen, Paisley, UK) were then transformed, as previously in this laboratory (Zhang et al., 2011), before DNA was purified using an endotoxin-free plasmid DNA purification kit (Neumann-Neander-Str., Germany, Macherey-Nagel), and the mutated sequence was confirmed through sequencing of the complete open reading frame (Eurofins MWG Operon, Ebersberg, Germany).

S631A-hERG plasmids previously studied in this laboratory were used for all experiments (Hancox et al., 1998b, McPate et al., 2008, Melgari et al., 2015). For this, hERG cDNA was subcloned into pGW1H expression vectors and the S631A mutation induced using PCR with a correcting polymerase (Vent, New England Biolabs). Sequencing was confirmed by LICOR technology (Hancox et al., 1998b, Paul et al., 2001).

2.2 Cell culture and transfection

Human embryonic kidney cells (HEK 293; European Collection of Cell Cultures, Porton Down, UK) were used for all work assessing the kinetic properties I_{hERG} (Sections 3.2.1, 3.2.2 and 4.2.1). As shown in Figure 5, these cells are devoid of a native I_{hERG}, although some endogenous current is present. As hERG is expressed well in these cells, I_{hERG} was sufficiently large in all experiments that the native current was deemed to not influence the data collected, and so in line with previous studies, it was not accounted for during data analysis (McPate et al., 2008, Zhang et al., 2011, El Harchi et al., 2012, Du et al., 2014, Zhang et al., 2016). HEK cells were incubated at 37°C, 5% CO_2, in DMEM containing glutamax-1 (DMEM; Gibco, Paisley, UK) and supplemented with 10% fetal bovine serum and 50μg ml^{-1} gentamycin (Gibco, Paisley, UK). Following passage using trypsin (Sigma-

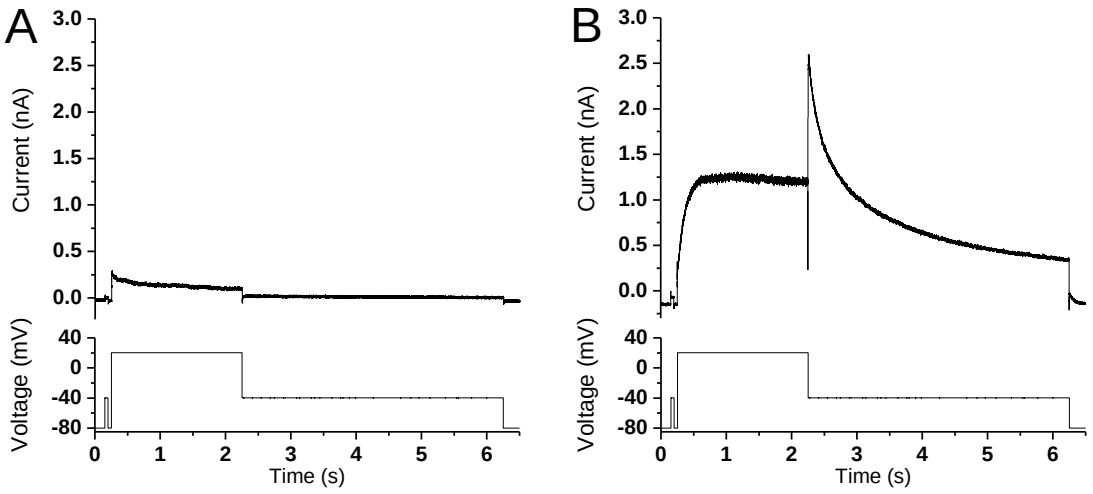

Figure 5: HEK 293 cells do not natively express hERG. **(A)** Representative trace elicited by the protocol in the lower panel, recorded from a HEK 293 which has not undergone transfection. **(B)** Representative trace elicited by the protocol in the lower panel, recorded from a HEK 293 cell which has been transfected with WT-hERG.

Aldrich, Gillingham, UK), cells were transfected with cDNA plasmids encoding either WT or mutant hERG channels using Lipofectamine 2000 (Invitrogen, Paisley, UK). During all WT experiments and the majority of I560T experiments, 1µg of cDNA was transfected. During studies of I_{hERG} inactivation however (which involve manoeuvres that result in large currents; Figure 9), it was seen that I560T I_{hERG} was too large to be accurately recorded when cells were transfected with 1µg of cDNA, and consequently only 0.15µg of mutant cDNA was used for this protocol. Similarly, due to the attenuation of inactivation and subsequent increase in I_{hERG} caused by the S631A mutation (Hancox et al., 1998b, McPate et al., 2008), a reduced volume of this cDNA (0.5µg) was also used. CD8-encoding cDNA (0.15µg) was additionally transfected into the cells (in pIRES, donated by Dr I Baró, University of Nantes, France) to allow detection of successful transfection using Dynabeads® (Invitrogen, Paisley, UK), as also seen previously (Zhang et al., 2011, Melgari et al., 2015).

Although these cells were also used for assessing the response of mutant hERG channels to pharmacological agents, a line of HEK 293 cells stably expressing WT hERG (donated by Dr

Craig January, University of Wisconsin) was used in comparative WT studies (Sections 3.2.3 and 4.2.2). These cells were treated as above, with the addition of 400 µg/mL geneticin (G418, Gibco) to the cell culture medium; and passage using enzyme free cell dissociation solution (Millipore, Watford, UK) as an alternative to trypsin. All cells were plated onto sterilized 13-mm glass coverslips in 40-mm Petri dishes containing their respective medium for electrophysical recordings.

2.3 Solutions for electrophysiological recordings

In keeping with similar studies performed in this lab (Du et al., 2014, Zhang et al., 2016), normal Tyrode's solution containing (in mM): 140 NaCl, 4 KCl, 2.5 $CaCl_2$, 1 $MgCl_2$, 10 Glucose, and 5 HEPES (titrated to pH of 7.45 with NaOH) was superfused over cells at 37°C ± 1°C. Patch-pipettes, fire-polished to 2.5–4 MΩ, were filled with a dialysis solution containing (in mM): 130 KCl, 1 MgCl2, 5 EGTA, 5 MgATP, and 10 HEPES (titrated to pH of 7.2 with KOH). Quinidine powder (Quinidine gluconate salt) and Sotalol (both Sigma-Aldrich, Gillingham, UK) were dissolved in Milli-Q water to produce initial stock solutions of 10mM and 50mM respectively. These were serially diluted in Milli-Q water to produce a range of stock solutions to be stored at -20°C. One the day of use, stock solutions were finally diluted in Tyrode's solution to produce the required concentrations as described in the results.

2.4 Experimental procedure and analysis

Measurements of I_{hERG} were made through whole-cell patch clamp recording of membrane currents using an Axopatch 200A amplifier featuring a 4-pole internal Bessel filter (Axon Instruments, Foster City, CA, USA) and a CV201 head stage. Electrode series resistance (typically 5-10 MΩ) was compensated by 70-80%. A Digidata 1440A interface (Molecular Devices, Sunnyvale, CA, USA) was used to record data at a bandwidth of 2 to 10kHz (depending on voltage protocol) and digitization rates of up to 25 kHz during as appropriate.

During action potential waveforms (Sections 3.2.2 and 4.2.1) I_{hERG} recordings were corrected online for P/N leak subtraction using an interspersed P/4 protocol (McPate et al., 2009a, El Harchi et al., 2010). Clampfit 10.2 (Axon Instruments), Origin 2017 (OriginLab Corporation, Northampton, MA, USA), Excel 2016 (Microsoft, Redmond, WA), and Prism 7 (Graphpad Inc, La Jolla, CA, USA) were all used for data analysis. Using these, a range of equations fully quantified the biophysical properties of I560T I_{hERG}:

Equation 1

Normalizing hERG tail current values (I) to the maximal tail current value observed during the protocol (I_{max}) and plotting these values against the appropriate voltage command (Vm) allowed the half-maximal activation voltage ($V_{0.5}$) and slope factor for I_{hERG} activation (k) to be calculated by fitting with a Boltzmann equation in the form of:

$$I=I_{max}/(1+\exp((V_{0.5}-V_m)/k)) \qquad \text{(See Figure 6 and Figure 20)}$$

Equation 2

The rate of I_{hERG} activation and the recovery from inactivation were calculated by fitting the appropriate data with an exponential equation using current (I) normalised against the maximal current recorded during the protocol (I_{max}); the rate constant (*K);* and the duration of the depolarising step (for rate of activation) or repolarising step (for rate of recovery from inactivation) preceding I_{hERG} 'tail' current measurement (x):

$$I = I_{max}(1-\exp(-K\ x)) \qquad \text{(See Figure 7 and Figure 11)}$$

Equation 3

I_{hERG} deactivation rates, described as a measure of the fast and slow components of the deactivation time-course (τ_f and τ_s respectively), were quantified as a function of the total current (I); the current amplitude at time 'x'; the measure of current represented by τ_f and τ_s (A_f and A_s respectively); and any residual current (C):

$$I = A_f \exp(-x/\tau_f) + A_s \exp(-x/\tau_s)+C \qquad \text{(See Figure 8)}$$

Equation 4

A Goldman-Hodgkin-Katz equation, modified to account for an absence of Na^+ in the intracellular solution, was used to calculate relative Na^+:K^+ permeability. The reverse potential (E); universal gas constant (R); temperature in Kelvin (T), and Faraday's constant (F) alongside the intra and extracellular concentration of ions ($[X]_i$ and $[X]_o$ respectively) were used to calculate relative ion permeability (pX).

$$E = (RT/zF)\ln(([K^+]_o + (pNa/pK) \times [Na^+]_o)/[K^+]_i)$$

Equation 5

Normalizing hERG tail current values (I) to the maximal value tail current observed during the protocol (I_{max}) and plotting these values against the appropriate voltage command (Vm) used to alter I_{hERG} availability allowed the half-maximal inactivation voltage ($V_{0.5}$) and slope factor for I_{hERG} inactivation (*k*) to be calculated by fitting with a Boltzmann equation in the form of:

$$I/I_{max} = 1-(1/(1+\exp[(V0.5-Vm)/k])) \qquad \text{(See Figure 9)}$$

Equation 6

Fractional inhibition of I_{hERG} by quinidine and sotalol was calculated using maximal hERG 'tail' currents, absolute maximal currents, or current integrals (as appropriate) before (I_{hERG}[Control]) and after (I_{hERG}[Drug]) application of drugs :

$$\text{Fractional inhibition} = 1-(I_{hERG}[Drug]/I_{hERG}[Control]) \text{ (See Figure 15, Figure 16 \& Figure 24)}$$

Equation 7

A standard Hill equation was used to establish concentration-response relations, where IC_{50} is the concentration of drug producing half-maximal I_{hERG} inhibition and *h* is the Hill coefficient of the fitting.

$$\text{Fractional inhibition} = 1/(1+(IC_{50}/[Drug])^h) \text{ (See Figure 15 and Figure 16)}$$

2.5 Statistics

All data are presented as mean ± standard error of the mean (SEM) and p values of less than 0.05 were considered significant. These were calculated, as appropriate, using a Student's t-test, Mann-Whitney test or one-way analysis of variance (ANOVA) with Bonferroni post hoc test. Statistical significance is denoted throughout by *, **, ** and **** represents p values of <0.05, <0.01, <0.001 and <0.0001 respectively.

2.6 Computational modelling

Modelling work was all kindly provided by Dr Christopher Dempsey. This used the recently published cryo-EM structure of hERG (Wang and MacKinnon, 2017); and a homology model of hERG based on a previously published rat EAG (rEAG) cryo-EM structure (Whicher and MacKinnon, 2016) which was built using Modeller 9.17 and quality assessed using Procheck software. Figures were made using PyMOL (version 1.4; Schroedinger, LLC, New York, NY).

2.7 Performance of *in vitro* work

Both the I560T and S631A plasmids were generated in the laboratory prior to my arrival. Transfection and cell culture were initially performed by Dr Zhang (University of Bristol), but these duties were passed on to myself following suitable training. I collected the majority of the electrophysiological data myself, with some also collected by Dr Zhang, in large part to ensure correct functioning of all systems whilst my practical and theoretical understanding was developed. I performed all data analysis and presentation.

Chapter 3 Effects of the I560T mutation on hERG function

3.1 Introduction

The I560T mutation is the first SQT1 causing mutation identified to occur within the S5 domain of hERG (Hancox et al., 2018). Prior to discovery of the I560T mutation, SQT1 mutations had been identified in both the N- and C-termini (E50D and R1135H respectively) and within the S5-pore linker (N588K) and pore region of the hERG protein (T618I) (Hancox et al., 2018), whilst additional inactivation attenuating mutations had been engineered in the pore (S620T, S631A) for studies of hERG structure function (Schonherr and Heinemann, 1996, Ficker et al., 1998, Hancox et al., 1998b, Herzberg et al., 1998, Zou et al., 1998). As may be expected, the mutations located within the pore-linker and pore-forming regions have been shown experimentally to have a more profound effect on channel function than those located at the more distal portions of the channel (Zou et al., 1998, McPate et al., 2005, Itoh et al., 2009, Hu et al., 2017), and so it is of interest to unravel the extent with which the I560T mutation affects the biophysical properties of hERG.

Whilst many loss-of-function hERG mutations have been found to cause LQTS through a reduction in protein trafficking (Thomas et al., 2003, Modell and Lehmann, 2006), no SQT1 mutations have yet been found to exert effects through increased membrane expression or hyperglycosylation of the protein (Hancox et al., 2018). In order to rule out this possibility, Harrell et al. (2015) performed western blotting to measure expression of I560T- and WT-hERG, demonstrating no significant change in either caused by the mutation. This suggests the documented QT interval abbreviation with this mutation is a direct result of changes to channel gating (Harrell et al., 2015).

S5 residues have been suggested to be energetically coupled to both S4 residues involved in the voltage sensing of activation and inactivation (Perry et al., 2013b), and pore-forming residues which are critical for channel inactivation (Perry et al., 2013a). Furthermore, a mutation to the nearby residue, H562, perturbed the hydrogen bonding believed to stabilise

the selectivity filter, caused a positive shift in half-maximal activation and slowed channel deactivation (Lees-Miller et al., 2009). Whilst confirmation of interactions between residues are outside the intended scope of this study, by fully characterising the biophysical properties of I560T-hERG, the work presented here could offer a basis for more targeted further work. In addition to this, by determining the effects of the mutation on binding of quinidine and sotalol, the study will offer insight into the structural effects of the mutation as well as potential therapeutic strategies for the patient. The interplay between S5 and the range of key hERG domains described in the literature suggests that the effects of the I560T mutation may extend beyond the only the voltage-dependence of inactivation as described by Harrell et al. (2015), and so additional hERG properties must be defined in order to characterise further the way in which the mutation facilitates shortening of the QT interval.

3.2 Results

3.2.1 Biophysical properties of I560T-hERG

3.2.1.1 Effects of the I560T mutation on hERG activation

The upper panels of Figure 6A show representative current traces elicited by application of the voltage protocol shown in the lower panels. Consistent with earlier studies (McPate et al., 2005, Zhang et al., 2011) a two second depolarising command was applied from a holding potential of -80mV to potentials between -40mV and 60mV. Subsequently, a repolarisation command to -40mV was applied to relieve channel inactivation, resulting in the archetypal resurgent I_{hERG} 'tails'. Figure 6Ai shows the well-established characteristics of WT I_{hERG}, with the current upon depolarisation rising rapidly and then plateauing; and the repolarisation command causing a rapid increase in hERG current (I_{hERG}) as inactivation was removed, followed by slower deactivation (Sanguinetti and Jurkiewicz, 1990, Sanguinetti et al., 1995, Spector et al., 1996, Zhou et al., 1998). By contrast, following the same protocol, I560T-hERG (Figure 6Aii) displayed a much larger initial increase in I_{hERG} and, following

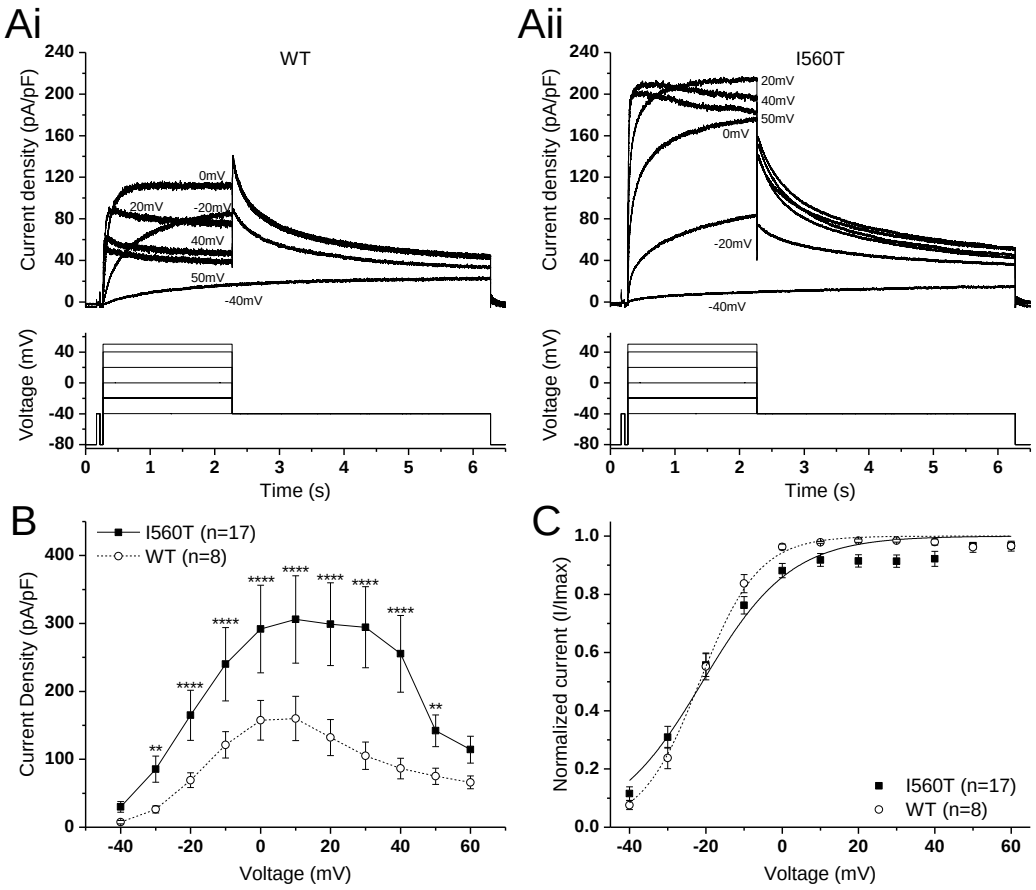

Figure 6: I-V relationship for WT and I560T-hERG. **(A)** Representative current traces for WT (i) and I560T (ii) hERG channels elicited by the protocol shown below, with only selected traces shown for clarity. **(B)** Mean I-V relations for end pulse WT and I560T $I_{hERG.}$ Current was normalised to capacitance reflecting cell membrane surface area. **(C)** Mean normalized tail current I-V relations. Currents were normalized to the peak current recorded during the protocol for each cell and fitted with Equation 1.

repolarisation, the mutant channel's tail current was typically smaller than that seen at the end of depolarisation across the positive voltage range.

The relationship between voltage and I_{hERG} (I-V relations) was determined by plotting the magnitude of the current following the depolarising pulse ("end pulse" current) against the applied voltage, with the magnitude of end pulse current reflecting both channel activation and inactivation. This is shown in Figure 5B, where WT I_{hERG} increased progressively up to 0-10mV and then declined at the more positive potentials as inactivation increased. I_{hERG} magnitude was plotted as current density (pA/pF) in order to normalize data for cell size (capacitance reflecting cell membrane surface area). Although I560T-hERG exhibited a

higher current density compared to the WT (e.g. following a 20mV command pulse; 298.8 ± 60.9pA/pF for I560T vs. 132.1 ± 26.5pA/pF for WT; n=17 vs. n=8; p<0.001), it followed a similar current progression at negative potentials with current density peaking at 10mV. Through the initial positive voltages however, I560T I_{hERG} remained comparatively higher, with little drop in current seen until commands to +40/+50 mV pulse were applied, whereas almost half the WT I_{hERG} had reduced prior to this. Rectification at 60mV increased however; thus, the end pulse I-V relation for I560T-hERG showed a region of negative slope, just shifted somewhat compared to the WT channel.

As peak tail currents represent the level of channel activation in the absence of inactivation, plotting these normalized values across the voltage range allows the voltage dependence of activation to be established (Figure 6C) (Sanguinetti and Jurkiewicz, 1990, Trudeau et al., 1995, Zhou et al., 1998, McPate et al., 2005). There was no change in the half maximal activation voltage ($V_{0.5}$) between the WT and mutated channels (-21.07 ± 1.29mV vs. -21.43 ± 1.41mV respectively; n= 8 vs. n=17; p>0.05), but a change in the slope of the activation relation (*k*) was identified (6.61 ± 0.15mV vs. 12.55 ± 2.14mV; n= 8 vs. n=17; p<0.01).

To establish the effects of the I560T mutation on the time-course of I_{hERG} activation, an 'envelope of tails' protocol was used (Figure 7) as employed in other studies (e.g. Zhang et al., 2011, El Harchi et al., 2012., Helliwell et al., 2018). From a holding potential of -80mV, a depolarising step to 20mV of variable duration was applied, followed by a 4 second repolarising step to -40mV. As the repolarising step removes I_{hERG} inactivation, varying the duration of the depolarising step (from 10ms to 810ms) allows I_{hERG} tail currents to be used to establish the rate at which the channel is activated. Representative currents for WT and I560T I_{hERG} following this protocol are shown in Figures 6Ai and 6Aii respectively. Plotting normalized peak tail currents and fitting them with Equation 2 (Figure 7B) shows a significant decrease in the mean time-constant of activation caused by the I560T mutation (65.4 ± 3.5ms for WT vs. 19.6 ± 1.7ms for I560T; n=5 vs. n=7; p<0.0001).

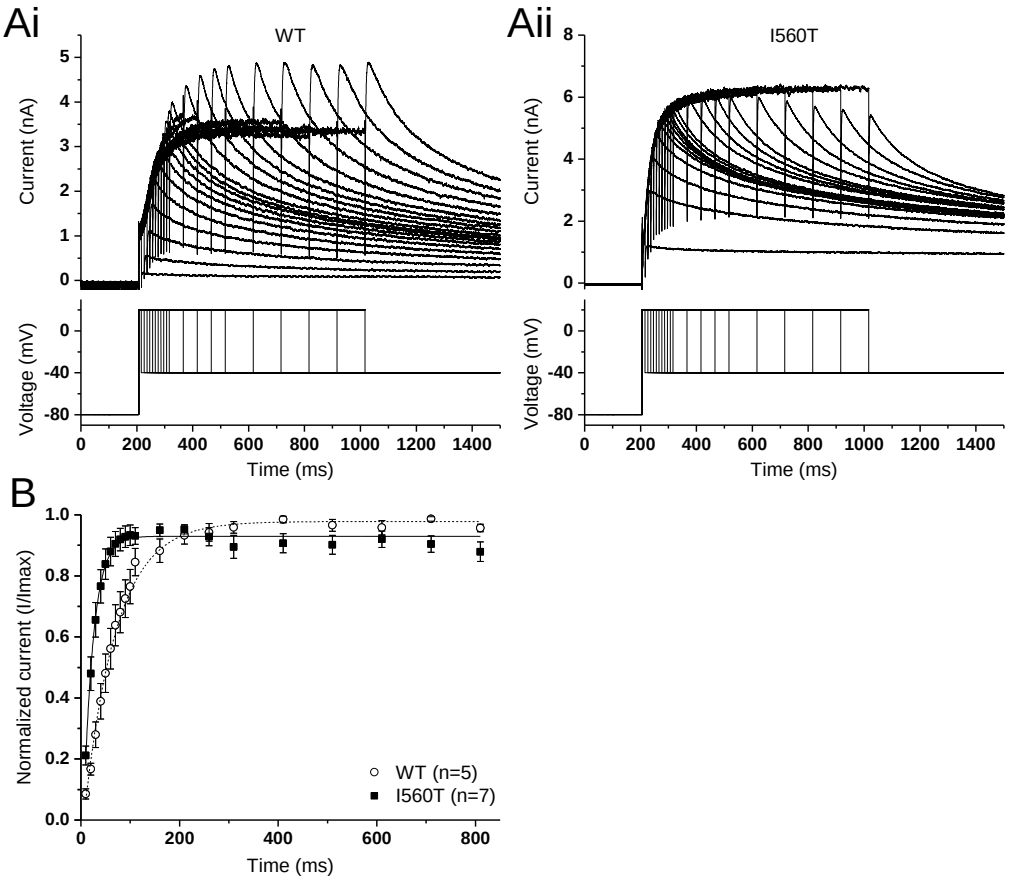

Figure 7: Time dependence of WT and I560T-hERG activation. **(A)** Representative traces for WT (i) and I560T (ii) I_{hERG} elicited by the 'envelope of tails' protocol shown in the lower panels. **(B)** Peak tail currents at each timepoint were normalised to the maximal current recorded during the protocol for each cell and fitted with Equation 2 to quantify the rate of channel activation.

3.2.1.2 Effects of the I560T mutation on the fully activated I-V relations

In order to quantify I_{hERG} deactivation and compare the fully activated I-V relation between WT and mutant channels, the protocol seen in the lower panel of Figure 8A was used, as seen previously (Spector et al., 1996, Hancox et al., 1998a, Zhou et al., 1998, McPate et al., 2005, Zhang et al., 2011). From a holding potential of -80mV, membrane potential was stepped to +40mV for 500ms to allow the channels to activate and inactivate fully. Following this, repolarising voltage commands were applied for 5 seconds at 10mV steps between -100mV and 40mV in order to relieve inactivation to different extents, producing resurgent current tails of different magnitudes, which then deactivated. This allowed the rate of

deactivation to be quantified across a wide voltage range. As can be seen in the representative traces of Figure 8Ai, WT tail currents rose as expected as the membrane potential became less negative, peaking at -20mV (McPate et al., 2005, Zhang et al., 2011). Similarly, tail current plateaus also increased as channel activation increased throughout the negative potentials, however at positive repolarising voltages range peak tail currents as substantial channel inactivation remained (see 20mV trace). I560T I_{hERG} followed a similar pattern under the same conditions (Figure 8Aii), albeit with a slightly more positive peak at -10mV.

Separate fast (τ_f) and slow (τ_s) components to hERG deactivation have previously been established and consequently a bi-exponential fitting (Equation 3) of the traces in Figure 8A can be used to quantify deactivation rates across the voltage range (Sanguinetti et al., 1995, Zhou et al., 1998, Wang et al., 2000, McPate et al., 2005, Zhang et al., 2011). At voltages above -20mV, the level of deactivation became too small to fit accurately. As can be seen in Figure 8B and 8C, τ_f and τ_s were modestly increased in I560T compared to WT at some voltages, although this was slightly more prominent for the fast component. As shown in Figure 8D however, the more significant increase in τ_f compared with τ_s was not sufficient to augment the proportion of deactivation mediated by either component to a significant level. Together, these data indicate a slight decrease in the rate of deactivation from a fully activated state.

By normalising both inward and outward tail currents to the maximal current recorded during the protocol for each cell, I-V relations from the fully activated state have also been establish as seen previously (Figure 8E) (Sanguinetti et al., 1995, Zhou et al., 1998, McPate et al., 2005, Zhang et al., 2011). This demonstrated a modest but statistically significant positive shift in the reversal potential (E_{rev}) of I_{hERG} caused by the mutation (-85.05 ± 0.53mV to -80.34 ± 1.4mV; n=5 vs. n=11; $p<0.05$; Figure 8E). Using a modified Goldman-Hodgkin-Katz equation (Equation 4) to calculate the relative Na^+:K^+ permeability ratio, this shift was shown

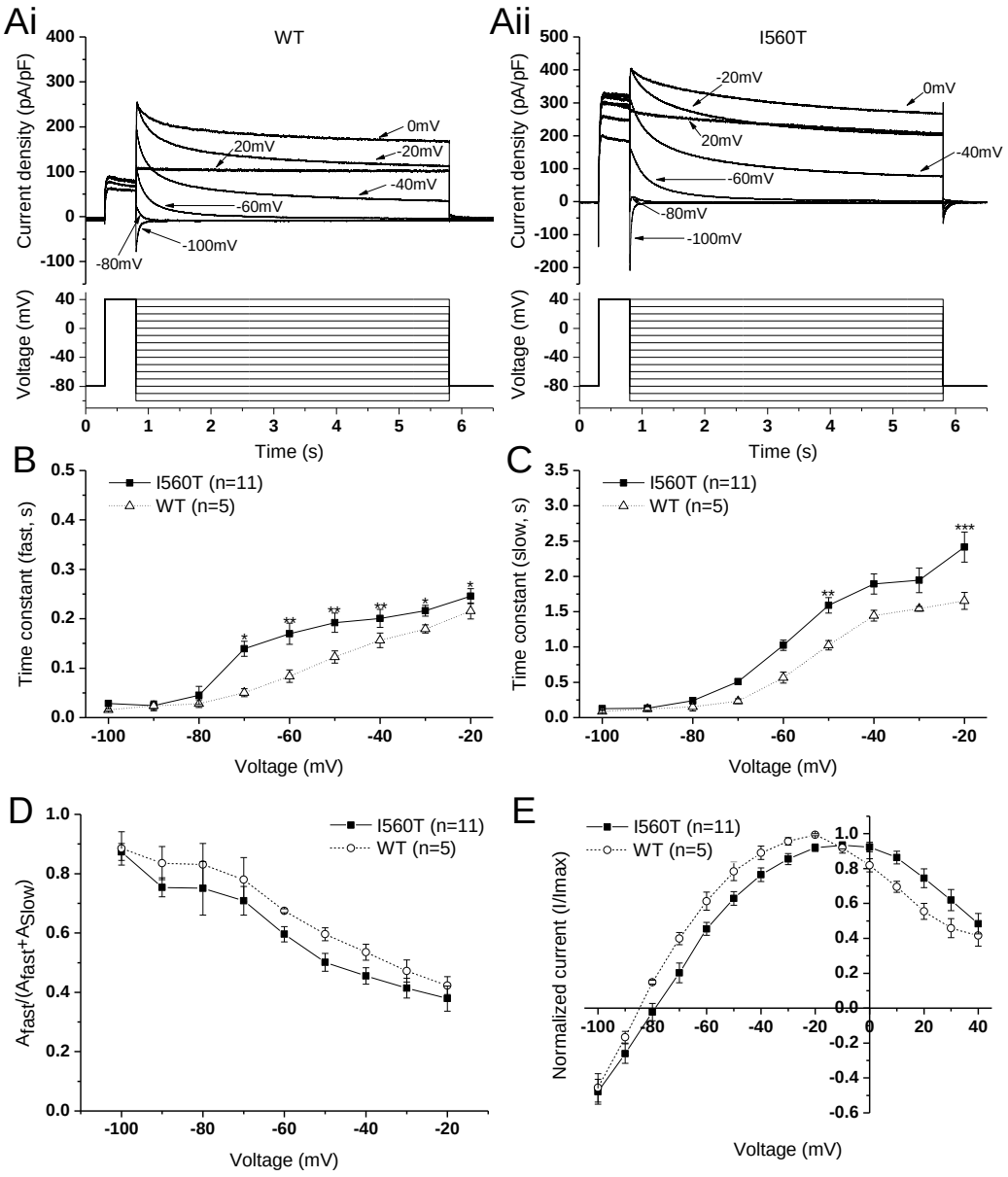

Figure 8: Fully activated I-V relations for WT and I560T-hERG. **(A)** Representative current traces elicited by the protocol shown in the lower panel of figures for WT (i) and I560T (ii) hERG, with only selected sweeps shown for clarity. **(B, C)** Fast (τ_f) and slow (τ_s) time constants of deactivation respectively, calculated by fitting current traces with Equation 3. **(D)** Fraction of deactivating current mediated by the fast component at voltages of -100mV to -20mV. **(E)** Peak tail currents at each voltage were normalized to the peak current recorded during the protocol for each cell to give the fully activated I-V relations.

to reflect a modest decrease the channel's selectivity towards K^+ as the Na^+:K^+ permeability ratio changed from 0.010 to 0.016.

3.2.1.3 Effects of the I560T mutation on hERG inactivation

Figure 9A and the lower panels of 8B show the voltage protocol used to study further inactivation properties of WT and I560T-hERG (Zou et al., 1998, McPate et al., 2005, Sun et al., 2011, El Harchi et al., 2012). From a holding potential of -80mV, cell membrane potential was stepped to 40mV and held at this potential for 500ms, allowing the channel to activate and inactivate fully. Subsequently, a brief 2ms pulse to different repolarization potentials (-140mV to 50mV) was applied to remove inactivation to varying degrees, before a third pulse returned the membrane potential to 40mV. As can be seen in Figure 9B, reapplication of depolarising commands to 40mV resulted in rapid I_{hERG} reflective of channel availability at each given voltage. By analysing the current following this third pulse (Figure 9Bi and 8Bii), the voltage dependence and time course of the inactivation gating was calculated. In order to correct for any deactivation, recorded traces were fitted with a single exponential fitting (Equation 5) and extrapolated back to the start of the third step, as described previously (Smith et al., 1996, Zou et al., 1998, McPate et al., 2005, Zhang et al., 2011).

For each cell, calculated peak currents were normalised to maximal current obtained during the protocol and plotted against voltage to establish voltage dependence (Figure 9C). The I560T mutation was shown to shift the $V_{0.5}$ of I_{hERG} inactivation positively by ~24mV (-41.79 ± 3.47mV for I560T vs. -66.25 ± 1.91mV for WT; n=6 vs. n=13; $p<0.001$), with an accompanying decrease in *k* value (-20.15 ± 0.62 for I560T vs. -25.31 ± 1.22 for WT; n=6 vs. n=13; $p<0.05$). As is apparent in the representative traces shown in Figure 9B, the mutated channel also increased the time-course of the development of inactivation, with a time constant more than double that seen in WT (2.31 ± 0.17 for WT vs. 4.72 ± 0.36 for I560T; n=6 vs. n=13; $p<0.001$; Figure 9D). This change in inactivation was also seen to affect steady state I_{hERG} greatly. Using the product of Equations 1 and 5, with $V_{0.5}$ and *k* values derived from the fitted activation and inactivation plots (Figure 10A), this 'window' current was calculated across a wide voltage range (Figure 10B) to show a significant increase in steady state I_{hERG} caused by the I560T mutation.

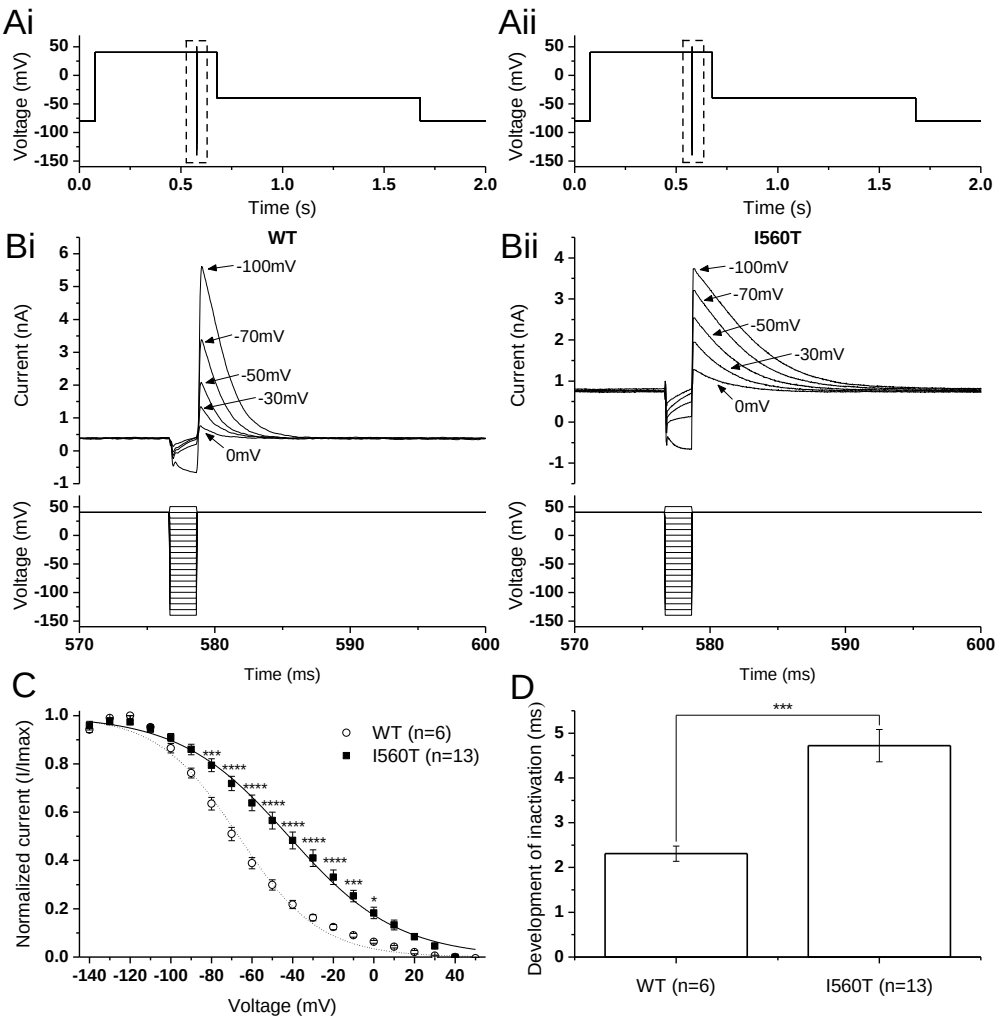

Figure 9: Voltage and time dependence of inactivation for WT and I560T-hERG. **(A)** Voltage protocols used to establish I_{hERG} inactivation. The highlighted sections are those magnified in lower panels of B. **(B)** Representative traces for WT (i) and I560T (ii) I_{hERG}. A pulse at every 10mV from -140mV to 50 mV was used to elicit current, with only selected traces shown here for clarity. **(C)** The voltage dependence of inactivation. Maximal I_{hERG} following the third pulse were normalized to the peak current recorded during the protocol for each cell and fitted with Equation 5. **(D)** Summary of the time-constant for the development of inactivation for WT and I560T I_{hERG} following repolarisation commands to 120mV.

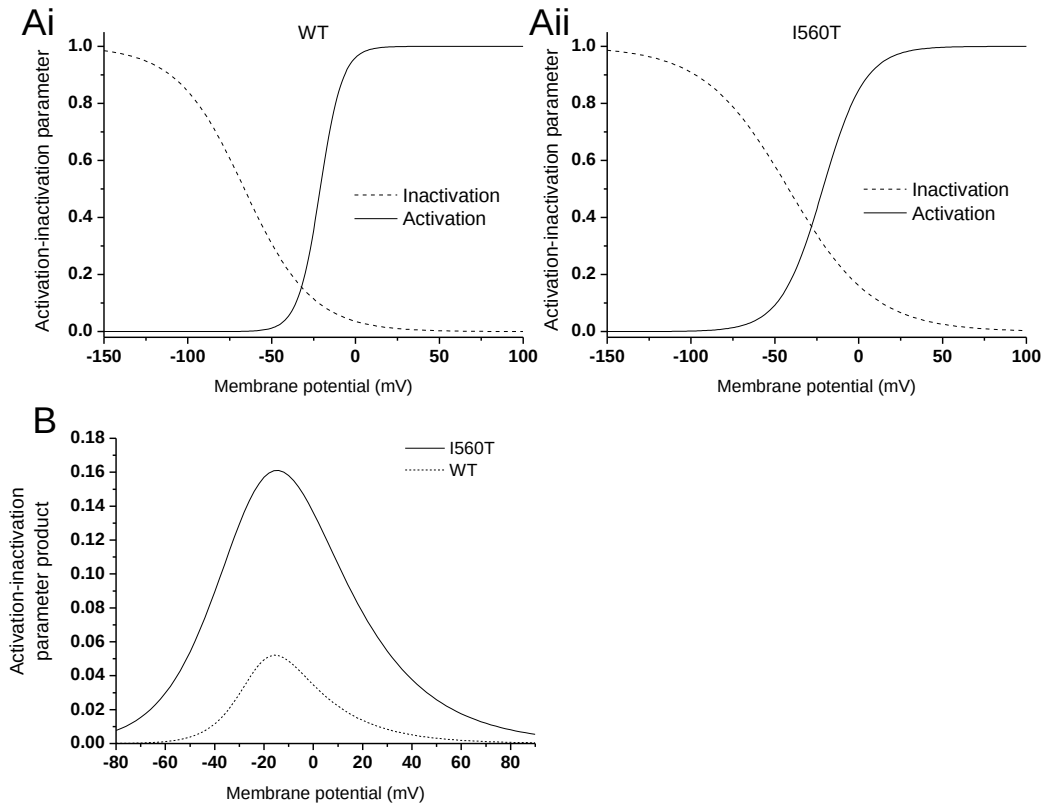

Figure 10: WT and I560T-hERG window current. **(A)** Superimposed activation and inactivation curves for WT (i) and I560T (ii) I_{hERG} respectively as initially plotted in Figure 6C and Figure 9C. **(B)** Product of activation and inactivation parameters plotted against voltage to show steady state WT and I560T I_{hERG}.

Additionally, the rate at which channels recover from inactivation has been investigated using the protocol shown in Figure 11A and expanded upon in the lower panels of Figure 11B. From a holding potential of -80mV, a depolarising step to 40mV was applied to allow the channels to reach a steady state of activation and inactivation. A brief, -40mV, repolarising pulse of 2ms to 20ms was then applied before a second depolarising pulse to 40mV. Plotting the normalized peak tail current (Figure 11C) allows investigation of the time-span necessary for complete transition to the open, activated state. As can be seen in Figure 11C, there was no significant difference between the time-constants for the recovery from activation between WT and I560T I_{hERG} (1.84 ± 0.08ms vs. 2.05 ± 0.17ms; n=10 vs. n=18; $p>0.05$).

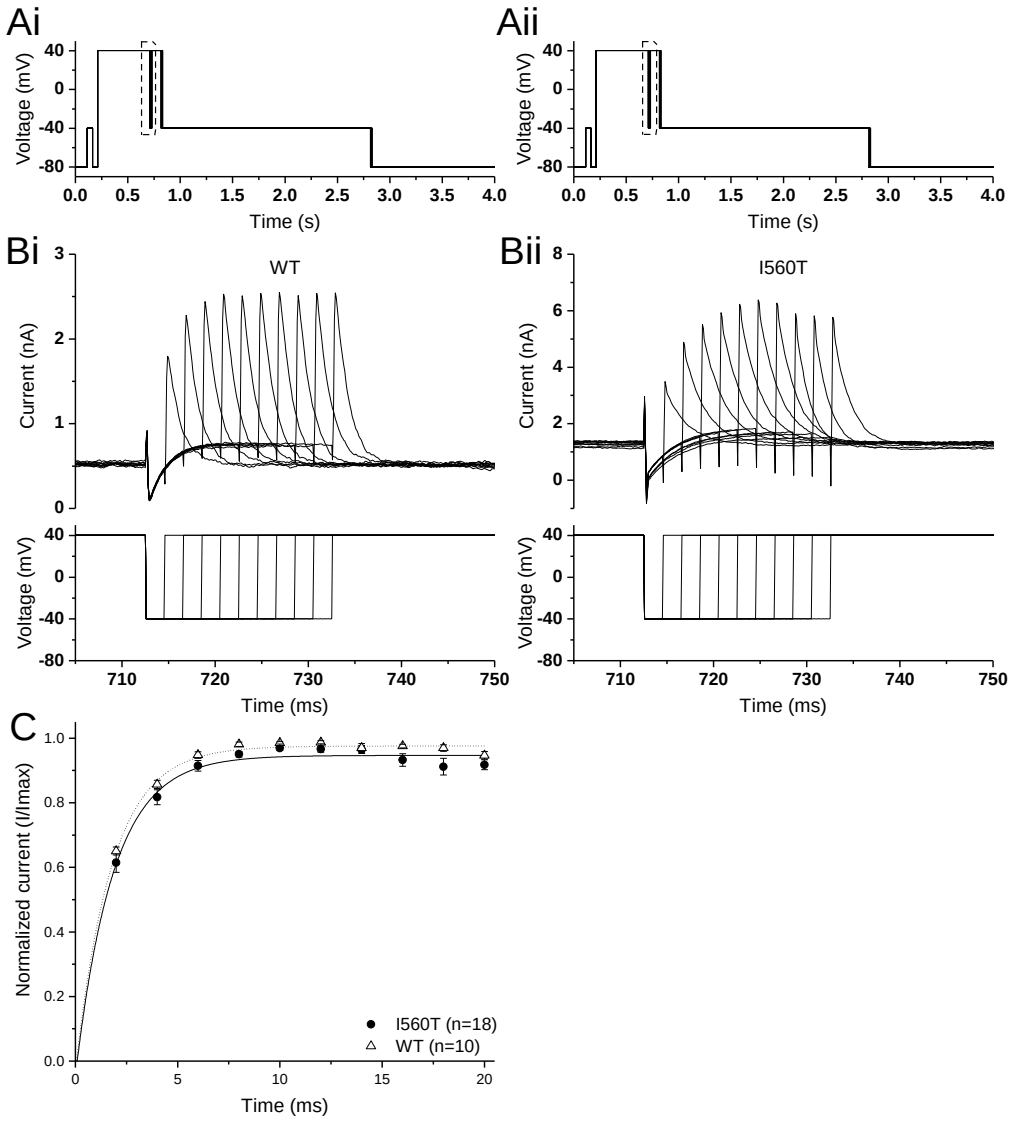

Figure 11: Time dependence of WT and I560T-I_{hERG} recovery from inactivation. **(A)** Voltage protocol used to establish rate of recovery, with the highlighted section being expanded upon in the lower panels of (B). **(B)** Representative traces for WT (i) and I560T (ii) I_{hERG}. **(C)** Peak tail currents at each timepoint were normalised to the maximal current recorded during the protocol for each cell and fitted with Equation 2 to quantify the rate of recovery from inactivation.

3.2.2 Physiological consequences of the I560T mutation

3.2.2.1 Effects of the I560T mutation on I_{hERG} profile during ventricular AP

The conventional voltage clamp techniques used above constitute an excellent means to understand basic channel kinetic properties through specific square voltage command protocols. Despite this, the use of physiological action potentials as stimuli during voltage clamp (AP clamp) in addition to the more traditional step protocols is valuable as it allows recordings to account for the more dynamic history of membrane potential experienced during physiological events (Hancox et al., 1998a, Noble et al., 1998). Figure 12A shows the mean I_{hERG} produced in response to a ventricular AP, with the AP itself shown simultaneously (McPate et al., 2009a, El Harchi et al., 2010). Following the initial peak of the AP at ~60ms in Figure 12Ai, hallmark I_{hERG} characteristics were exhibited in the WT with current limited during the early stages of the AP and, as the membrane potential decreased, inactivation was progressively removed and so I_{hERG} increased, peaking in phase 3 of the AP. From the start of phase 2 however, I560T I_{hERG} continued to increase in a relatively linear fashion, with peak current still occurring in phase 3 of the action potential (Figure 12Aii).

Figure 12B, which shows instantaneous I-V relationship established throughout the ventricular AP, with repolarisation occurring from the right to the left of the plots, highlights that although both WT and I560T I_{hERG} peaked late during the ventricular AP, the mutation caused a significant positive shift in the voltage at which this occurs (Figure 12B; I560T -11.9 ± 3.4mV vs. WT -29.7 ± 2.7mV; n=19 vs. n=5; $p<0.05$, and so I560T I_{hERG} peaked earlier during repolarisation. In addition to this earlier timing, the total charge passed by the channel (current integral) was 2.6-fold larger than that of WT I_{hERG} (Figure 14B; $p<0.01$). Figure 12C shows the instantaneous changes in conductance throughout repolarisation. As can be seen in Figure 12Ci, WT G-V relations increased progressively throughout the early stages of the AP before peaking between -50mV and -80mV. Conversely, following the I560T mutation,

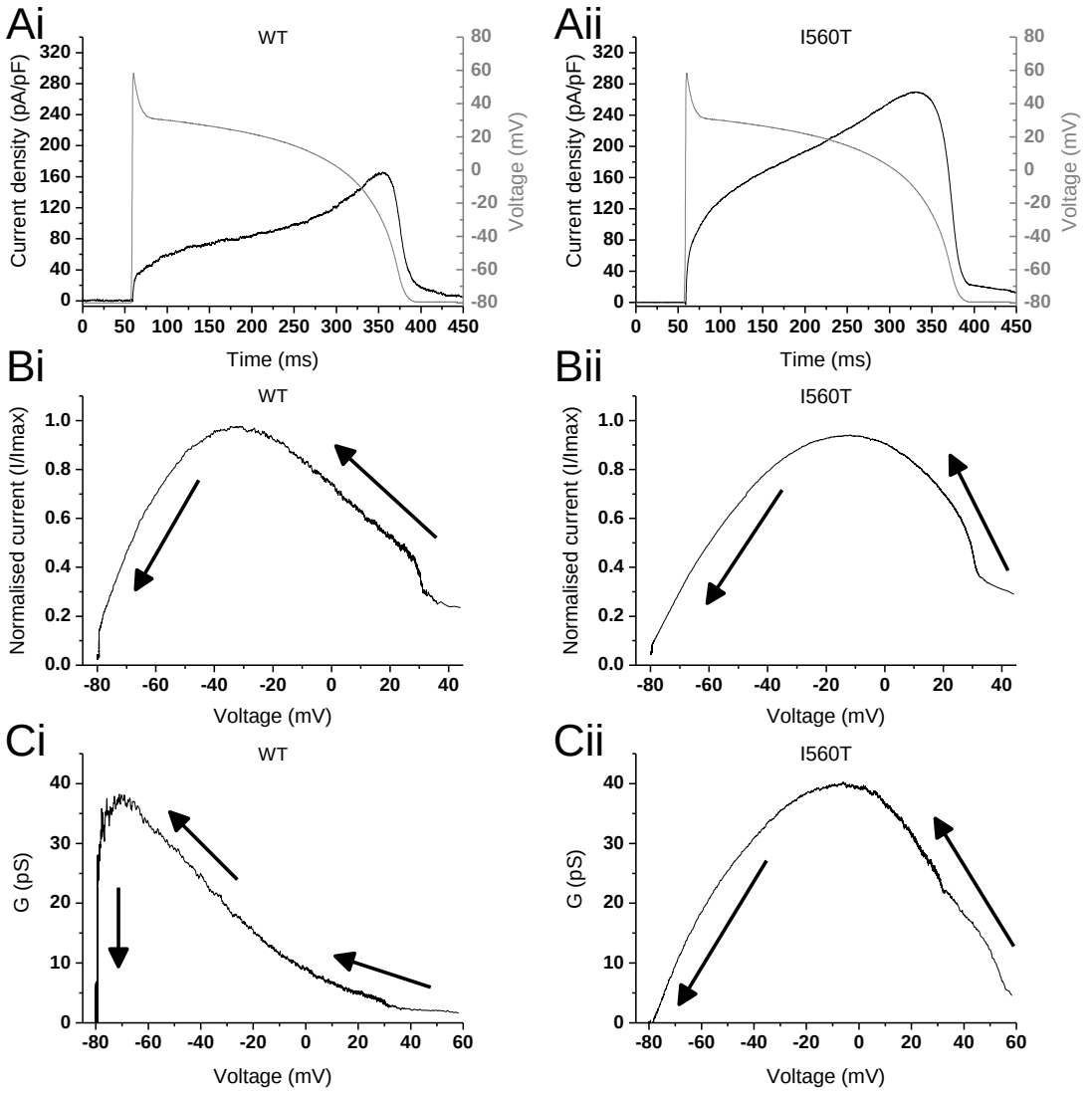

Figure 12: WT and I560T-I_{hERG} response to a ventricular AP. **(A)** Mean WT (i) and I560T (ii) I_{hERG} profile (shown in black) during a ventricular AP (shown in grey). Current was normalised to capacitance reflecting cell membrane surface area. **(B)** Mean I-V relations recorded during repolarisation in a ventricular action potential. Current was normalised to the maximal current recorded during the protocol for each cell, with these values used to establish mean current at each given voltage. **(C)** Mean G-V relations recorded during repolarisation in a ventricular AP. For (B, C) the arrows represent the direction of repolarisation. For all figures, n=5 for WT and n=19 for I560T.

ionic driving force increased much earlier in the AP (between 20mv and -30mV) and also remained high over a larger voltage range (Figure 12Cii).

3.2.2.2 Effects of the I560T mutation on I_{hERG} profile I_{hERG} during atrial and Purkinje fibre AP

To establish whether the different voltage, duration and plateau phases of action potentials in other cardiac tissue types would affect I560T I_{hERG} to a similar extent as the ventricular AP, both atrial and Purkinje fibre (PF) stimuli were also applied to the cells (Figure 13), as used previously (El Harchi et al., 2009, El Harchi et al., 2010, Milnes et al., 2010). As can be seen, the plateau phase of the atrial AP (Figure 13Ai) is both shorter in duration and occurs at a voltage more negative than the ventricular AP, and as a result the elicited I_{hERG} was much smaller. Although this lower plateau reduced hERG activation, inactivation was also diminished and therefore a more dome-shaped I_{hERG} profile was produced. I560T I_{hERG} again produced a larger current integral (Figure 14B; 2.3-fold; $p<0.001$) than WT, but the reduced involvement of inactivation meant the current profile was similar under both the WT and the mutant condition. This was supported by peak I_{hERG} occurring at same stage of the AP in WT cells as cells expressing I560T-hERG (Figure 13Aii, -24.0 ± 2.5mV vs. -24.4 ± 2.3mV; n=15 vs. n=16; $p>0.05$).

The PF AP (Figure 13B) is an intermediary between the atrial and ventricular APs, with its plateau phase being at an intermediate with regards to both duration and voltage. This was reflected in the profile of WT I_{hERG} which underwent some inactivation during the early stages of repolarisation and peaked during phase 3 at voltage comparable to that of the ventricular AP (Figure 13Bii; -35.1 ± 0.8mV; n=7) before the channel deactivated. Similar to other APs, I560T I_{hERG} carried a 2.2-fold greater charge throughout the waveform compared to WT I_{hERG} (Figure 14Bi; $p<0.05$). As can be seen in Figure 13Bii, the mutant channels also caused peak I_{hERG} to occur significantly earlier during repolarisation (-17.5 ± 3.5mV; n=7; $p<0.001$). In summary, these data show that the I560T mutation increased I_{hERG} in response to APs from all cell types investigated. This occurred in a relatively proportional manner during all

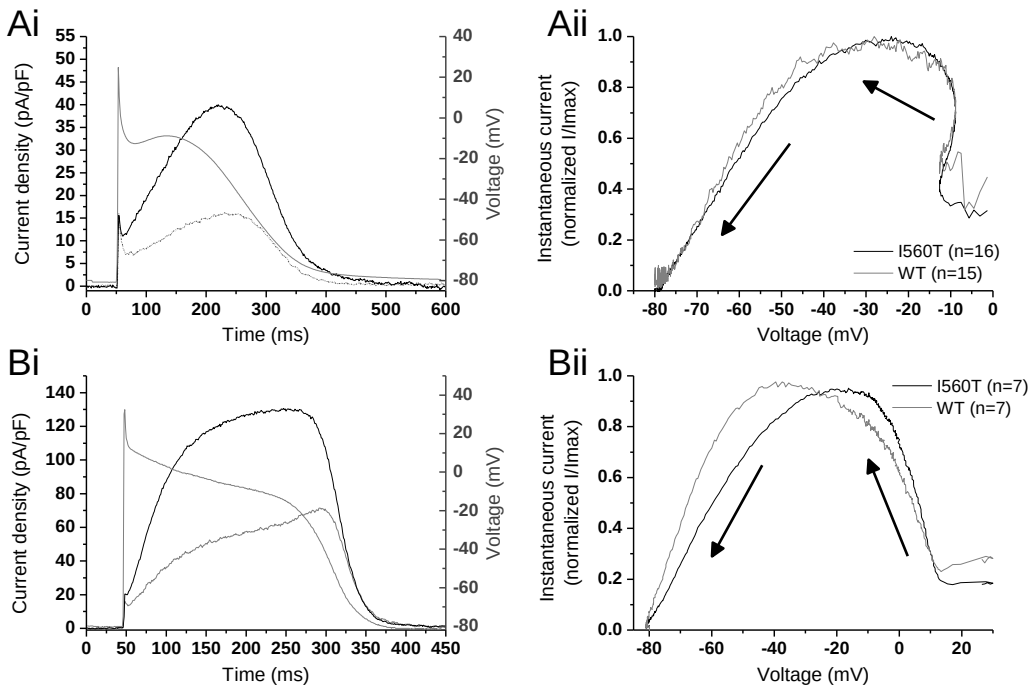

Figure 13: WT and I560T-I_{hERG} response to atrial and Purkinje fibre APs. **(Ai)** Mean profile of WT and I560T I_{hERG} during atrial AP. **(Aii)** Mean I-V relations recorded during repolarisation in an atrial AP. **(Bi)** Mean profile of WT and I560T I_{hERG} during Purkinje fibre AP. **(Bii)** Mean I-V relations during Purkinje fibre AP. For all figures, WT I_{hERG} is shown in grey whilst I560T I_{hERG} is in black. For (Ai and Bi), current was normalised to capacitance reflecting cell membrane surface area. For (Aii and Bii) the arrows represent the direction of repolarisation and current was normalised to the maximal current recorded during the protocol for each cell, with these values used to establish mean current at each given voltage.

APs, and therefore the ratio of total I_{hERG} was little different between AP types (Figure 14A, B). In addition to this, peak I_{hERG} occurred earlier during repolarisation only in response to ventricular and PF APs.

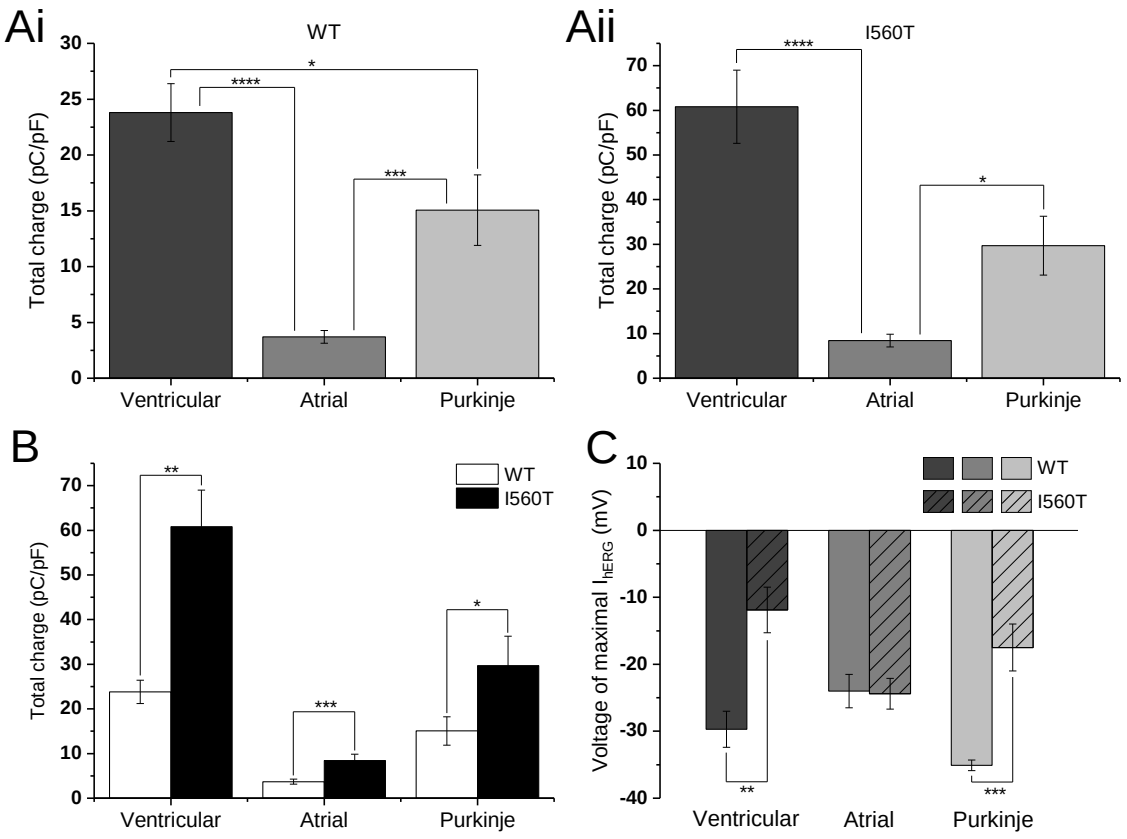

Figure 14: Comparison of WT and I560T-I_{hERG} density and timing during ventricular, atrial and PF APs. **(A)** Comparison of total charge passed during different AP conditions in WT (i) and I560T (ii) hERG-expressing cells. **(B)** Comparison of total WT and I560T I_{hERG} during each AP. For both of (A, B), total charge was calculated by integrating current traces normalized to cell capacitance. **(C)** Mean voltage at which peak I_{hERG} occurred during each AP for WT and I560T channels. In all figures, as above, for WT n=5, 15 and 7 and for I560T data n=19, 16 and 7 for ventricular, atrial and PF APs respectively.

3.2.3 Response of I560T-hERG to quinidine and sotalol

3.2.3.1 Response of WT and I560T-hERG to quinidine

The response of I_{hERG} to quinidine and sotalol was measured using a standard step protocol used in previous studies from this laboratory (e.g. McPate et al., 2008, Zhang et al., 2011, El Harchi et al., 2012). This was comprised of a 2 second depolarising command to 20mV followed by a 4 second repolarising command to -40mV, followed by a return to the -80mV holding potential (lower panels of Figure 15A). A 12 second start-to-start interval was used, with superfusion of drug occurring until I_{hERG} reached a steady state.

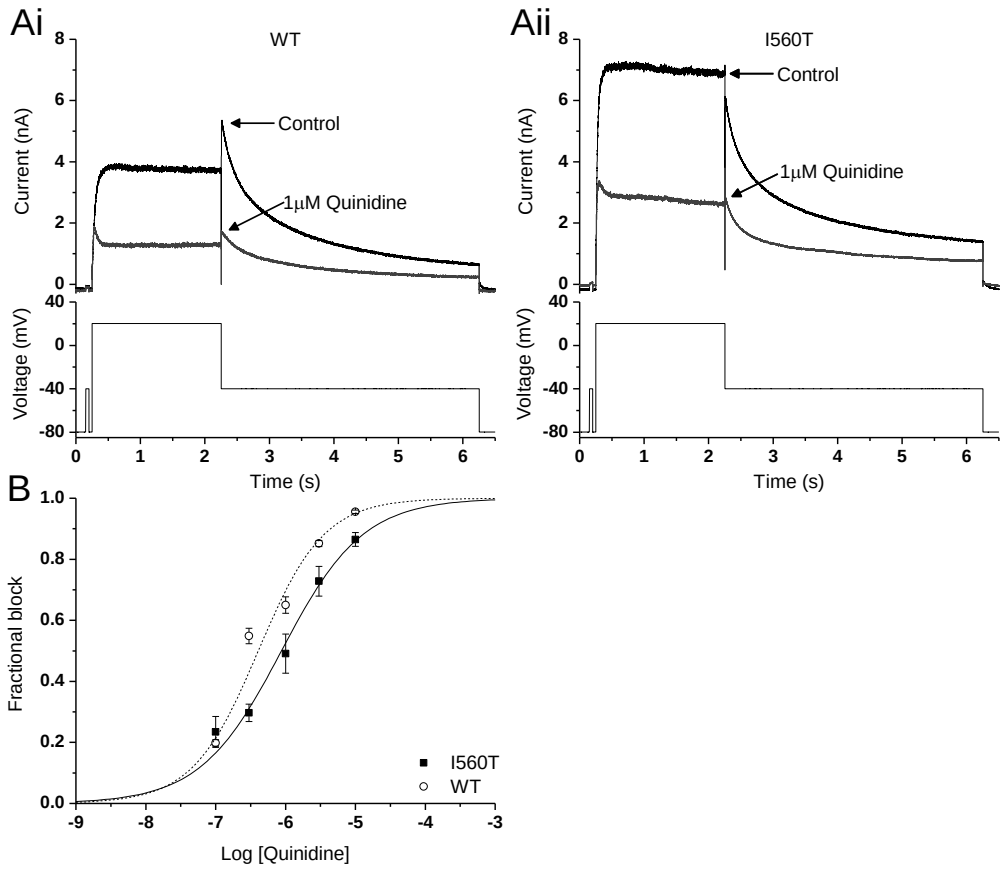

Figure 15: Inhibition of WT and I560T-I_{hERG} by quinidine. **(A)** Representative traces of WT (i) and I560T (ii) I_{hERG} in the absence (black) and presence (grey) of 1μM quinidine. **(B)** Concentration-response relations for inhibition of WT and mutant $I_{hERG,}$ with fractional block calculated using Equation 6. A minimum of 5 cells were used for each concentration of drug.

The class Ia antiarrhythmic quinidine has been shown to prolong the QT interval in SQTS patients (Gaita et al., 2004, Wolpert et al., 2005) and inhibit I_{kr} *in vitro* (Paul et al., 2002, Wolpert et al., 2005), whilst its binding is only modestly altered by the attenuation of inactivation (Lees-Miller et al., 2000a, McPate et al., 2006, McPate et al., 2008). Consequently, its effectiveness in inhibiting I560T I_{hERG} has been evaluated in this work. The upper panels of Figure 15A show representative traces of WT and I560T I_{hERG} in the absence (black) and presence (grey) of 1μM quinidine, with the application of quinidine clearly reducing I_{hERG} throughout the protocol for both WT and mutant cells. Plotting I_{hERG} tail currents in response to 0.1-10μM quinidine (Figure 15B; Equation 7) established a half-maximal inhibitory concentration (IC_{50}) 2.3-fold larger for I560T I_{hERG} than that of the WT (0.88 ± 0.14μM for I560T vs. 0.38 ± 0.03μM for WT; $p<0.01$), with derived *h* values of 0.86 ± 0.06 (WT) and 0.7 ± 0.09 (I560T; $p>0.05$).

3.2.3.2 Response of WT and I560T-hERG to sotalol

In contrast to quinidine, binding of the class III antiarrhythmic sotalol to hERG has been shown as heavily dependent upon inactivation gating (Numaguchi et al., 2000, Brugada et al., 2004, Wolpert et al., 2005), and so its evaluation in parallel to quinidine may aid understanding of the mutation's effects on relatively well understood drug binding mechanisms as well as providing insight into the potential therapeutic benefits of the drug. The upper panels of Figure 16A shows representative traces of WT and I560T I_{hERG} in the absence (black) and presence (grey) of 100μM sotalol. Plotting I_{hERG} tail currents in response to 1-1000μM sotalol (Figure 16) shows no significant difference in IC_{50} between the WT and mutant channels (135.6 ± 47.4 for WT vs. 88.74 ± 35.3 for I560T; $p>0.05$; Equation 7), and also no significant difference in *h* values (0.49 ± 0.08 for WT vs. 0.35 ± 0.06 for I560T; $p>0.05$).

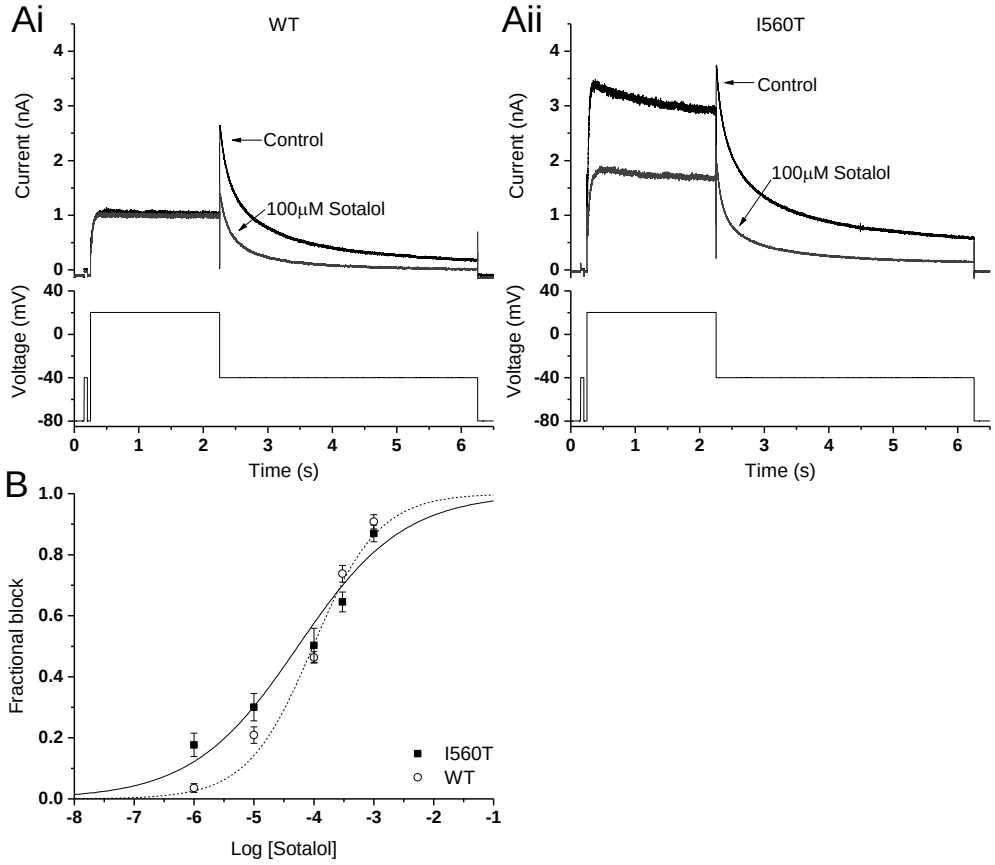

Figure 16: Inhibition of WT and I560T-I_{hERG} by sotalol. **(A)** Representative traces of WT (i) and I560T (ii) I_{hERG} in the absence (black) and presence (grey) of 100μM sotalol. **(B)** Concentration-response relations for inhibition of WT and mutant $I_{hERG,}$ with fractional block calculated using Equation 6. A minimum of 5 cells were used for each concentration of drug.

	WT IC_{50} (μM)	**I560T IC_{50} (μM)**	**WT *h***	**I560T *h***
Quinidine	0.38 ± 0.03	0.88 ± 0.14 **(p<0.01)**	0.86 ± 0.06	0.7 ± 0.09
Sotalol	135.6 ± 47.4	88.74 ± 35.3 (p>0.05)	0.49 ± 0.08	0.35 ± 0.06

Table 2: Summary of WT and I560T-hERG response to quinidine and sotalol.

3.3 Summary I560T data

Property	WT	I560T	Significance
I_{hERG} properties during voltage clamp			
Current density at 20mV (pA/pF)	132.1 ± 26.5 (n=8)	298.8 ± 60.9 (n=17)	**p<0.001**
$V_{0.5\ (activation)}$ (mV)	-21.07 ± 1.29 (n=8)	-21.43 ± 1.41 (n=17)	p>0.05
k (activation, mV)	6.61 ± 0.15 (n=8)	12.55 ± 2.14 (n=17)	**p<0.01**
Activation time constant (ms)	65.4 ± 3.5 (n=5)	19.6 ± 1.7 (n=7)	**p<0.0001**
E_{rev} (mV)	-85.05 ± 0.53 (n=5)	-80.34 ± 1.4 (n=11)	**p<0.05**
Time constant for recovery from inactivation (ms)	1.84 ± 0.08 (n=10)	2.05 ± 0.17 (n=18)	p>0.05
$V_{0.5\ (inactivation)}$ (mV)	-66.25 ± 1.91 (n=6)	-41.79 ± 3.47 (n=13)	**p<0.001**
k (inactivation, mV)	-20.15 ± 0.62 (n=6)	-25.31 ± 1.22 (n=13)	**p<0.05**
Time constant (ms)	2.31 ± 0.17 (n=6)	4.72 ± 0.36 (n=13)	**p<0.001**
Voltage of maximal I_{hERG} during AP clamp			
Ventricular AP (mV)	-29.7 ± 2.7 (n=5)	-11.9 ± 3.4 (n=19)	**p<0.05**
Atrial AP (mV)	-24.0 ± 2.5 (n=15)	-24.4 ± 2.3 (n=16)	p>0.05
Purkinje fibre AP (mV)	-35.1 ± 0.8 (n=7)	-17.5 ± 3.5 (n=7)	**p<0.001**
Current integral during AP clamp			
Ventricular AP (pC/pF)	23.8 ± 2.6 (n=5)	60.8 ± 8.2 (n=19)	**p<0.01**
Atrial AP (pC/pF)	3.7 ± 0.6 (n=15)	8.4 ± 1.4 (n=16)	**p<0.001**
Purkinje fibre AP (pC/pF)	15.1 ± 3.2 (n=7)	29.7 ± 6.6 (n=7)	**p<0.05**

Table 3: Summary of collected data for WT and I560T-hERG.

3.4 Discussion

3.4.1 Effects of the I560T mutation on hERG properties

Although a partial electrophysiological characterisation of I560T I_{hERG} has been previously published (Harrell et al., 2015), this study provides a more complete evaluation of the mutation's effects, describing for the first time for I560T-hERG: the time-dependence of activation; the fully activated I-V relation; ion selectivity; deactivation rates; the rate of recovery from inactivation; the time course of inactivation; and the current timing and voltage dependence (I-V relations) during cardiac action potentials. In addition, the pharmacological information on quinidine and sotalol is novel.

Where direct comparison is possible, the results presented here are generally in agreement with those published previously, with a comparative increase in current density (I560T I_{hERG} 2.3-fold larger than that of WT in my work, 2.5-fold previously; Figure 6B) and no change in the half maximal voltage of activation seen in either study (Figure 6C; Harrell et al., 2015). My work, however, has shown a greater positive shift in inactivation $V_{0.5}$ (~24mV vs. ~14mV; Figure 9C). Both investigations were performed at 37°C using similar recording solutions and techniques, with the only major difference in methods being in the use of a COS-7 cell line in the original work by Harrell et al. (2015). It is possible that this difference is related to unknown, natively expressed co-assembling proteins; proteins involved with post-translational modification of hERG; or proteins associated with biogenesis and assembly which exist to varying extents in different cell lines (Vandenberg et al., 2012, Li et al., 2017), but exact determination of the variation is outside the scope of this work. Despite the larger shift in inactivation demonstrated by my work, the recorded $V_{0.5, (inactivation)}$ published by Harrell et al. (2015) is significantly (~29mV) more positive than my own findings. Similarly, their $V_{0.5, (inactivation)}$ for WT-hERG, was also dramatically shifted compared to established literature from this and other laboratories (Zou et al., 1998, McPate et al., 2005, Vandenberg et al., 2006, Zhang et al., 2011, Harrell et al., 2015), and consequently it is possible that the shift in inactivation caused by the I560T mutation was previously underestimated. Irrespective of

these differences, the positively shifted $V_{0.5\ (inactivation)}$, alongside the change seen in slope (*k*) value, results in considerably less I_{hERG} inactivation occurring across the majority of physiological voltages (Figure 9C), including those at which AP plateaus occur. As has been described in studies of other mutations which attenuate inactivation, the resulting increase in I_{hERG} will drive repolarisation and QT interval shortening (McPate et al., 2005, McPate et al., 2009a).

In addition to changes in the voltage dependence of inactivation, conventional voltage clamp demonstrated more widespread effects of the I560T mutation on gating properties of hERG, with changes in the rate of activation, deactivation and inactivation all seen. The faster time course of activation (Figure 7) would lead to increased I_{hERG} activation at a very early stage of an AP, however it is also notable that the time course is still significantly slower than that of the development of inactivation presented in this study (Figure 9D). The differences in voltage during the relevant protocols makes the exact time courses difficult to compare, but the decreased speed in the development of inactivation demonstrated by my work (Figure 9D) combined with this increase in rate of activation are anticipated to contribute to increased I_{hERG}.

A slower rate of deactivation has been shown as the primary mechanism through which R1135H-hERG causes SQT1 (Itoh et al., 2009), with this being demonstrated using *in silico* simulations as sufficient to abbreviate the QT interval clinically (Wilders and Verkerk, 2010). Similarly, a faster time course of deactivation has been shown to cause LQTS (Chen et al., 1999). Although the I560T mutation only causes a modest decrease in the rate of deactivation at some voltages (Figure 8B, C), the increase in I_{hERG} that this causes may contribute to some extent to the abbreviation of the QT interval. Despite this QT shortening, these slowed rates of deactivation may be in fact confer protection against arrhythmia, as the residual I_{hERG} could be protective against subsequent premature stimulation (See Figure 4C). Thus, the I560T mutation may confer some protection against re-entrant circuits (Lu et al., 2001, Du et al., 2010).

With hERG's inactivation being dependent upon collapse of the selectivity filter (Liu et al., 1996, Hoshi and Armstrong, 2013), it is perhaps no surprise that mutations affecting inactivation also commonly cause changes in E_{rev} and ion permeability (Jiang et al., 2005, Vandenberg et al., 2012). This is in agreement with previous data showing the hERG S5 mutation, L532P, to cause a similar shift in inactivation $V_{0.5}$ (+32mV) accompanied by an identical ~1.6-fold increase in Na^+:K^+ permeability ratio (Zhang et al., 2011) and the larger shift in inactivation caused by N588K (+90mV) to link to a ~2.7-fold increase in Na^+:K^+ permeability ratio (McPate et al., 2005). Despite these associations, the separate processes of inactivation gating and ion selectivity mean that this effect has not been described for all mutations (Fan et al., 1999, Sun et al., 2011), but mutations to a range of further residues involved in inactivation gating in the S5-P linker have also been shown to influence K^+ selectivity (Jiang et al., 2005, Tseng, 2006), and the differences in impact on ion selectivity are at least partially a consequence of the direction in which the residues face within the α-helices (Liu et al., 2002). Similarly, mutations within the selectivity filter itself have been shown to affect selectivity to different extents (Lees-Miller et al., 2000b, Sun et al., 2011). In work that linked residues more distal to the selectivity filter to ion selectivity, K^+ selectivity was shown to be dependent upon interactions between the selectivity filter and S5 through energetic linkage of given residues (Perry et al., 2015), and so my work is in agreement with previous work suggesting that both S5 residues, and those which attenuate inactivation can also affect ion selectivity.

The increased current seen across a wide range of physiologically relevant voltages (Figure 6B) and during ventricular, atrial and Purkinje fibre AP commands (Figure 12A & Figure 13Ai, Bi) constitute compelling evidence of how I560T I_{hERG} can accelerate repolarization and drive a reduction in QTc interval. This larger current passed during repolarisation by the channels in both upper and lower cardiac chambers as well as throughout the Purkinje fibres would shorten phases two and three of the AP, lowering the membrane potential more quickly and activating I_{k1} sooner to re-establish the resting potential; and this would be

further reinforced by the earlier timing of peak I_{hERG} during ventricular and PF APs (Figure 12B, Figure 13Aii, Bii). As QTc interval has a direct relationship with the effective refractory period (ERP), which is vital in the protection of cardiac tissues against fibrillation (Gaita et al., 2003), it is reasonable to conclude that that mutation-driven shortening of the QTc interval could predispose to arrhythmogenesis by abbreviating refractoriness (expanded upon below in Section 3.4.3). To summarise: the data obtained show that the I560T mutation affects a range of hERG properties, each of which contribute to increased I_{hERG} and augmentation of I_{hERG} timing to varying extents during cardiac action potentials. In turn, these alterations likely contribute to the abbreviation of the QT interval, predisposing the patient to arrhythmia.

3.4.2 Structural context of the I560T mutation

The underlying structural mechanism(s) by which the I560T mutation causes these changes in I_{hERG} kinetics are currently unclear and this has not been helped by the lack of a detailed hERG structure, with previous structural inferences depending on the use of homology modelling (Lees-Miller et al., 2009, Perry et al., 2010, Zhang et al., 2011, Cavalli et al., 2012, Durdagi et al., 2012, Perry et al., 2013b, Melgari et al., 2015, Saxena et al., 2016, Wang et al., 2016, Phan et al., 2017). Recently, however, the first cryo-electron microscopy (cryo-EM) structure of hERG was published using an open pore, activated (depolarised) conformation (Wang and MacKinnon, 2017). Using this structure (Figure 3B, Figure 17A), it can be seen that the I560 side chain faces membrane lipids, with a distance too great to suggest direct interaction with other residues in the S5 domain; adjacent S6 domain or the opposing S4 domain. The notion that I560 does not interact directly with the voltage sensing domain is further supported by mapping the residues to a closed pore rEAG structure with a high level of homology to hERG (Whicher and MacKinnon, 2016). As can be seen in Figure 17, modelling I560 using both the new Cryo-EM structure and the rEAG structure which has been used in hERG analysis previously (de la Peña et al., 2018, Helliwell et al., 2018,

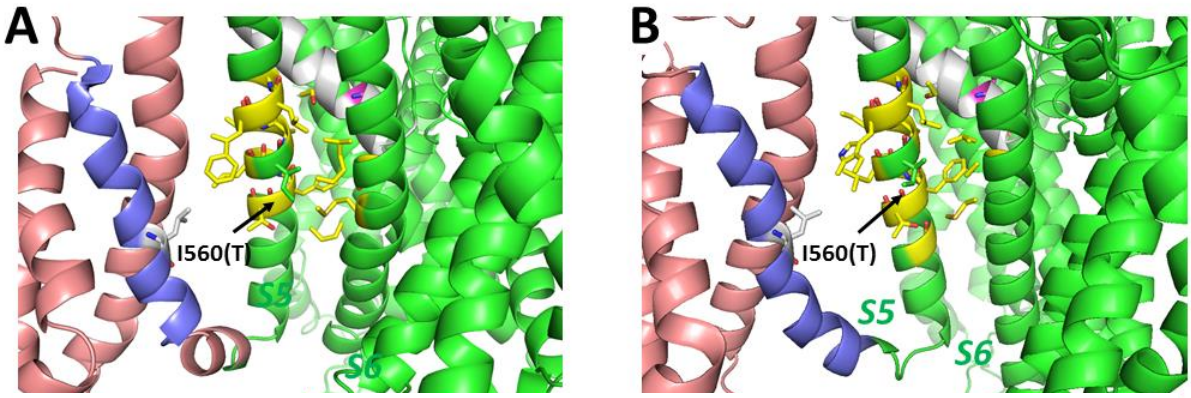

Figure 17: Structural context of the I560 residue. **(A)** Construct of hERG built using the recent cryo-EM structure (Wang and MacKinnon, 2017). **(B)** hERG model built on rEAG cryo-EM structure (Whicher and MacKinnon, 2016). In both, residues near I560 (within 7Å) are highlighted in yellow, but the distance between these and I560 is still too great for direct interactions. Provided by Dr Christopher Dempsey (University of Bristol).

Perissinotti et al., 2018) shows highly comparable results, with the residue facing membrane lipids under both conditions.

A separate study investigated 'energetic coupling' between S4 and S5 residues by introducing double mutations and establishing whether their effects on inactivation were additive or overlapping (Perry et al., 2013b). This work showed a coupling between I560 and hydrophobic residues involved in the voltage sensing of inactivation on the S4 domain (L529 and V535). In the context of another homology model (Kv1.2/2.1 chimera; Long et al, 2007) the distance between I560 and S4 residues was stated to be too large for a direct interaction, supporting findings from the more recent models. The energetic coupling data however, suggests an allosteric effect on S4 possibly via modulation of interactions with the lipid membrane, and this represents a potential mechanism for the attenuation of inactivation caused by the I560T mutation. One possible explanation, which is consistent with the S4/S5 energetic coupling data, as well as the data described above which highlighted coupling between the selectivity filter and S5 (Perry et al., 2015), is that of threonine induced bending of transmembrane α-helices. It is well documented that rather than interact with lipid chains, the polar sidechains of both serine and threonine preferentially form hydrogen bonds with amino acid residues three or four residues closer to the N-terminal than themselves

(Ballesteros et al., 2000, del Val, 2012, Xu et al., 2016). Consequently, the isoleucine to threonine substitution may facilitate the formation of a hydrogen bond between T560 and T556 or F557 in hERG and would increase the bending angle of the helix. This will alter the way in which a number of local amino acids could interact with multiple key hERG structures, potentially affecting interactions between S5 and the S4 regions responsible for both activation and inactivation gating (Perry et al., 2013b) as well as with the pore domain (Lees-Miller et al., 2009, Perry et al., 2015). This is supported by the cryo-EM structure and the tight 'knobs-into-holes' packing (steric contacts occurring between complimentary helices; Eilers et al. (2002)) it shows between residues on the pore helix (including T618) and the nearby A651 and A656 (Figure 18A). Even minor perturbation of these interactions as may be caused by the amino acid substitution and the possible induction of helices bending and it is likely that this will influence channel gating and ion selectivity considering the critical role the pore helix has in channel function (Hancox et al., 1998b, Lees-Miller et al., 2009, Perry et al., 2013a). The cryo-EM structure also highlights a region of S1 which interacts with the pore helix and S5 (Figure 18B), and it is possible that an alteration to this interaction may have further effects for activation, inactivation and deactivation gating (Zhang et al., 2005, Colenso et al., 2013, Phan et al., 2017).

Although the pursuit of a complete structural basis for the mechanisms by which the I560T mutation interferes with the biophysical properties of hERG is outside the scope of my work, the current literature provides potential mechanisms by which the diverse effects found in my study could be caused. Although this is aided by the recently published Cryo-EM structure and more widely used homology models, hERG's range of gated states mean that more work needs to be done to capture accurately the arrangement of hERG in order to understand mutations in the context of its different conformational states.

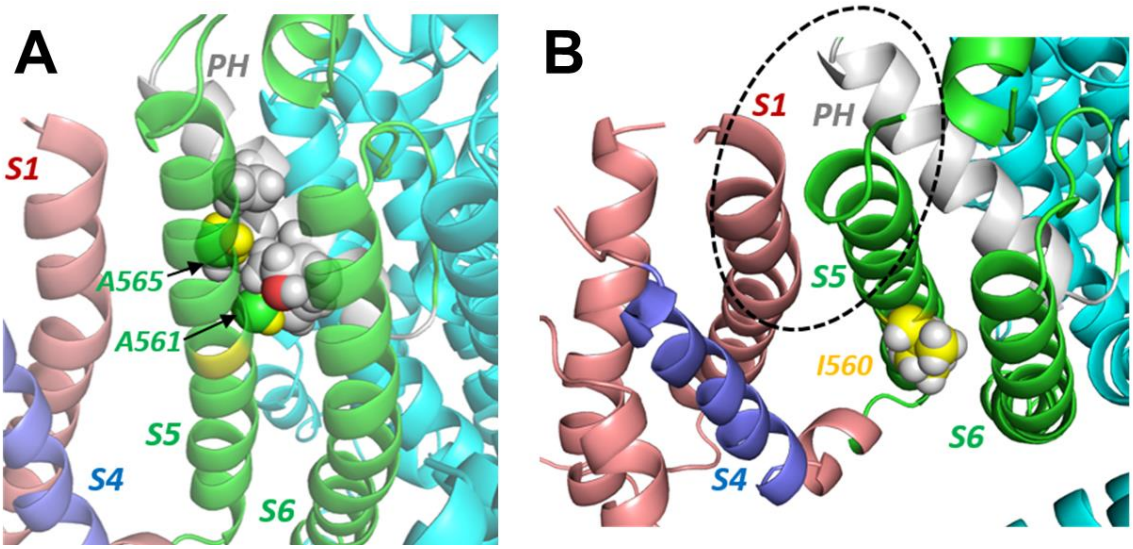

Figure 18: S5 interactions which may be perturbed by the I560T mutation. **(A)** The residue adjacent and one further helical turn from I560 (A561 and A565) tightly pack with complementary pore helices, forming interactions with A614, L615, T618 and F619 **(B)** The I560 residue cannot interact with S4 of the VSD, but the extracellular half of the S5 helix can interact with both S1 and the pore helix through interactions occurring within the dotted circle (side chains not shown). For both figures, constructs were built using the recent cryo-EM structure (Wang and MacKinnon, 2017) and provided by Dr Christopher Dempsey (University of Bristol).

3.4.3 Mechanisms of arrhythmogenesis

The proband in the initial work by Harrell et al. (2015) suffered from palpitations and near syncope triggered by paroxysmal atrial fibrillation (AF) and atrial flutter which was treated using catheter ablation (CA). Following this, a QTc interval of 319ms was recorded, but there is no report of the measured QTc interval prior to CA or the timespan over which this developed and so it is not possible to describe the degree of shortening caused by the CA. This is further complicated by case reports in which catheter CA has been successfully used to treat SQTS (Pavão et al., 2014) and LQTS has been triggered by CA (Mantziari et al., 2011). To my best knowledge, this the only patient described in the literature to have SQTS defined following CA, and so it is possible that either the onset is an unfortunate and rare consequence of the difficulties in understanding and detecting ablation targets (Dharmaprani et al., 2018, Jansen et al., 2018) combined with the I560T mutation increasing propensity for

arrhythmia; or that the presenting AF caused by the I560T mutation resulted in difficulties in accurately measuring the QT interval prior to ablation. Regardless, this increase in susceptibility to arrhythmia is reinforced by the sudden death of the proband's brother and father (Harrell et al., 2015). Interestingly, studies have however shown AF patients with a shorter QTc interval to have reduced recurrent episodes of AF following CA compared to those with a longer QTc interval, although it must be noted that the lowest QTc interval in these were still higher than that of the I560T-hERG patient (Liu et al., 2015, Ma et al., 2016).

As described, the increased current density carried by I560T-I_{hERG} will accelerate repolarisation and shorten the APD and the ERP (McPate et al., 2005, Rudic et al., 2014, Hancox et al., 2018). In turn, this causes a decrease in excitation wavelength which supports the formation of re-entry circuits and re-entrant arrhythmias. The transmural dispersion of repolarisation, that is the extent of difference between the maximal and minimal duration of repolarisation throughout the cardiac wall (Sicouri et al., 2010), has also been shown to be increased in SQTS as differences in ionic conductance across tissue layers or cell types can be accentuated by mutations (Elming et al., 1998, Okin et al., 2000, Bjerregaard et al., 2006, Hancox et al., 2018), and this further increases the susceptibility to re-entry. These re-entrant circuits lead to the formation of spiral waves which circulate around an arrhythmogenic substrate and cause the atrial or ventricular fibrillation (VF) symptomatic of SQTS (Cerrone et al., 2006).

In silico modelling by Harrell et al. (2015) which used their established properties of I560T-hERG for the induction of I_{Kr} in the left ventricular wall model calculated an abbreviated QT interval of 287ms as compared with 388ms in their WT simulations. Application of a protocol modelling VF through simulation of a premature stimuli showed WT I_{Kr} to cause immediate termination of spiral waveforms, whereas the alteration in kinetics seen in I560T-hERG resulted in sustained spiral wave rotation which would be expected to cause severe VF clinically. The proband was never recorded as suffering VF, but the results are consistent with the sudden death experienced by the probands brother and father. No *in silico*

simulations investigating the atrial consequences of the I560T mutation to increase understanding of the atrial symptoms suffered by the patient have been performed, and so the differences seen during my atrial AP clamp work (Figure 13A) are key for understanding the patient's symptoms. The more than doubling of I_{hERG} caused by the I560T mutation will certainly drive repolarisation and facilitate circuit re-entry in the atria in addition to the ventricles. Further modelling must be done using atrial conditions to increase understanding of the effects of the I560T mutation, and in addition to this, the more detailed properties of I_{hERG} found by my work should be applied to ventricular *in silico* modelling to demonstrate further the arrhythmogenic properties of the mutation.

Previous comparable work on N588K-hERG showed the mutation to augment the difference in peak current between the waveforms of different tissue types significantly. Whilst WT ventricular I_{hERG} was 2.9-fold greater than that of atrial I_{hERG} and 1.7-fold greater than that of PF I_{hERG}, the N588K mutation augmented ventricular I_{hERG} to 6.6-fold that of atrial and 2.6-fold that of WT, showing the mutation to affect current during each waveform to differing extents, contributing to the development of heterogeneity during repolarisation (McPate et al., 2009a). This work, however, has shown that the more modest nature of the I560T mutation causes total I_{hERG} to be augmented to a similar extent across all waveforms (Figure 14), and so the aforementioned *in silico* work will be also useful in understanding the differences in arrhythmogenesis between a mutation which severely attenuates inactivation and this more modest mutation.

3.4.4 Response of I560T-hERG to quinidine and sotalol

This study is the first to investigate the effects of the I560T mutation on sensitivity of I_{hERG} to antiarrhythmic drugs. Quinidine and sotalol were chosen due to their known I_{Kr} blocking properties and prior use in the treatment of SQT1 (Wolpert et al., 2005, McPate et al., 2008, Hu et al., 2017, Hancox et al., 2018). Additionally, much is known about the binding

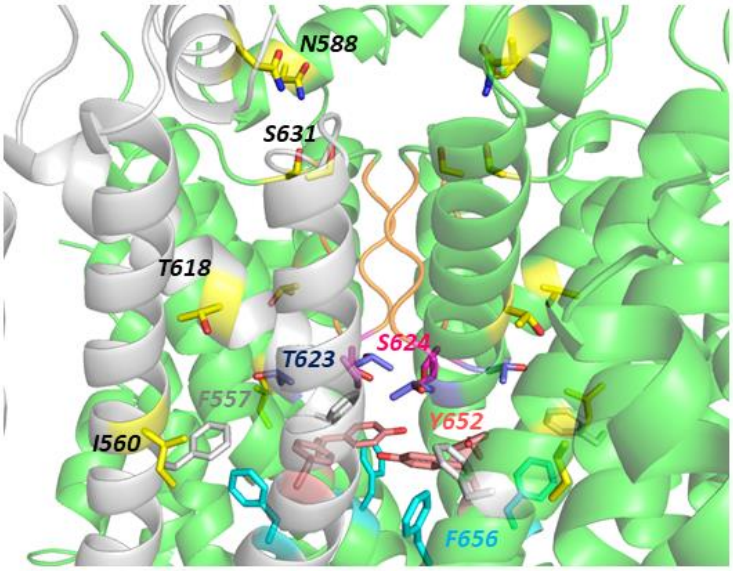

Figure 19: Pore region of the hERG channel with key drug binding residues highlighted on each protein. Discussed residues associated with SQTS are also shown. Construct built using the recent cryo-EM structure (Wang and MacKinnon, 2017) and provided by Dr Christopher Dempsey (University of Bristol).

properties of both drugs and so they make an excellent comparative tool for probing the way in which the I560T mutation affects key mechanisms of drug binding to hERG.

Site directed mutagenesis work on a range of structurally diverse drugs has highlighted two residues, Y652 and F656 (see Figure 19), to be consistently vital for high affinity drug binding (Mitcheson et al., 2000, Perry et al., 2004, Kamiya et al., 2006, Duan et al., 2007, Jo et al., 2008, Zhang et al., 2016), and separate studies showed mutation of these residues to reduce quinidine potency by at least 30-fold (Lees-Miller et al., 2000a, Sanchez-Chapula et al., 2003). These sites lie within the S6 helix which lines the K^+ conduction pathway and so drug binding is proposed to occur commonly below the selectivity filter (Helliwell et al., 2018). For some drugs, including methanesulphonanilide class III antiarrhythmics such as sotalol, inactivation gating has also been shown as a key in stabilising drug binding, and this has been demonstrated using mutations shown to attenuate inactivation (Lees-Miller et al., 2000a, Ficker et al., 2001, McPate et al., 2008, Perrin et al., 2008, Du et al., 2014, Zhang et al., 2016, Helliwell et al., 2018). This occurs as the process of inactivation gating is believed to involve rotation of the S6 helices, and this leaves key residues facing into a more

favourable direction for binding to certain drugs (Chen et al., 2002, Helliwell et al., 2018). Consequently, perturbations to inactivation affect drugs to varying extents, with studies showing the IC_{50} of quinidine to increase only 3.5-5.8-fold in response to the S631A or N588K mutations (Lees-Miller et al., 2000a, Wolpert et al., 2005, McPate et al., 2008). These known properties of quinidine agree well with my finding of a modest, 2.3-fold increase in IC_{50} caused by the I560T mutation's moderate effects on inactivation (Figure 15).

A recent study also highlighted the importance of the S5 residue F557 (see Figure 19) in drug binding (Saxena et al., 2016). A range of structurally diverse hERG blockers (not including quinidine) were applied, showing the mutation of F557 to have an effect comparable to that of Y652 mutations. This is interesting in the case of the I560T mutation due to the aforementioned potential for threonine-induced bending of the S5 helix (see Section 3.4.2). If this bending is occurring then it will involve T560 bonding either with F557 itself or the adjacent T556, which is likely to affect the positioning and availability of F557 through either direct or allosteric modulation. Consequently, it is feasible that both this mechanism and the reduced inactivation gating have a modest effect on binding which both contribute to the increased IC_{50} of quinidine.

The N588K mutation causes a larger shift in the IC_{50} of quinidine during patch-clamp experiments than does the I560T mutation, with a reported IC_{50} of 3.5-4.35μM (Wolpert et al., 2005, McPate et al., 2008). Despite this being higher than the mean serum concentration measured in patients during a standard regime involving an oral quinidine dosage of 1000mg/day (~2.9μM; Schimpf et al., 2007), the drug still retains effectiveness clinically (Wolpert et al., 2005, Giustetto et al., 2015). N588K patients receiving oral administration of quinidine show a prolongation of the QT interval and of the ERP as a result of treatment; and dosage also rendered VF non-inducible for patients in whom it had been inducible (Gaita et al., 2004, Giustetto et al., 2006, Giustetto et al., 2015). As the IC_{50} of quinidine for I560T-hERG is lower than both that reported for N588K and the plasma concentration of the drug,

it is more than likely that the increased IC_{50} caused by the mutation is not sufficient to disrupt quinidine's therapeutic properties.

In prior work, sotalol binding has been shown as highly dependent upon inactivation gating, with attenuation of this causing a 20-fold increase in IC_{50} (Brugada et al., 2004). Consequently, it was anticipated that the attenuation in inactivation caused by the I560T mutation would lead to a larger reduction in affinity for sotalol than quinidine, possibly akin to the T618I mutation which caused a +25mV shift in inactivation associated with a 3.2-fold increase in IC_{50} of sotalol and only a 1.4-fold increase in IC_{50} of quinidine using comparable experiments (El Harchi et al., 2012). This however, was a contrast to the results produced, with the I560T mutation causing no change in binding to sotalol (Figure 16). The reasoning behind these differences is unclear. The more modest effect of the I560T mutation on inactivation compared with other mutations used in study of sotalol (Numaguchi et al., 2000, Brugada et al., 2004, Perrin et al., 2008) likely contributes to the reduced effect on binding, and the differences between T618I and I560T-hERG may be attributed to the more distal location of the mutation compared to the channel pore.

In vitro, sotalol was also shown as an effective hERG blocker and a strong candidate for use in patients with the T618I mutation, with no more than a 1.7-fold increase in IC_{50} caused by the mutation under AP clamp conditions (Sun et al., 2011, El Harchi et al., 2012). However subsequent *in vivo* work has shown sotalol not to prolong the QTc interval or to reduce susceptibility to ventricular arrhythmias (Giustetto et al., 2015, Hu et al., 2017). Although quinidine also failed to prevent arrhythmias in some T618I cases, it was successful in prolonging QT interval and has in general been seen as the most effective treatment for SQT1 (Giustetto et al., 2015, Hu et al., 2017, Hancox et al., 2018). Despite my work showing I560T to have a lesser effect on sotalol binding compared to that of quinidine, I believe that suggesting quinidine supplementation for the identified I560T patient would be more appropriate due to a combination of the retained effectiveness of the drug in N588K patients and the history of use in SQT1 patients (Gaita et al., 2004, Wolpert et al., 2005, Giustetto et

al., 2006, Giustetto et al., 2015). The limited availability of quinidine in many countries, however, means that it may not be a possible therapeutic option, with one 2013 study showing it only as 'readily available' in 14% of countries (Viskin et al., 2013b, Mazzanti et al., 2017a). Consequently, the proof of retention of binding to sotalol may also be of value clinically.

3.5 Conclusion

The I560T mutation produces a range of effects on hERG properties, with the increase in current density and the positive shift in the voltage dependence of inactivation being the most consequential. These changes are expected to increase I_{Kr} during cardiac action potentials and shift the timing of the current during the during the PF and ventricular APs which elicit the highest levels of I_{hERG}. As a result, AP repolarisation and therefore QT interval and the ERP will be accelerated, increasing susceptibility to arrhythmia. Despite the alteration to I_{hERG} kinetics, there is relatively little change in the binding properties of quinidine and no change in the affinity of sotalol. While both may offer an effective therapeutic option, the clinical history of quinidine usage suggests it may be of most value in cases of I560T-induced SQT1.

Chapter 4 Effects of the S631A hERG mutation in the context of SQTS

4.1 Introduction

The use of the S631A hERG mutation within the laboratory predates the identification of SQTS as a clinical entity, with the first work published in 1996 (Schonherr and Heinemann, 1996). S631 in hERG corresponds to a pore residue (T449) which was previously shown to be critical for inactivation in *Shaker* B channels (Lopez-Barneo et al., 1993); and in the non-inactivating rat and drosophila EAG channels an alanine rather than serine is present at position 631 (Warmke et al., 1991, Ludwig et al., 1994). Consequently, Schonherr and Heinemann (1996) created the S631A mutation to investigate its effects on hERG channel gating, showing the mutation to eliminate inactivation under their conditions. Subsequent work has shown that inactivation is not removed, but is markedly positively shifted, resulting in a reduction in current rectification at positive voltages (Hancox et al., 1998b, Zou et al., 1998, Fan et al., 1999, McPate et al., 2008). The mutation has also been shown to have no significant effect channel activation (Schonherr and Heinemann, 1996, Zou et al., 1998, Fan et al., 1999, McPate et al., 2008) or ion selectivity (Fan et al., 1999) and its use has helped to demonstrate the critical role of hERG inactivation during the ventricular AP (Hancox et al., 1998b). Furthermore, a number of pharmacological studies have used the mutation to investigate the effects of the attenuation of inactivation on drug binding (Lees-Miller et al., 2000a, Paul et al., 2001, Weerapura et al., 2002a, McPate et al., 2008).

The identification of a patient expressing S631A-hERG, over 20 years after the initial study of the mutation, represented the first observation of an SQTS mutation with an effect on inactivation as profound as that seen for the N588K mutation (McPate et al., 2005, Akdis et al., 2017, Hancox et al., 2018). A female proband, who's most recent QTc interval was 323ms, had a father and sister who presented with QTc intervals of 324ms and 340ms respectively; and an aunt and two cousins died suddenly of unreported causes. Although the S631A mutation was identified in all three family members with shortened QTc intervals, a

lack of further symptoms resulted in no treatment being received by the family members, whilst the proband herself received an ICD which has not triggered since implantation (Akdis et al., 2017).

Some existing hERG literature describes the comparable nature of the effects of the N588K and S631A mutations, with similarities being drawn between the mutations' effects on the voltage dependence of activation and inactivation as well as upon retention of drug binding (Schonherr and Heinemann, 1996, Zou et al., 1998, Fan et al., 1999, Paul et al., 2001, Cordeiro et al., 2005, McPate et al., 2005, McPate et al., 2008). Now that the mutation has been identified clinically, the aim of the study comprising this chapter was to supplement the current literature and provide data on how the S631A mutation affects I_{hERG} during APs from different cardiac regions. It is predicted that further similarities with N588K may be found, with previous work showing profound differences between WT and N588K I_{hERG} profiles during cardiac APs (Brugada et al., 2004, Cordeiro et al., 2005, McPate et al., 2009a). As drug binding can vary between the square voltage command protocols and physiological waveforms (Kirsch et al., 2004, Yao et al., 2005, Milnes et al., 2010, El Harchi et al., 2012), this work also aims to use quinidine during AP clamp in order to supplement the current literature and investigate the notion from previous work that quinidine is likely to be an effective adjunctive therapy for patients with the S631A mutation. In contrast to the I560T mutation, conventional voltage clamp has been widely used in previous studies to characterise S631A-hERG kinetics (Schonherr and Heinemann, 1996, Hancox et al., 1998b, Zou et al., 1998, Fan et al., 1999, McPate et al., 2008), and so the use of AP clamp here represents a novel area of research hoping to bring clear, translatable findings.

4.2 Results

4.2.1 Physiological consequences of the S631A mutation

4.2.1.1 Effects of the S631A mutation on I-V relations

As described above, conventional voltage clamp has been previously used to characterise the S631A mutation (Schonherr and Heinemann, 1996, Hancox et al., 1998b, Zou et al., 1998, Fan et al., 1999, McPate et al., 2008), and so the majority of this section focusses upon the novel use of AP clamp with conventional voltage clamp used only to establish I-V relations of WT and S631A channels. This is important to ensure the reported properties of S631A-hERG are reflected under the current laboratory conditions and has been done using the protocols shown in the lower panels of Figure 20A and 20B. From a holding potential of -80mV, a 2 second depolarising command was applied, followed by a 4 second repolarising command to -40mV (as in Chapter 3, Figure 6). For WT I_{hERG}, depolarising commands increased by 10mV from -40 to 60mV. Due to the large attenuation of inactivation caused by the S631A mutation (Schonherr and Heinemann, 1996, Hancox et al., 1998b, Zou et al., 1998), this protocol was modified to include voltages up to 100mV in order to capture fully the positively shifted I_{hERG} rectification, as has previously been shown effective for the comparable N588K mutation (Cordeiro et al., 2005, McPate et al., 2005). Additionally, 20mV steps were used over this wider voltage range for S631A to increase the likelihood of maintaining cell integrity throughout the duration of the protocol (McPate et al., 2005).

As can be seen in Figure 20C WT I_{hERG} exhibited the expected I-V relations as previously demonstrated in Figure 6Ai and 6B. Through decreasingly negative membrane potentials I_{hERG} rose and peaked at 0-10mV. Subsequently, inactivation became more dominant and I_{hERG} rectification occurred across the range of positive membrane potentials. As a consequence, using a repolarisation voltage of -40mV removed channel inactivation, and archetypal I_{hERG} tail currents were evident following repolarisation from the positive membrane potentials (Figure 20A) (Sanguinetti et al., 1995, Schonherr and Heinemann, 1996, Spector et al., 1996, Zhou et al., 1998). As previously reported (Schonherr and

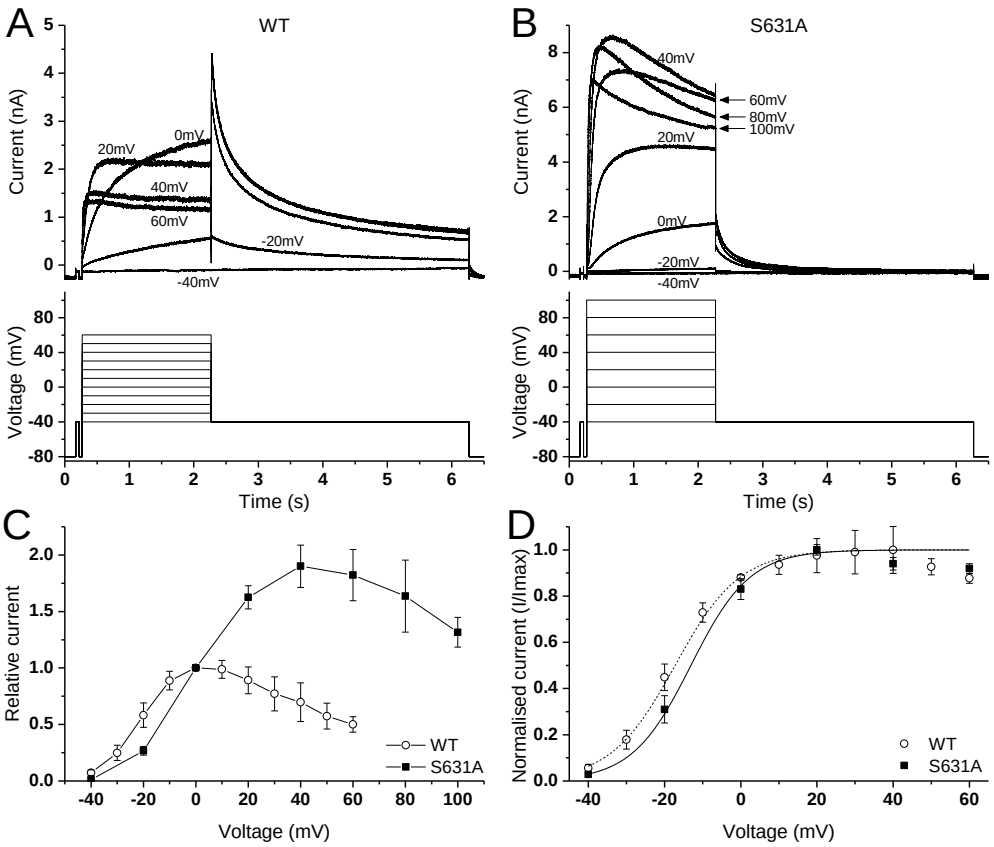

Figure 20: I-V relationship for WT and S631A-hERG. Representative current traces for WT **(A)** and S631A-hERG. **(B)** hERG channels elicited by the protocol shown below, with only selected traces shown for clarity. **(C)** Mean I-V relations for end pulse WT and S631A IhERG. Current was normalised to current recorded at 0mV. **(D)** Mean normalized tail current I-V relations. Currents were normalized to the peak current recorded during the protocol for each cell and fitted by Equation 1. In (C, D) for WT n=7 and for S631A n=5.

Heinemann, 1996, Hancox et al., 1998b, McPate et al., 2008), S631A I_{hERG} continued to increase throughout positive test potentials and only began to decrease as the membrane potential reached 40-60mV (Figure 20C). S631A tail currents were also smaller than those elicited by the test pulse at all positive voltages (Figure 20B).

By plotting normalised I_{hERG} tails against the voltage at which they were elicited and fitting with Equation 1, the voltage dependence of activation was quantified (Figure 20D). The S631A mutation caused no significant change in the half maximal voltage of activation (-14.4 ± 1.8mV for S631A vs. -16.8 ± 3.0mV for the WT; n=5 vs. n=7; p>0.05) and there was also no change in *k* value (5.3 ± 1.0 for S631A vs. 8.0 ± 1.5 for WT; p>0.05). Overall, these data

are in agreement with previous conclusions regarding the S631A mutation and show it to have no effect on the voltage dependence of I_{hERG} activation but to cause shifted rectification of I_{hERG} across a positive voltage range (Schonherr and Heinemann, 1996, Zou et al., 1998, McPate et al., 2008). This is indicative of the known property of attenuated inactivation possessed by S631A-hERG, and as the data presented here are consistent with those which have been reported previously, the remainder of S631A experiments focus solely on the novel use of AP clamp to characterise better the mutation's effects on I_{hERG} during physiological waveforms.

4.2.1.2 Effects of the S631A mutation on I_{hERG} profile during ventricular AP

As shown in Section 3.2.2 (Figure 12Ai), during the initial depolarising upstroke of the ventricular AP and the early stages of repolarisation WT I_{hERG} was limited by channel inactivation, but increased progressively towards the end of the plateau phase and then peaked during phase 3 of the action potential (Figure 21Ai). The attenuation of inactivation, however, caused S631A I_{hERG} to increase more rapidly throughout the early stages of repolarisation and produce a dome-shaped profile which reached its peak much earlier in the AP (Figure 21Aii). By plotting instantaneous I-V relations during AP repolarisation (Figure 21B), the voltage at which each channel exhibited peak I_{hERG} was identified. The S631A mutation caused a significant positive shift in this of over 50mV (-32.2 ± 2.3mV for WT vs. 21.5 ± 2.6mV for S631A; n=6 vs. n=7; $p<0.0001$), demonstrating that it can be expected to alter significantly the profile and timing of I_{hERG} during a ventricular AP. As above (Figure 12Ci), conductance-voltage relations increased progressively throughout repolarisation for WT I_{hERG}, peaking between –50mV and -80mV before dropping rapidly as the holding potential of -80mV was re-established (Figure 21Ci). S631A G-V relations however show a much-augmented profile, as conductance rose abruptly early during repolarisation, then reached a plateau for the majority of the action potential (Figure 21Cii). Thus, S631A hERG conducted earlier and over a larger voltage range than WT hERG during a ventricular AP.

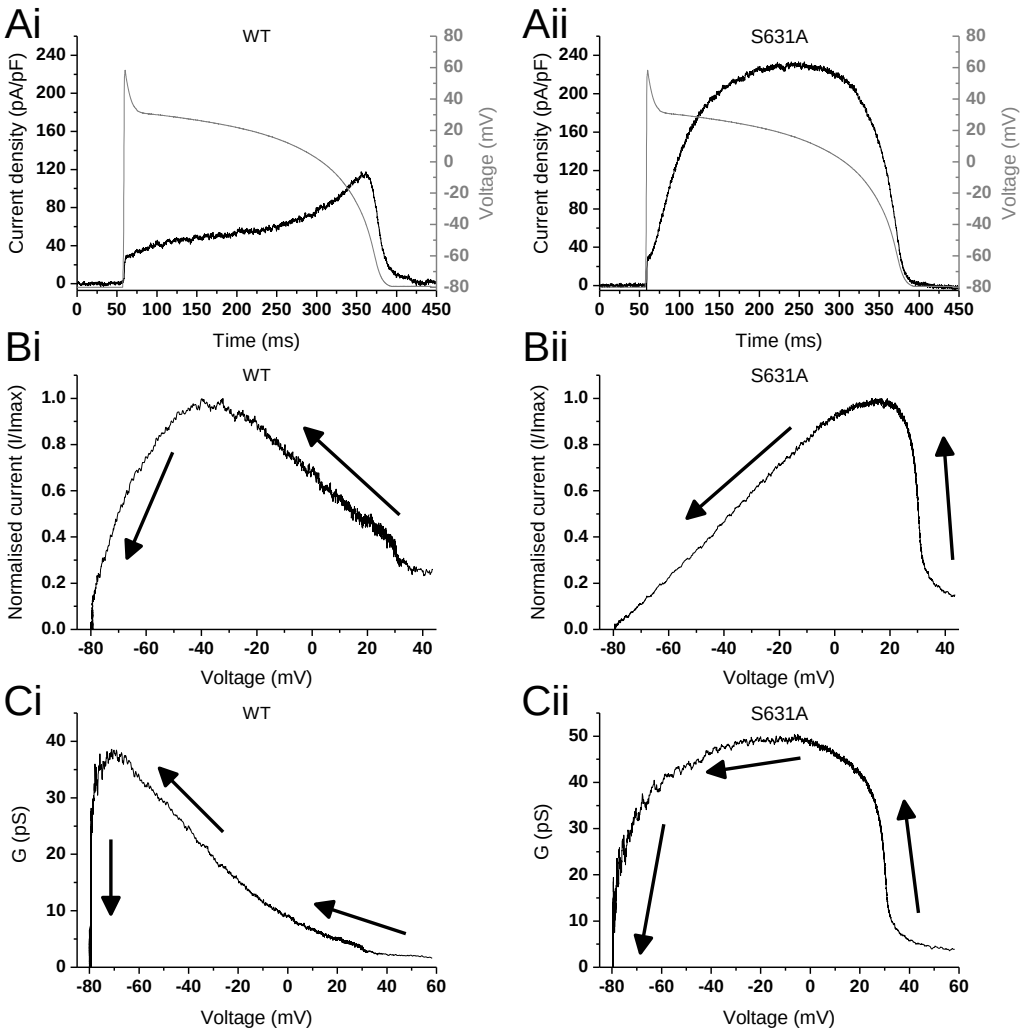

Figure 21: WT and S631A-I_{hERG} response to a ventricular AP. **(A)** Representative traces of WT and S631A-I_{hERG} profile (shown in black) during a ventricular AP (shown in grey). Current was normalised to capacitance reflecting cell membrane surface area. **(B)** Representative I-V relations recorded during repolarisation in a ventricular action potential. Current was normalised to the maximal current recorded during the protocol for each cell **(C)** Representative G-V relations recorded during repolarisation in a ventricular AP. For (B, C) the arrows represent the direction of repolarisation. For WT figures, representative traces were selected from a total of 6 experiments. For S631A figures, representative traces were selected from a total of 7 experiments.

4.2.1.3 Effects of the S631A mutation on I_{hERG} profile during atrial and Purkinje fibre AP

As established in Chapter 3 (Figure 13Ai), due to the less positive peak and more negative plateau phase, WT I_{hERG} was much smaller during atrial AP than during ventricular AP, with reduced involvement of inactivation giving a dome-shaped I_{hERG} profile which peaked during phase 3 of the AP (Figure 22Ai). Similarly, during the atrial AP, S631A I_{hERG} produced a dome-shaped profile, but with the peak occurring earlier during the plateau phase (Figure 22Aii). The lower plateau phase causes WT I_{hERG} to be more evenly distributed throughout repolarisation, with a much flatter peak between -20mV and -40mV (Figure 22Bi). In contrast S631A I_{hERG} increased more abruptly, peaking at a less negative voltage (-25.7 ± 3.0mV for WT vs. -13.8 ± 0.7mV for S631A; n=6 vs. n=6; $p<0.01$) and subsequently declining in a more linear fashion (Figure 22B).

The WT I_{hERG} profile in response to Purkinje fibre AP again showed signs of inactivation during the plateau phase, with peak I_{hERG} occurring in phase three of the AP (Figure 22Ci). Similar to the atrial and in particular ventricular S631A I_{hERG} profile, S631A I_{hERG} rose rapidly following the initial AP upstroke of the PF AP, presenting a dome-like profile (Figure 22Cii); and also peaked earlier during repolarisation, with maximal I_{hERG} being positively shifted by ~35mV (-38.1 ± 2.0mV for WT vs. -3.9 ± 1.8mV for S631A; n=6 vs. n=6; $p<0.0001$; Figure 22D). Figure 23A and 23B show comparison of maximal I_{hERG} current (normalised to capacitance reflecting cell membrane surface area) between the different cardiac AP waveforms. This highlights that augmentation of peak I_{hERG} occurred proportionately across the different APs, with no significant change in the ratio between waveforms.

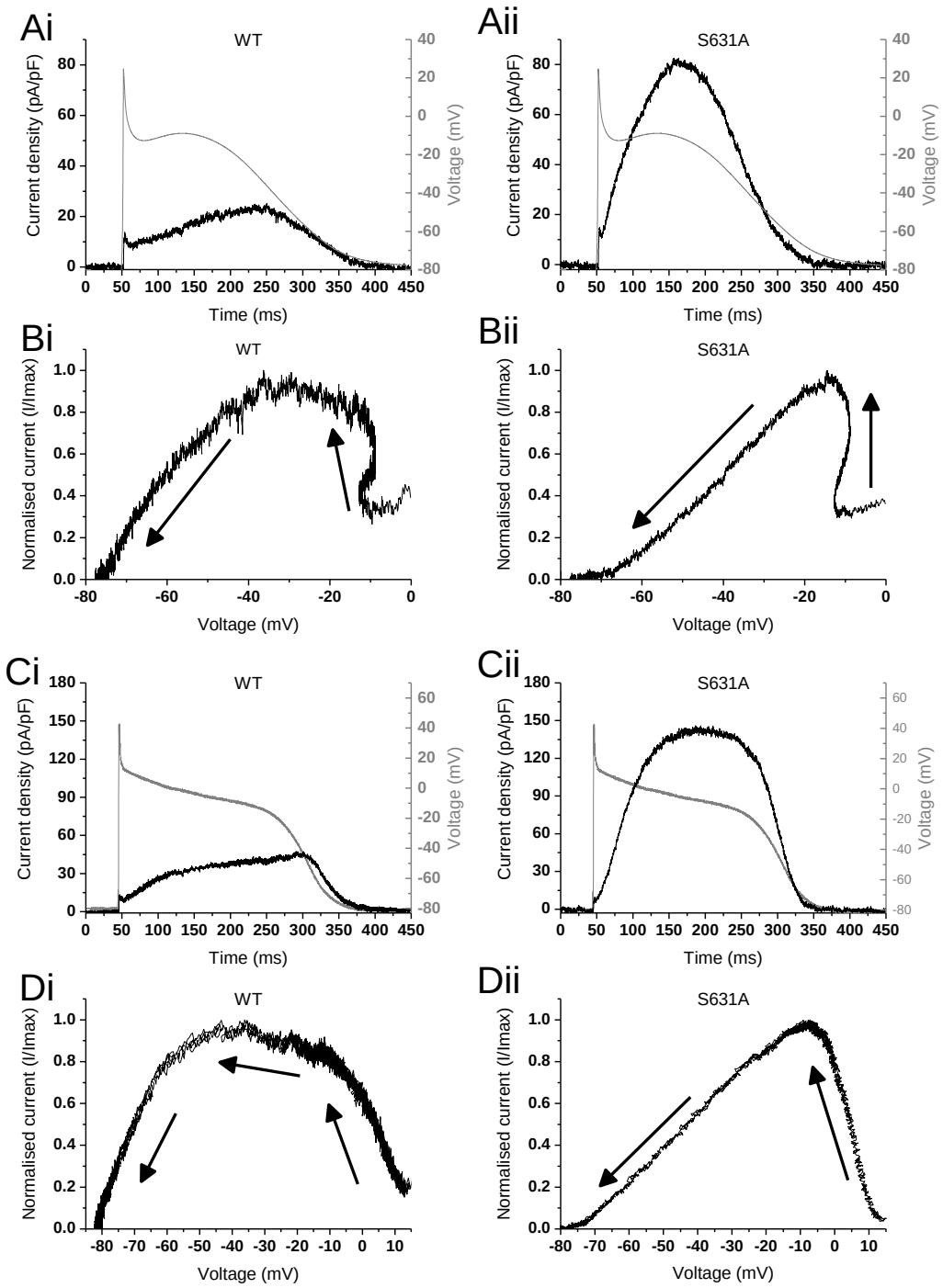

Figure 22: WT and S631A-I_{hERG} response to atrial and Purkinje fibre APs. **(A)** Representative profiles of WT (i) and S631A (ii) I_{hERG} during an atrial AP. **(B)** Representative I-V relations recorded during repolarisation in an atrial AP for WT (i) and S631A (ii) cells. **(C)** Representative profile of WT (i) and S631A (ii) I_{hERG} during Purkinje fibre AP. **(D)** Representative I-V relations during Purkinje fibre AP. For (A, C) the current traces (black) overlay the protocol used (grey) and current was normalised to capacitance reflecting cell membrane surface area. For (B, D) the arrows represent the direction of repolarisation and current was normalised to the maximal current recorded during the protocol for each cell. For all waveforms and both WT and S631A figures, representative traces were selected from 6 experiments.

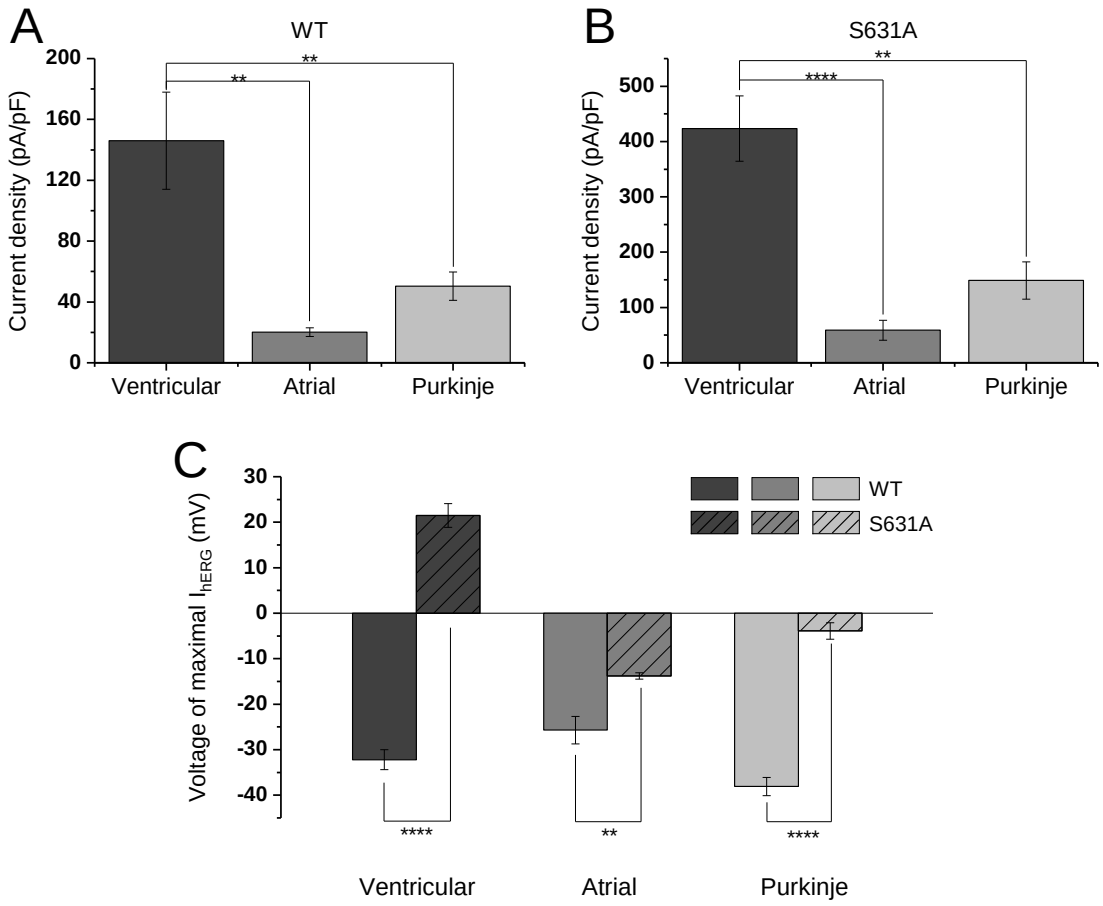

Figure 23: Comparison of WT and S631A-I_{hERG} density and timing during ventricular, atrial and PF APs. **(A)** Peak WT-I_{hERG} density during ventricular, atrial and PF APs, with current normalised to capacitance reflecting cell membrane surface area. **(B)** Peak S631A-I_{hERG} density during ventricular, atrial and PF APs, with current normalised to capacitance reflecting cell membrane surface area. **(C)** Mean voltage at which peak repolarising I_{hERG} occurred during each AP waveform. For all WT experiments n=6; for ventricular S631A experiments n=7; for PF and atrial S631A experiments n=6.

4.2.2 Response of S631A-hERG to quinidine

Previous work using voltage clamp has shown the attenuation of inactivation to have only a modest effect on I_{hERG} blockage by quinidine (Lees-Miller et al., 2000a, McPate et al., 2006, McPate et al., 2009a), however it is known that variation in drug potency can occur between different voltage clamp waveforms (Kirsch et al., 2004, Yao et al., 2005, Milnes et al., 2010,

El Harchi et al., 2012). Consequently, using AP clamp to investigate the effects of quinidine on WT and, for the first time, S631A I_{hERG} will work towards an increased understanding of the mutation and potential therapeutic strategies. Following on from the results shown in Section 3.2.3.1 and in line with other published data (Paul et al., 2002, McPate et al., 2008, El Harchi et al., 2012), a concentration of 1μM quinidine was selected to partially block I_{hERG} during a ventricular action potential.

Figure 24A shows representative traces for WT and S631A I_{hERG} in response to a ventricular AP in the absence (black) or presence (grey) of 1μM quinidine, with a reduction in I_{hERG} magnitude throughout the AP following the application of quinidine visible for both channels. This has been quantified in Figure 24B, where the reduction in peak repolarising current (Bi) and inhibition of total current integral (Bii) have been calculated. Figure 24Bi shows the fractional block of maximal I_{hERG} was decreased from 71.9 ± 3.5% in the WT to 57.1 ± 5.1% for S631A-hERG (n=5 vs. n=6; $p<0.05$), whereas Figure 24Bii shows that the reduction in total charge carried throughout the AP was not significantly different for the mutated channels (74.0 ± 2.4% for WT vs. 63.0 ± 6.2% for S631A; n=5 vs. n=6; $p>0.05$). Taken together, these results show that under AP clamp, the S631A mutation only modestly affects the affinity of hERG for quinidine.

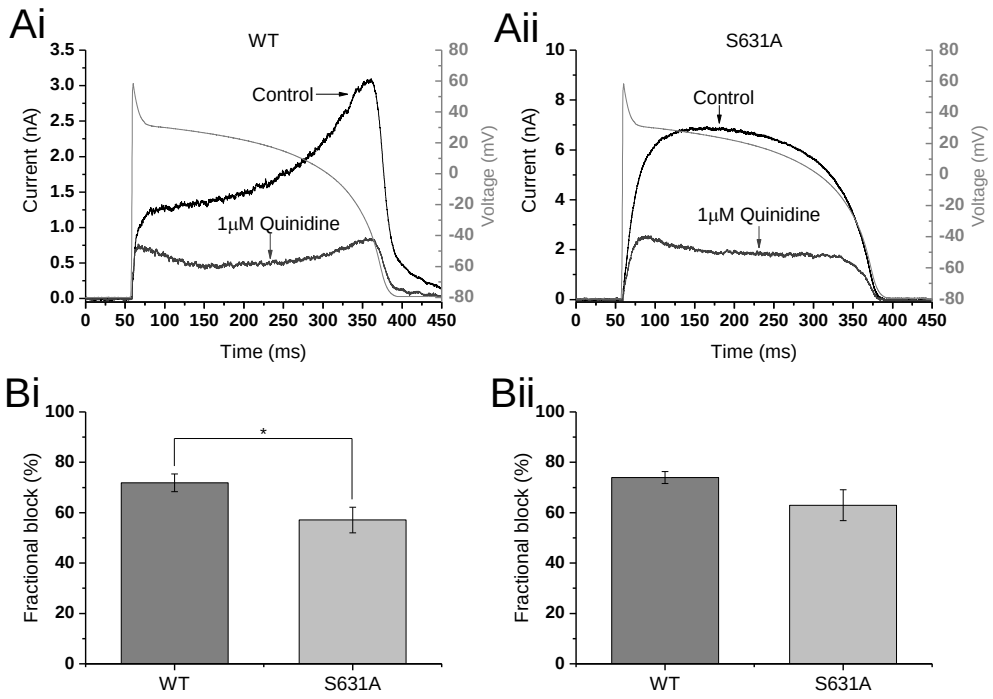

Figure 24: Inhibition of WT and S631A-I_{hERG} by quinidine. **(A)** Representative traces of WT (i) and S631A (ii) I_{hERG} in the absence (black) and presence (grey) of 1μM quinidine during a ventricular AP. **(Bi)** Reduction in maximal I_{hERG} recorded during the AP following the application of 1 μM quinidine. **(Bii)** Reduction in current integral following the application of 1μM quinidine. A minimum of 5 cells were used for each concentration of drug. For WT experiments n=5; for S631A experiments n=6.

4.3 Summary of S631A data

Property	WT	S631A	Significance
I_{hERG} properties during voltage clamp			
$V_{0.5\ (activation)}$ (mV)	16.8 ± 3.0 (n=7)	-14.4 ± 1.8 (n=5)	p>0.05
k (activation, mV)	8.0 ± 1.5 (n=7)	5.3 ± 1.0 (n=5)	p>0.05
Voltage of maximal I_{hERG} during AP clamp			
Ventricular AP (mV)	-32.2 ± 2.3 (n=6)	21.5 ± 2.6 (n=7)	**p<0.0001**
Atrial AP (mV)	-25.7 ± 3.0 (n=6)	-13.8 ± 0.7 (n=6)	**p<0.01**
Purkinje fibre AP (mV)	-38.1 ± 2.0 (n=6)	-3.9 ± 1.8 (n=6)	**p<0.0001**
Response to quinidine			
Reduction in maximal I_{hERG} (%)	71.9 ± 3.5 (n=6)	57.1 ± 5.1 (n=6)	**p<0.05**
Reduction in current integral (%)	74.0 ± 2.4 (n=6)	63.0 ± 6.2 (n=6)	p>0.05

Table 4: Summary of collected data for WT and S631A-hERG.

4.4 Discussion

4.4.1 Physiological consequences of the S631A mutation

In line with previous studies, the I-V relations demonstrated in Figure 20 show that the S631A mutation caused no change in the voltage dependence of activation but positively shifted I_{hERG} rectification (Schonherr and Heinemann, 1996, Zou et al., 1998, Fan et al., 1999, McPate et al., 2008). Previous comparable work has shown the S631A mutation to cause a ~90mV shift in the inactivation $V_{0.5}$ (McPate et al., 2008), and this is the underlying basis for the ~40mV shift in current rectification compared with WT channels. As a consequence of this shift it could be predicted that very little inactivation would occur during the AP clamp commands, as during each physiological waveform the plateau phase occurs at a voltage less positive than the range of current rectification, and only during the ventricular AP does the membrane potential reach a voltage likely to cause significant inactivation. Thus, over the vast majority of physiologically relevant voltages, channel inactivation can be considered essentially to be removed. This is evident in Figure 21A, 21A and 21C where a dome-shaped S631A-I_{hERG} profile was produced in response to ventricular, atrial and PF APs, whereas under WT conditions the limiting of current by inactivation was clearly evident during the ventricular and PF AP. Quantifying this augmentation by plotting the instantaneous I-V relations (Figure 21B, 22B and 22D) shows a positive shift in peak I_{hERG} during each AP, corresponding to maximal current occurring earlier in the AP and consequently abbreviating repolarisation (Figure 23C).

In each case, this shift produced by the mutation is greater than that caused by the I560T mutation and highly comparable to that caused by the N588K mutation. The S631A mutation caused a positive shift of ~50mv, ~10mV and ~35mV during ventricular, atrial and PF APs respectively, whereas previous work using similar conditions showed the N588K mutation to augment peak I_{hERG} by ~60mV, ~15mV and ~30mV respectively, also showing a dome-shaped profile (McPate et al., 2005, McPate et al., 2009a). This is in agreement with voltage clamp studies which show N588K to shift the voltage of half maximal inactivation by ~80-

105mV, similar to the ~90-100mV shifts reported for S631A (Zou et al., 1998, Cordeiro et al., 2005, McPate et al., 2005, McPate et al., 2008), whilst also having no effect on the voltage dependence of activation. Such similarities make it possible to take findings associated with the N588K mutation and predict that the results may be similar in the context of the S631A mutation (Hancox and Stuart, 2018). For example, prior *in silico* study of the N588K mutation has shown that the mutation increases I_{Kr} ~5-fold (Adeniran et al., 2011). My own work was limited by the necessity of using different concentrations of DNA for transfection of each construct, and this prevented a direct comparison of IhERG magnitude. The N588K-based *in silico* work however suggest that a similar increase in I_{Kr} may be caused by the S631A mutation. As described above, an increase in I_{hERG} amplitude will drive repolarisation and QT interval shortening, and in the case of the N588K mutation, this was shown to predispose to the uni-directional conduction block which facilitates re-entrant arrhythmia (Adeniran et al., 2011). An increase in local electrical heterogeneity and a reduction in the substrate size required to maintain spiral waves was also shown to be caused by the mutation, further highlighting ways in which the S631A may contribute to ventricular arrhythmogenesis (Adeniran et al., 2011).

At present, the S631A mutation has not been associated clinically with any supraventricular arrhythmia (Akdis et al., 2017), however SQTS is typically characterised by atrial in addition to ventricular arrhythmia (Maury et al., 2008, Rudic et al., 2014, Chen et al., 2016, Hancox et al., 2018), and atrial consequences have been identified in SQT1 patients with the I560T and T618I mutations as well as with the N588K mutation (Brugada et al., 2004, Giustetto et al., 2015, Harrell et al., 2015). Given the small sample size of S631A patients, it would be naïve to rule out the potential for S631A-induced atrial arrhythmia and this is supported by the data presented in Figure 22. As seen during the ventricular AP, the earlier timing of I_{hERG} during an atrial AP will abbreviate repolarisation and would be expected to facilitate re-entry by reducing the ERP (Adeniran et al., 2011, Rudic et al., 2014, Hancox et al., 2018). Atrial simulations have also shown an increase in I_{Kr} amplitude and the augmentation of I_{hERG}

timing caused by the N588K mutation to increase propensity for AF (Loewe et al., 2014), and so it is feasible that this could also be experienced by the S631A patients, although further clinical investigations would need to be performed to confirm this.

As highlighted in Figure 23C, during each AP waveform I_{hERG} timing was shifted to differing extents, and consequently the S631A mutation contributes to heterogeneity across the various cardiac tissues. As described above, this amplified heterogeneity further increases the susceptibility to arrhythmia (McPate et al., 2009a, Adeniran et al., 2011), however, as with the I560T mutation, further *in silico* work must be done in order to characterise fully the S631A mutation to understand better its effects in different tissue types.

4.4.2 Molecular context of the S631A mutation

As shown in Figure 25, the S631A residue is located outside the selectivity filter and within the outer residues of the pore helix (Wang and MacKinnon, 2017). As described in Section 4.1, the mutation was originally induced with the aim of attenuating inactivation, and consequently the mechanisms by which this occurs are much clearer than those of I560T (Schonherr and Heinemann, 1996, Hancox et al., 1998b). Following the initial S631A studies, the critical nature of the S631A residue in rapid inactivation was reinforced by work showing that, in the homologous, non-inactivating EAG, mutation of residues equivalent to hERG 631 and 620 to serine was sufficient to recapitulate hERG's rapid inactivation (Ficker et al., 2001) and a number of different mutations to the S631 residue attenuate inactivation (Fan et al., 1999). Interestingly, other mutations to the residue (S631V, S631K and S631E) which disrupted inactivation to a larger extent were also shown to shift the voltage dependence of activation of the channel, although the mechanisms underlying this are unclear (Fan et al., 1999).

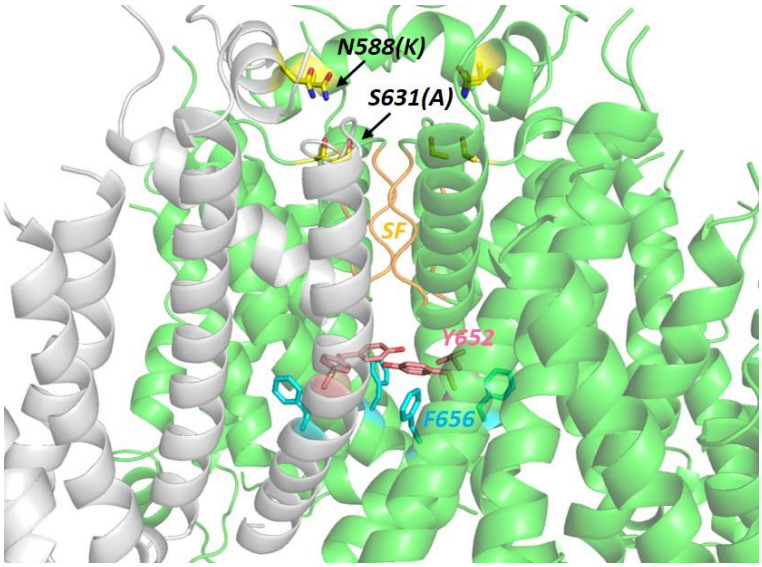

Figure 25: Structural context of the S631 residue. S631 lies above the selectivity filter (SF; shown in orange) and within the outer residues of the pore helix. The N588K residue (S5-P linker) is also highlighted, as are the key drug binding residues Y652 and F656 which sit below the SF. Construct built using the cryo-EM structure (Wang and MacKinnon, 2017) and provided by Dr Christopher Dempsey (University of Bristol).

The highly comparable nature of the S631A and N588K mutations is of particularly interest due to the spatial difference between the two residues. Unlike S631, N588 lies within the S5-P linker (Figure 25) (Liu et al., 2002, Brugada et al., 2004, Wang and MacKinnon, 2017). Mutations to a number of residues within the S5-P linker have been shown to attenuate inactivation (Liu et al., 2002, Vandenberg et al., 2004, Clarke et al., 2006), possibly due to perturbations to the linker's ability to interact with both the channel pore and the voltage sensing domain (Liu et al., 2002, Clarke et al., 2006), and so N588K represents a clinically relevant mechanism for attenuated inactivation distinct from that of S631A. This difference in location is key in the study of pharmacological agents as it means that similarities in alterations to dug binding between the two mutations are caused by a disturbance of the inactivation process, whereas any differences are likely related to more localised changes.

With this in mind, studies have shown that binding of drugs with a variety of structures including dofetilide, flecainide, disopyramide, quinidine, propafenone and amiodarone are similarly affected by the two mutations (McPate et al., 2008, Perrin et al., 2008, Melgari et

al., 2015) thus highlighting the process of inactivation to be of varying importance for drug binding, but this to be irrespective of the specific mutations to the N588 and S631. This has been supported by site-directed mutagenesis which simultaneously relocated the key drug binding residues Y652 and F656 (shown in Figure 25) along the S6 helices and attenuated inactivation and showed that S6 helices rotate during inactivation gating, facing the residues into a state compatible with high affinity drug binding (Chen et al., 2002). Consequently, it is believed that it is this rotation rather than inactivation as such which is key for drug binding (Chen et al., 2002, Helliwell et al., 2018). This is further supported by the studies of the non-inactivating EAG which show that although it also possesses residues homologous to Y652 and F656, it is not susceptible to high affinity block by potent hERG inhibitors (Ficker et al., 1998, Herzberg et al., 1998).

As a result of my work and prior studies it can be predicted with confidence that *in vivo* the S631A mutation will result in a reduced the effect of a number of drugs. As described in Section 3.4.4 however, the reduction in affinity for quinidine caused by the N588K mutation was not large enough prevent it from being useful clinically and the drug has consistently been used in the treatment of SQT1. Prior studies using traditional, square-pulse voltage clamp have shown the S631A mutation to cause a 1.25-3.5-fold (Lees-Miller et al., 2000a, McPate et al., 2008) decrease in potency of quinidine compared to WT channels, but to my knowledge no previous study has investigated the how different this is under AP clamp conditions. The data presented in Figure 24 supports a modest change in sensitivity to quinidine with only a ~15% reduction in the fractional inhibition of peak I_{hERG} and no significant change in reduction of current integral throughout the ventricular AP. The use of 1μM quinidine in my work is notably lower that the mean serum concentration (~2.9μM) measured in patients (Schimpf et al., 2007), and so as with the I560T mutation, this data is supportive of the use of quinidine as an adjunctive agent for patients with the S631A mutation. As far as has been reported, none of the patients identified in the study by Akdis et al. (2017) appear to be receiving additional medication.

With regard to the aforementioned reduced clinical availability of quinidine (Viskin et al., 2013a, Mazzanti et al., 2017a), it is worth noting that in the case of N588K, disopyramide was shown to be a more effective hERG blocker than quinidine *in vitro* (McPate et al., 2006) and the inhibition of N588K and S631A I_{hERG} by disopyramide was similar (Paul et al., 2001, McPate et al., 2008). In a small clinical study, two patients with the N588K mutation receiving disopyramide as an alternative to quinidine both experienced prolongation of the QTc interval and an increase in the effective refractory period (Schimpf et al., 2007), with subsequent *in silico* work demonstrating this QTc interval prolongation to be a result of I_{Kr} block whilst the increase in ERP was due to inhibition of both I_{Kr} and I_{Na} (Whittaker et al., 2017), and so it is feasible to recommend disopyramide as an alternative in areas where quinidine is unavailable. In summary, the mechanisms which link attenuated inactivation to changes in drug sensitivity reinforce to use of the N588K mutation as a comparable tool, and the available data combined with the data presented in Figure 24 make a strong case to support the use of quinidine as an adjunct therapy in SQT1 patients with the S631A mutation.

4.5 Conclusion

The S631A mutation has long been reported to have a profound effect on hERG channel gating and drug binding properties. This study's application of AP clamp to cells expressing S631A-hERG has demonstrated that the attenuation of inactivation caused by the mutation significantly augments I_{hERG} profile during ventricular, atrial and PF APs. This can be expected to abbreviate repolarisation and therefore QT interval *in vivo* and increase susceptibility to both ventricular and atrial arrhythmia. Application of quinidine blocked both WT and S631A I_{hERG} to a similar extent, suggesting it may work as an effective therapeutic option for S631A-induced SQT1, a conclusion reinforced by previous conventional voltage clamp studies (Lees-Miller et al., 2000a, McPate et al., 2006, McPate et al., 2008, Perrin et al., 2008).

Chapter 5 General Discussion

5.1 Clinical relevance of findings

Much work has been done previously using heterologous expression of hERG channels in mammalian cell lines. Prior work conducted using approaches similar to those adopted here has demonstrated an underlying electrophysiological basis for symptoms experienced by SQT1 patients (Brugada et al., 2004, McPate et al., 2005, Wilders and Verkerk, 2010, Sun et al., 2011, Zhang et al., 2011, El Harchi et al., 2012) as well as demonstrating mutation driven changes in affinity for drugs which have been taken forward clinically and proven effective *in vivo* (McPate et al., 2006, Schimpf et al., 2007, El Harchi et al., 2012, Giustetto et al., 2015). Data generated by such work has also provided a basis for *in silico* recapitulation of SQT1, helping to increase understanding of the links between QT interval abbreviation, tissue excitability and arrhythmogenesis (Adeniran et al., 2011, Loewe et al., 2014, Whittaker et al., 2017). Accordingly, my findings follow a similar trend by using proven patch clamp techniques to determine channel properties under the conditions of the I560T and S631A mutation.

Using traditional voltage clamp and square voltage command protocols, the most significant finding regarding the I560T mutation was that of a ~24mV shift in the half maximal voltage of inactivation. Despite structurally distinct locations, this is highly comparable to both the T618I (25mV) and L532P (32mV) mutations studied under comparable conditions, although unlike I560T, the T618I and L532P mutations have both also been reported to shift the half maximal voltage of activation (Sun et al., 2011, Zhang et al., 2011, El Harchi et al., 2012, Harrell et al., 2015). This attenuation of inactivation resulted in peak I_{hERG} occurring earlier during ventricular repolarisation for all both mutations, with positive shifts of ~35mV (T618I) and ~45mV (L532P) recorded (Zhang et al., 2011, El Harchi et al., 2012). For both, this is more significant than the shift in I_{hERG} caused by the I560T mutation (~18mV) recorded using AP clamp in my work. Despite the I560T mutation appearing to have a more modest effect on hERG properties, similar to the L532P mutation it has been associated *in vivo* with atrial

fibrillation, which is not true for the more prevalent T618I mutation (Hassel et al., 2008, Sun et al., 2011, Harrell et al., 2015, Hu et al., 2017). The reason(s) for this difference are not currently known. However, such comparisons highlight the need for provision of data regarding basic channel properties, such as that presented throughout Chapters 3 and 4, which can be used for *in silico* studies to help build our understanding of how altered channel function can cause arrhythmia and how this differentiates between tissue types. This is reinforced by comparison of the S631A and N588K mutations, as the work done on both mutations prior to the identification of a patient harbouring the S631A mutation bore predictions on drug binding and I_{hERG} profile during physiological waveforms which were further supported by my work (Hancox et al., 1998b, Lees-Miller et al., 2000a, McPate et al., 2006, McPate et al., 2008, McPate et al., 2009a).

In vitro study of SQT1 mutations is generally consistent with the alterations to QTc interval suffered by patients. Although no AP clamp data regarding the E50D or R1135H mutations are available, their reported properties mostly differ from WT channels with respect to I_{hERG} amplitude and deactivation rates, with only a modest shift in inactivation also described for E50D (but no data published). Consequently, it can be predicted that timing of peak I_{hERG} will not be altered significantly during physiological waveforms and thus a less prominent clinical effect will occur (Itoh et al., 2009, Hu et al., 2017). This is reflected in the QTc intervals recorded in patients with these mutations, with the R1135H and E50D mutations reducing QTc intervals to 329-379ms and 366-381ms respectively, and further supported by knowledge that the patient identified with the E50D mutation having no history of SCD within the family (Itoh et al., 2009, Redpath et al., 2009). The two mutations associated with a more intermediate level of inactivation attenuation (I560T and T618I) are clinically linked with a greater reduction in QTc interval, with the largest study of T618I patients showing a mean QTc interval of 313ms and the only I560T patient's QTc interval reported at a similar 319ms (Harrell et al., 2015, Hu et al., 2017); whilst the N588K mutation's almost total attenuation of inactivation over physiological voltages resulted in a mean QTc interval of 284ms in the

widest analysis (Hu et al., 2017). In this respect, the S631A mutation is a relative outlier, with the average QTc interval of the three afflicted patients being 329ms, much higher than those reported for the similar N588K mutation (Akdis et al., 2017). The reasons for this are unclear, but a much larger number of patients with the N588K mutation have been identified, with 16 used in the aforementioned analysis (Akdis et al., 2017, Hu et al., 2017), and so perhaps clarity or a change in the defined QTc interval associated with the S631A mutation will occur if further patients are identified.

Despite my work being consistent with other studies in the literature with clear, translatable results, there are some inherent limitations that should be considered, as doing so may identify a number of areas in which further work may be beneficial with regards to both the I560T and S631A mutations and perhaps also SQT1 as a whole and wider hERG channel function. The principal potential limitations of the results in this thesis are considered below, along with the opportunities these create for future work.

5.2 SQTS patients are heterozygous

SQTS is inherited in an autosomal dominant fashion, with successfully genotyped patients presenting as heterozygous for their SQTS mutations (Hu et al., 2017, Hancox et al., 2018). This heterozygosity means that the hERG channels in patients will be formed of heteromers of WT and mutant subunits, rather than the homologous channels used in this study. Despite this, the vast majority of studies of SQT1 mutations have used homozygous expression (Hancox et al., 1998b, Zou et al., 1998, Lees-Miller et al., 2000a, Brugada et al., 2004, Cordeiro et al., 2005, McPate et al., 2005, McPate et al., 2009a, Sun et al., 2011, El Harchi et al., 2012, Hu et al., 2017), with limited work being published using co-expression of WT and mutant channels. The data available however, does suggest heterologous channels can cause graded alterations to channel properties (Wu et al., 2014, Wu et al., 2015, Hu et al., 2017). Transient co-expression of T618I and WT-hERG in HEK cells increased peak I_{hERG} 1.75-fold, whereas expression of T618I-hERG alone resulted in a 2.19-fold increase in

current (Hu et al., 2017), showing that whilst co-expression reduced the effect of the mutation compared to expression of T618I alone, a significant change in I_{hERG} still occurred. Unfortunately, further information regarding differences in hERG kinetics or make-up of channels cannot be drawn from the study by Hu et al. (2017) and there is no way to determine the number of WT/T618I-hERG subunits which contribute to the channels that they studied.

Earlier work by Wu et al. (2014), however, aimed to address issues of stoichiometry of inactivation mutants more precisely using concatemers of WT and mutant subunits with attenuated inactivation in order to establish the effects of stoichiometry on channel function. By expressing hERG channels containing one, two or three mutant subunits with no (G628C/S631C) or attenuated (S620T or S631A) inactivation, this work showed that in channels containing the subunits with the G628C/S631C or S620T mutation, the presence of a single mutated subunit in a tetramer was sufficient to disrupt channel function to the same extent as in a mutant homomer; and in channels with subunits possessing the S631A mutation the number of mutant subunits contributing to the channel had a graded effect (Wu et al., 2014). This grading however, is not linear and the presence of one, two, three or four subunits caused a positive shift in the $V_{0.5}$ of inactivation by 53mV, 56mV, 68mV and 77mV respectively (Wu et al., 2014). From this it can be inferred that the results shown in Section 4.2.1 will be clinically relevant during heterozygous expression, with ~70% of the attenuation of inactivation with homozygous expression occurring when only one or two mutant subunits contributed to the channel (Wu et al., 2014). In addition to this, the reduced attenuation of inactivation recorded in heterozygous S631A channels may account for the less abbreviated QTc intervals recorded in patients compared to those with the N588K mutation. If, as with S620T, a single mutant N588K subunit disrupts channel function to the same extent as in a mutant homomer, then the larger clinical effect documented can be expected, but more work will be required to confirm this hypothesis.

Subsequent work using the same hERG concatemers showed that a mix of WT and mutant subunits can also affect drug binding, with the IC_{50} of cisapride and dofetilide being lower in heterologous channels containing subunits with the S631A mutation than in monomeric S631A-hERG channels (Wu et al., 2015). This means it is possible that the results presented in Section 4.2.2 may overestimate the *in vivo* effect of the mutation on drug binding, (which was modest, even under homozygous expression conditions). Whilst work with I560T concatemers or dimers has yet to be performed, my data (Figure 15B and Figure 16B) establish the potential maximal alterations in potency of quinidine and sotalol with this mutation. Collectively the evidence suggests that whilst heterozygosity can moderate the impact of a mutation, significant changes in channel properties still occur and so the mechanisms by which the I560T and S631A mutations have been shown as linked to arrhythmias by my work will still bear clinical relevance. Similarly, prior work with concatemeric channels and the modest shifts in drug potency seen here with homozygous mutant expression provide a rational basis for the clinical application of drugs studied in my experiments.

5.3 In vivo formation of hERG channels

As described in Section 1.2.1, unlike hERG 1b, hERG 1a is capable of forming functional monomers in humans, however native channels are likely to be formed of hERG 1a/1b heteromers (Phartiyal et al., 2008, Jones et al., 2014, McNally et al., 2017) and the current conducted by the heteromeric channel more closely resembles that of native I_{Kr} (London et al., 1997). Although evidence to support a physiological role of hERG 1b is relatively limited, at least two cases of LQTS associated with hERG 1b mutations (A8V and R25W) have been identified (Sale et al., 2008, Crotti et al., 2013). More recently, cardiomyocytes derived from human iPSCs have been studied using shRNA to knockdown hERG 1b and using transformation with a hERG 1a-specific PAS domain fragment which has been previously shown to modulate I_{hERG} through interactions with hERG 1b only (Trudeau et al., 2011,

Jones et al., 2014). Both of these techniques shifted the I_{hERG} profile from one consistent with hERG 1a/1b heteromers to one consistent with hERG 1a homomers and inhibition of hERG 1b was also seen as proarrhythmic, thus the work showed the hERG 1b subunit as critical in human hERG function and consequently key in cardiac repolarization (Trudeau et al., 2011, Jones et al., 2014).

Work comparing the properties of heterologous N588K-hERG 1a/1b channels against WT-hERG 1a/1b and monomeric hERG 1a channels showed that the inclusion of N588K-hERG 1b subunits amplified the attenuation of inactivation caused by the N588K mutation, with no further effects on other channel properties (McPate et al., 2009b), possibly due to the reduced number N-termini which have previously been shown to interact with the S4-5 linker and stabilise inactivation (Wang et al., 1998, El Harchi et al., 2018). The similarities between the extent of I_{hERG} inactivation attenuation for hERG1a produced by N588K and S631A mutation make it possible to suggest that hERG1b incorporation is likely have a similar effect for S631A-hERG and it also cannot be ruled out that either I560T 1a/1b heteromers may display properties slightly different to those of the monomers used in my work; and so this presents a clear opportunity for further study. Despite these potential differences in properties, the findings of prior work in which *in vitro* results with hERG1a align with *in vivo* data are supportive of the clinical relevance of my study (McPate et al., 2005, McPate et al., 2009a, El Harchi et al., 2012, Hu et al., 2017). In addition to this, drug binding assays comparing affinity for 1a/1b heteromers against traditional hERG 1a monomers have highlighted differences in affinity, with some drugs having higher affinity for monomeric channels, others for heteromeric channels, and these differences in IC_{50} being as large as 8-fold in some cases (Abi-Gerges et al., 2011, El Harchi et al., 2018). Of note, little difference in the IC_{50} for sotalol in the presence of hERG 1b has been found and neither study evaluate differences in affinity for quinidine (Abi-Gerges et al., 2011, El Harchi et al., 2018). The impact of mutations on this has not been investigated, and so further work could also be done to confirm the retention of drug binding in heteromeric hERG1a/1b SQT1 channels.

In addition to the major pore-forming subunit, potential β-subunits merit some consideration. Although hERG and KCNE2 interact in heterologous expression systems (Abbott et al., 1999, Mazhari et al., 2001, Anantharam and Abbott, 2005), KCNE2 is only strongly expressed in the Purkinje fibres and atrial pacemaker cells, and so an *in vivo* interaction within the cardiac chambers is unlikely (Pourrier et al., 2003, Lundquist et al., 2005). In addition to this, heterologous expression of N588K-hERG and KCNE2 showed little difference in I_{hERG} profile during ventricular, atrial or PF APs when compared with expression of N588K-hERG alone (McPate et al., 2009a). Furthermore, it has been shown *in vitro* that hERG preferentially interacts with KCNE1 over KCNE2 and that (in addition to the well-established role of KCNE1 in I_{Ks}) mutation to KCNE1 can cause LQTS by modifying I_{Kr} (Ohno et al., 2007, Um and McDonald, 2007). Although a number of studies characterise the effects of KCNE1 mutations on I_{hERG} (Bianchi et al., 1999, Ohno et al., 2007, Nof et al., 2011, Du et al., 2013), to the best of my knowledge no work has yet been completed determining whether and how SQT1 mutations influence interactions with KCNE1, and so this may offer another interesting area of further study both in the context of the two mutations studied here and within the wider SQT1 setting.

To summarize: heterozygous expression of WT and I560T/S631A mutations to mimic more closely the situation in SQT1 patients could lead to quantitative differences in the extent of alterations of particular I_{hERG} properties, but these are unlikely to alter the fundamental observations regarding which processes are altered by either mutation. Incorporation of hERG1b into heteromeric channels could also potentially produce a quantitative difference in effects of inactivation attenuation and co-expression with potential accessory subunits (KCNE1 or KCNE2) might also modulate I_{hERG}, though any modulation of kinetic changes produced by hERG mutations by these subunits is likely to be modest. Whilst limits on the time available for a research MSc placed further work to address these issues outside the scope of my own work, future investigations along these lines may be of value in further

explorations of the roles of these mutations in SQT1 and of the underlying residues in I_{hERG} channel gating.

5.4 Conclusion

Following the recent clinical identification of the I560T and S631A hERG mutations in the SQTS, this study has aimed to characterise the kinetics and pharmacology of the mutant channels more extensively than prior work, using both conventional voltage clamp and AP clamp. For I560T hERG, I have identified a larger positive shift in the voltage dependence of inactivation alongside wider changes in channel properties than those previously reported (Harrell et al., 2015), which combine to produce alterations to the channels response to physiological waveforms, thus increasing susceptibility to arrhythmia. As could be predicted from the previous literature on the S631A mutation (Schonherr and Heinemann, 1996, Hancox et al., 1998b, Zou et al., 1998, Wu et al., 2014), a larger augmentation of I_{hERG} profile during cardiac repolarisation was seen in cells expressing S631A-hERG, demonstrating its ability to drive repolarisation and abbreviate the QT interval. Although both mutations augmented I_{hERG} to different extents and clearly have a different underlying structural basis for their effects, they both showed a similar retention of binding to quinidine and I560T-hERG additionally showed the same affinity for sotalol as WT-hERG. In summary, the work presented here demonstrates the underlying mechanisms of I560T-induced SQT1 and the consequences of both the I560T and S631A mutations during physiological waveforms. In addition to this, therapeutic agents likely to be effective in attenuating the increased I_{Kr} in patients with each mutation have been identified.

Publications

The work in Chapter 4 describing the effects of the S631A hERG mutation on I_{hERG} during ventricular, atrial and Purkinje fibre APs, and the channel's response to quinidine under AP clamp has been recently published and can be found under:

Butler, A., Y. Zhang, A. G. Stuart, C. E. Dempsey and J. C. Hancox (2018). "Action potential clamp characterization of the S631A hERG mutation associated with short QT syndrome." Physiol Rep 6(17): e13845.

Bibliography

Abbott, G. W., F. Sesti, I. Splawski, M. E. Buck, M. H. Lehmann, K. W. Timothy, M. T. Keating and S. A. Goldstein (1999). "MiRP1 forms IKr potassium channels with HERG and is associated with cardiac arrhythmia." Cell **97**(2): 175-187.

Abi-Gerges, N., H. Holkham, E. Jones, C. Pollard, J. Valentin and G. Robertson (2011). "hERG subunit composition determines differential drug sensitivity." Br J Pharmacol **164**(2b): 419-432.

Ackerman, M. J., S. G. Priori, S. Willems, C. Berul, R. Brugada, H. Calkins, A. J. Camm, P. T. Ellinor, M. Gollob, R. Hamilton, R. E. Hershberger, D. P. Judge, H. Le Marec, W. J. McKenna, E. Schulze-Bahr, C. Semsarian, J. A. Towbin, H. Watkins, A. Wilde, C. Wolpert and D. P. Zipes (2011). "HRS/EHRA expert consensus statement on the state of genetic testing for the channelopathies and cardiomyopathies this document was developed as a partnership between the Heart Rhythm Society (HRS) and the European Heart Rhythm Association (EHRA)." Heart Rhythm **8**(8): 1308-1339.

Adeniran, I., M. J. McPate, H. J. Witchel, J. C. Hancox and H. Zhang (2011). "Increased vulnerability of human ventricle to re-entrant excitation in hERG-linked variant 1 short QT syndrome." PLoS Comput Biol **7**(12): e1002313.

Akdis, D., A. M. Saguner, A. Medeiros-Domingo, A. Schaller, C. Balmer, J. Steffel, C. Brunckhorst and F. Duru (2017). "Multiple clinical profiles of families with the short QT syndrome." EP Europace: eux186-eux186.

Anantharam, A. and G. W. Abbott (2005). "Does hERG coassemble with a beta subunit? Evidence for roles of MinK and MiRP1." Novartis Found Symp **266**: 100-112; discussion 112-107, 155-108.

Anttonen, O., M. J. Junttila, H. Rissanen, A. Reunanen, M. Viitasalo and H. V. Huikuri (2007). "Prevalence and prognostic significance of short QT interval in a middle-aged Finnish population." Circulation **116**(7): 714-720.

Ballesteros, J. A., X. Deupi, M. Olivella, E. E. Haaksma and L. Pardo (2000). "Serine and threonine residues bend alpha-helices in the chi(1) = g(-) conformation." Biophys J **79**(5): 2754-2760.

Barhanin, J., F. Lesage, E. Guillemare, M. Fink, M. Lazdunski and G. Romey (1996). "K(V)LQT1 and lsK (minK) proteins associate to form the I(Ks) cardiac potassium current." Nature **384**(6604): 78-80.

Bartos, D. C., E. Grandi and C. M. Ripplinger (2015). "Ion Channels in the Heart." Compr Physiol **5**(3): 1423-1464.

Baskar, S. and P. F. Aziz (2015). "Genotype-phenotype correlation in long QT syndrome." Glob Cardiol Sci Pract **2015**(2).

Bianchi, L., Z. Shen, A. T. Dennis, S. G. Priori, C. Napolitano, E. Ronchetti, R. Bryskin, P. J. Schwartz and A. M. Brown (1999). "Cellular dysfunction of LQT5-minK mutants: abnormalities of IKs, IKr and trafficking in long QT syndrome." Hum Mol Genet **8**(8): 1499-1507.

Bjerregaard, P., A. Jahangir and I. Gussak (2006). "Targeted therapy for short QT syndrome." Expert Opin Ther Targets **10**(3): 393-400.

Brugada, R., K. Hong, R. Dumaine, J. Cordeiro, F. Gaita, M. Borggrefe, T. M. Menendez, J. Brugada, G. D. Pollevick, C. Wolpert, E. Burashnikov, K. Matsuo, Y. S. Wu, A. Guerchicoff, F. Bianchi, C. Giustetto, R. Schimpf, P. Brugada and C. Antzelevitch (2004). "Sudden death associated with short-QT syndrome linked to mutations in HERG." Circulation **109**(1): 30-35.

Carro, C., A. F. Cereda, G. Annoni and S. M. Marianeschi (2017). "Epicardial cardioverter–defibrillator implantation in a 4-month-old infant bridged to heart transplantation." Interactive CardioVascular and Thoracic Surgery **25**(5): 832-833.

Cavalli, A., R. Buonfiglio, C. Ianni, M. Masetti, L. Ceccarini, R. Caves, M. W. Chang, J. S. Mitcheson, M. Roberti and M. Recanatini (2012). "Computational design and discovery of "minimally structured" hERG blockers." J Med Chem **55**(8): 4010-4014.

Cerrone, M., S. Noujaim and J. Jalife (2006). "The short QT syndrome as a paradigm to understand the role of potassium channels in ventricular fibrillation." Journal of Internal Medicine **259**(1): 24-38.

Charpentier, F., J. Merot, G. Loussouarn and I. Baro (2010). "Delayed rectifier K(+) currents and cardiac repolarization." J Mol Cell Cardiol **48**(1): 37-44.

Chen, J., G. Seebohm and M. C. Sanguinetti (2002). "Position of aromatic residues in the S6 domain, not inactivation, dictates cisapride sensitivity of HERG and eag potassium channels." Proc Natl Acad Sci U S A **99**(19): 12461-12466.

Chen, J., A. Zou, I. Splawski, M. T. Keating and M. C. Sanguinetti (1999). "Long QT syndrome-associated mutations in the Per-Arnt-Sim (PAS) domain of HERG potassium channels accelerate channel deactivation." J Biol Chem **274**(15): 10113-10118.

Chen, L., K. J. Sampson and R. S. Kass (2016). "Cardiac Delayed Rectifier Potassium Channels in Health and Disease." Card Electrophysiol Clin **8**(2): 307-322.

Cheng, Y. M. and T. W. Claydon (2012). "Voltage-Dependent Gating of hERG Potassium Channels." Front Pharmacol **3**.

Clarke, C. E., A. P. Hill, J. Zhao, M. Kondo, R. N. Subbiah, T. J. Campbell and J. I. Vandenberg (2006). "Effect of S5P alpha-helix charge mutants on inactivation of hERG K+ channels." J Physiol **573**(Pt 2): 291-304.

Colenso, C. K., R. B. Sessions, Y. H. Zhang, J. C. Hancox and C. E. Dempsey (2013). "Interactions between Voltage Sensor and Pore Domains in a hERG K+ Channel Model from Molecular Simulations and the Effects of a Voltage Sensor Mutation." Journal of Chemical Information and Modeling **53**(6): 1358-1370.

Cordeiro, J. M., R. Brugada, Y. S. Wu, K. Hong and R. Dumaine (2005). "Modulation of I(Kr) inactivation by mutation N588K in KCNH2: a link to arrhythmogenesis in short QT syndrome." Cardiovasc Res **67**(3): 498-509.

Courneya, C. A. M. and M. J. Parker (2011). Cardiovascular physiology: A clinical approach, Lippincott Williams & Wilkins.

Crotti, L., D. J. Tester, W. M. White, D. C. Bartos, R. Insolia, A. Besana, J. D. Kunic, M. L. Will, E. J. Velasco, J. J. Bair, A. Ghidoni, I. Cetin, D. L. Van Dyke, M. J. Wick, B. Brost, B. P. Delisle, F. Facchinetti, A. L. George, P. J. Schwartz and M. J. Ackerman (2013). "Long QT Syndrome–Associated Mutations in Intrauterine Fetal Death." Jama **309**(14).

Curran, M. E., I. Splawski, K. W. Timothy, G. M. Vincent, E. D. Green and M. T. Keating (1995). "A molecular basis for cardiac arrhythmia: HERG mutations cause long QT syndrome." Cell **80**(5): 795-803.

de la Peña, P., P. Domínguez and F. Barros (2018). "Functional characterization of Kv11.1 (hERG) potassium channels split in the voltage-sensing domain." Pflugers Arch **470**(7): 1069-1085.

del Val, C. (2012). "Ser/Thr Motifs in Transmembrane Proteins: Conservation Patterns and." **245**(11): 717-730.

Dharmaprani, D., L. Dykes, A. D. McGavigan, P. Kuklik, K. Pope and A. N. Ganesan (2018). "Information Theory and Atrial Fibrillation (AF): A Review." Front Physiol **9**: 957.

Dhutia, H., A. Malhotra, S. Parpia, V. Gabus, G. Finocchiaro, G. Mellor, A. Merghani, L. Millar, R. Narain, N. Sheikh, E. R. Behr, M. Papadakis and S. Sharma (2016). "The prevalence and significance of a short QT interval in 18,825 low-risk individuals including athletes." Br J Sports Med **50**(2): 124-129.

Du, C., A. El Harchi, H. Zhang and J. C. Hancox (2013). "Modification by KCNE1 variants of the hERG potassium channel response to premature stimulation and to pharmacological inhibition." Physiol Rep **1**(6).

Du, C., Y. Zhang, A. El Harchi, C. E. Dempsey and J. C. Hancox (2014). "Ranolazine inhibition of hERG potassium channels: drug-pore interactions and reduced potency against inactivation mutants." J Mol Cell Cardiol **74**: 220-230.

Du, C. Y., I. Adeniran, H. Cheng, Y. H. Zhang, A. El Harchi, M. J. McPate, H. Zhang, C. H. Orchard and J. C. Hancox (2010). "Acidosis impairs the protective role of hERG K(+) channels against premature stimulation." J Cardiovasc Electrophysiol **21**(10): 1160-1169.

Duan, J.-j., J.-h. Ma, P.-h. Zhang, X.-p. Wang, A.-r. Zou and D.-n. Tu (2007). "Verapamil blocks HERG channel by the helix residue Y652 and F656 in the S6 transmembrane domain." Acta Pharmacologica Sinica **28**: 959.

Durdagi, S., S. Deshpande, H. J. Duff and S. Y. Noskov (2012). "Modeling of open, closed, and open-inactivated states of the hERG1 channel: structural mechanisms of the state-dependent drug binding." J Chem Inf Model **52**(10): 2760-2774.

Eilers, M., A. B. Patel, W. Liu and S. O. Smith (2002). "Comparison of helix interactions in membrane and soluble alpha-bundle proteins." Biophys J **82**(5): 2720-2736.

El Harchi, A., M. J. McPate, Y. Zhang, H. Zhang and J. C. Hancox (2009). "Action potential clamp and chloroquine sensitivity of mutant Kir2.1 channels responsible for variant 3 short QT syndrome." J Mol Cell Cardiol **47**(5): 743-747.

El Harchi, A., D. Melgari, H. Zhang and J. Hancox (2018). "Investigation of hERG1b influence on hERG channel pharmacology at physiological temperature." **9**(2): 92-103.

El Harchi, A., D. Melgari, Y. H. Zhang, H. Zhang and J. C. Hancox (2012). "Action Potential Clamp and Pharmacology of the Variant 1 Short QT Syndrome T618I hERG K+ Channel." PLOS ONE **7**(12): e52451.

El Harchi, A., H. Zhang and J. C. Hancox (2010). "The S140G KCNQ1 atrial fibrillation mutation affects 'I(KS)' profile during both atrial and ventricular action potentials." J Physiol Pharmacol **61**(6): 759-764.

Elming, H., E. Holm, L. Jun, C. Torp-Pedersen, L. Kober, M. Kircshoff, M. Malik and J. Camm (1998). "The prognostic value of the QT interval and QT interval dispersion in all-cause and cardiac mortality and morbidity in a population of Danish citizens." Eur Heart J **19**(9): 1391-1400.

Fan, J. S., M. Jiang, W. Dun, T. V. McDonald and G. N. Tseng (1999). "Effects of outer mouth mutations on hERG channel function: a comparison with similar mutations in the Shaker channel." Biophys J **76**(6): 3128-3140.

Ficker, E., W. Jarolimek and A. M. Brown (2001). "Molecular determinants of inactivation and dofetilide block in ether a-go-go (EAG) channels and EAG-related K(+) channels." Mol Pharmacol **60**(6): 1343-1348.

Ficker, E., W. Jarolimek, J. Kiehn, A. Baumann and A. M. Brown (1998). "Molecular determinants of dofetilide block of HERG K+ channels." Circ Res **82**(3): 386-395.

Finley, M. R., Y. Li, F. Hua, J. Lillich, K. E. Mitchell, S. Ganta, R. F. Gilmour, Jr. and L. C. Freeman (2002). "Expression and coassociation of ERG1, KCNQ1, and KCNE1 potassium channel proteins in horse heart." Am J Physiol Heart Circ Physiol **283**(1): H126-138.

Gaborit, N., S. Le Bouter, V. Szuts, A. Varro, D. Escande, S. Nattel and S. Demolombe (2007). "Regional and tissue specific transcript signatures of ion channel genes in the non-diseased human heart." J Physiol **582**(Pt 2): 675-693.

Gaita, F., C. Giustetto, F. Bianchi, R. Schimpf, M. Haissaguerre, L. Calo, R. Brugada, C. Antzelevitch, M. Borggrefe and C. Wolpert (2004). "Short QT syndrome: pharmacological treatment." J Am Coll Cardiol **43**(8): 1494-1499.

Gaita, F., C. Giustetto, F. Bianchi, C. Wolpert, R. Schimpf, R. Riccardi, S. Grossi, E. Richiardi and M. Borggrefe (2003). "Short QT Syndrome: a familial cause of sudden death." Circulation **108**(8): 965-970.

Giustetto, C., F. Di Monte, C. Wolpert, M. Borggrefe, R. Schimpf, P. Sbragia, G. Leone, P. Maury, O. Anttonen, M. Haissaguerre and F. Gaita (2006). "Short QT syndrome: clinical findings and diagnostic–therapeutic implications." European Heart Journal **27**(20): 2440-2447.

Giustetto, C., R. Schimpf, A. Mazzanti, C. Scrocco, P. Maury, O. Anttonen, V. Probst, J.-J. Blanc, P. Sbragia, P. Dalmasso, M. Borggrefe and F. Gaita (2011). "Long-Term Follow-Up of Patients With Short QT Syndrome." Journal of the American College of Cardiology **58**(6): 587-595.

Giustetto, C., C. Scrocco, D. Giachino, C. Rapezzi, B. Mognetti and F. Gaita (2015). "The lack of effect of sotalol in short QT syndrome patients carrying the T618I mutation in the KCNH2 gene." HeartRhythm Case Rep **1**(5): 373-378.

Gollob, M. H., C. J. Redpath and J. D. Roberts (2011). "The Short QT Syndrome: Proposed Diagnostic Criteria." Journal of the American College of Cardiology **57**(7): 802-812.

Guerrier, K., D. Kwiatkowski, R. J. Czosek, D. S. Spar, J. B. Anderson and T. K. Knilans (2015). "Short QT Interval Prevalence and Clinical Outcomes in a Pediatric Population." Circ Arrhythm Electrophysiol **8**(6): 1460-1464.

Gussak, I., P. Brugada, J. Brugada, R. S. Wright, S. L. Kopecky, B. R. Chaitman and P. Bjerregaard (2000). "Idiopathic short QT interval: a new clinical syndrome?" Cardiology **94**(2): 99-102.

Hancox, J. C., A. J. Levi and H. J. Witchel (1998a). "Time course and voltage dependence of expressed HERG current compared with native "rapid" delayed rectifier K current during the cardiac ventricular action potential." Pflugers Arch **436**(6): 843-853.

Hancox, J. C., M. J. McPate, A. El Harchi and Y. H. Zhang (2008). "The hERG potassium channel and hERG screening for drug-induced torsades de pointes." Pharmacol Ther **119**(2): 118-132.

Hancox, J. C. and A. G. Stuart (2018). "Rational prediction of pharmacological treatment options for a novel KCNH2- linked variant of the Short QT Syndrome." Annals of Circulation(3): 008-009.

Hancox, J. C., D. G. Whittaker, C. Du, A. G. Stuart and H. Zhang (2018). "Emerging therapeutic targets in the short QT syndrome." Expert Opin Ther Targets **22**(5): 439-451.

Hancox, J. C., H. J. Witchel and A. Varghese (1998b). "Alteration of HERG current profile during the cardiac ventricular action potential, following a pore mutation." Biochem Biophys Res Commun **253**(3): 719-724.

Harrell, D. T., T. Ashihara, T. Ishikawa, I. Tominaga, A. Mazzanti, K. Takahashi, Y. Oginosawa, H. Abe, K. Maemura, N. Sumitomo, K. Uno, M. Takano, S. G. Priori and N. Makita (2015). "Genotype-dependent differences in age of manifestation and arrhythmia complications in short QT syndrome." Int J Cardiol **190**: 393-402.

Hassel, D., E. P. Scholz, N. Trano, O. Friedrich, S. Just, B. Meder, D. L. Weiss, E. Zitron, S. Marquart, B. Vogel, C. A. Karle, G. Seemann, M. C. Fishman, H. A. Katus and W. Rottbauer (2008). "Deficient zebrafish ether-a-go-go-related gene channel gating causes short-QT syndrome in zebrafish reggae mutants." Circulation **117**(7): 866-875.

Helliwell, M. V., Y. Zhang, A. El Harchi, C. Du, J. C. Hancox and C. E. Dempsey (2018). "Structural implications of hERG K(+) channel block by a high affinity minimally-structured blocker." J Biol Chem.

Herzberg, I. M., M. C. Trudeau and G. A. Robertson (1998). "Transfer of rapid inactivation and sensitivity to the class III antiarrhythmic drug E-4031 from HERG to M-eag channels." J Physiol **511 (Pt 1)**: 3-14.

Hoshi, T. and C. M. Armstrong (2013). "C-type inactivation of voltage-gated K(+) channels: Pore constriction or dilation?" J Gen Physiol **141**(2): 151-160.

Hoshi, T., W. N. Zagotta and R. W. Aldrich (1991). "Two types of inactivation in Shaker K+ channels: effects of alterations in the carboxy-terminal region." Neuron **7**(4): 547-556.

Hu, D., Y. Li, J. Zhang, R. Pfeiffer, M. H. Gollob, J. Healey, D. T. Harrell, N. Makita, H. Abe, Y. Sun, J. Guo, L. Zhang, G. Yan, D. Mah, E. P. Walsh, H. B. Leopold, C. Giustetto, F. Gaita, A. Zienciuk-Krajka, A. Mazzanti, S. G. Priori, C. Antzelevitch and H. Barajas-Martinez (2017). "The Phenotypic Spectrum of a Mutation Hotspot Responsible for the Short QT Syndrome." JACC: Clinical Electrophysiology **3**(7): 727-743.

Huang, H., M. K. Pugsley, B. Fermini, M. J. Curtis, J. Koerner, M. Accardi and S. Authier (2017). "Cardiac voltage-gated ion channels in safety pharmacology: Review of the landscape leading to the CiPA initiative." J Pharmacol Toxicol Methods **87**: 11-23.

Itoh, H., T. Sakaguchi, T. Ashihara, W.-G. Ding, I. Nagaoka, Y. Oka, Y. Nakazawa, T. Yao, H. Jo, M. Ito, K. Nakamura, T. Ohe, H. Matsuura and M. Horie (2009). "A novel KCNH2 mutation as a modifier for short QT interval." International Journal of Cardiology **137**(1): 83-85.

Jansen, H., J. Siebels, R. Ventura, J. Hebe and C. Sohns (2018). "Mapping and ablation of cardiac arrhythmias : Never forget where you are coming from." Herzschrittmacherther Elektrophysiol.

Jiang, M., M. Zhang, I. V. Maslennikov, J. Liu, D. M. Wu, Y. V. Korolkova, A. S. Arseniev, E. V. Grishin and G. N. Tseng (2005). "Dynamic conformational changes of extracellular S5-P linkers in the hERG channel." J Physiol **569**(Pt 1): 75-89.

Jo, S.-H., H.-K. Hong, S. H. Chong, K. H. Won, S. J. Jung and H. Choe (2008). "Clomipramine block of the hERG K+ channel: Accessibility to F656 and Y652." European Journal of Pharmacology **592**(1): 19-25.

Jones, D. K., F. Liu, R. Vaidyanathan, L. L. Eckhardt, M. C. Trudeau and G. A. Robertson (2014). "hERG 1b is critical for human cardiac repolarization." Proc Natl Acad Sci U S A **111**(50): 18073-18077.

Jones, E. M., E. C. Roti Roti, J. Wang, S. A. Delfosse and G. A. Robertson (2004). "Cardiac IKr channels minimally comprise hERG 1a and 1b subunits." J Biol Chem **279**(43): 44690-44694.

Kamiya, K., R. Niwa, J. S. Mitcheson and M. C. Sanguinetti (2006). "Molecular determinants of HERG channel block." Mol Pharmacol **69**(5): 1709-1716.

Kirsch, G. E., E. S. Trepakova, J. C. Brimecombe, S. S. Sidach, H. D. Erickson, M. C. Kochan, L. M. Shyjka, A. E. Lacerda and A. M. Brown (2004). "Variability in the measurement of hERG potassium channel inhibition: effects of temperature and stimulus pattern." J Pharmacol Toxicol Methods **50**(2): 93-101.

Lees-Miller, J. P., Y. Duan, G. Q. Teng and H. J. Duff (2000a). "Molecular determinant of high-affinity dofetilide binding to HERG1 expressed in Xenopus oocytes: involvement of S6 sites." Mol Pharmacol **57**(2): 367-374.

Lees-Miller, J. P., Y. Duan, G. Q. Teng, K. Thorstad and H. J. Duff (2000b). "Novel gain-of-function mechanism in K(+) channel-related long-QT syndrome: altered gating and selectivity in the HERG1 N629D mutant." Circ Res **86**(5): 507-513.

Lees-Miller, J. P., C. Kondo, L. Wang and H. J. Duff (1997). "Electrophysiological characterization of an alternatively processed ERG K+ channel in mouse and human hearts." Circ Res **81**(5): 719-726.

Lees-Miller, J. P., J. O. Subbotina, J. Guo, V. Yarov-Yarovoy, S. Y. Noskov and H. J. Duff (2009). "Interactions of H562 in the S5 Helix with T618 and S621 in the Pore Helix Are Important Determinants of hERG1 Potassium Channel Structure and Function." Biophys J **96**(9): 3600-3610.

Li, K., Q. Jiang, X. Bai, Y. F. Yang, M. Y. Ruan and S. Q. Cai (2017). "Tetrameric Assembly of K(+) Channels Requires ER-Located Chaperone Proteins." Mol Cell **65**(1): 52-65.

Liu, J., M. Zhang, M. Jiang and G. N. Tseng (2002). "Structural and functional role of the extracellular s5-p linker in the HERG potassium channel." J Gen Physiol **120**(5): 723-737.

Liu, N., S.-N. Wen, Y.-F. Ruan, T. Zhang, S.-N. Li, J.-H. Wu, C.-X. Jiang, R.-B. Tang, D.-Y. Long, R. Bai, R.-H. Yu, X. Du, J.-Z. Dong and C.-S. Ma (2015). "QTc interval prolongation predicts the ablation outcome in hypertensive patients with paroxysmal atrial fibrillation." European Heart Journal Supplements **17**(suppl_B): B32-B38.

Liu, Y., M. E. Jurman and G. Yellen (1996). "Dynamic rearrangement of the outer mouth of a K+ channel during gating." Neuron **16**(4): 859-867.

Loewe, A., M. Wilhelms, F. Fischer, E. P. Scholz, O. Dössel and G. Seemann (2014). "Arrhythmic potency of human ether-à-go-go-related gene mutations L532P and N588K in a computational model of human atrial myocytes." EP Europace **16**(3): 435-443.

London, B., M. C. Trudeau, K. P. Newton, A. K. Beyer, N. G. Copeland, D. J. Gilbert, N. A. Jenkins, C. A. Satler and G. A. Robertson (1997). "Two isoforms of the mouse ether-a-go-go-related gene coassemble to form channels with properties similar to the rapidly activating component of the cardiac delayed rectifier K+ current." Circ Res **81**(5): 870-878.

Long, S. B., X. Tao, E. B. Campbell and R. MacKinnon (2007). "Atomic structure of a voltage-dependent K+ channel in a lipid membrane-like environment." Nature **450**: 376.

Lopez-Barneo, J., T. Hoshi, S. H. Heinemann and R. W. Aldrich (1993). "Effects of external cations and mutations in the pore region on C-type inactivation of Shaker potassium channels." Receptors Channels **1**(1): 61-71.

Lu, Y., M. P. Mahaut-Smith, A. Varghese, C. L. Huang, P. R. Kemp and J. I. Vandenberg (2001). "Effects of premature stimulation on HERG K(+) channels." J Physiol **537**(Pt 3): 843-851.

Ludwig, J., H. Terlau, F. Wunder, A. Bruggemann, L. A. Pardo, A. Marquardt, W. Stuhmer and O. Pongs (1994). "Functional expression of a rat homologue of the voltage gated either a go-go potassium channel reveals differences in selectivity and activation kinetics between the Drosophila channel and its mammalian counterpart." Embo j **13**(19): 4451-4458.

Lundquist, A. L., L. J. Manderfield, C. G. Vanoye, C. S. Rogers, B. S. Donahue, P. A. Chang, D. C. Drinkwater, K. T. Murray and A. L. George, Jr. (2005). "Expression of multiple KCNE genes in human heart may enable variable modulation of I(Ks)." J Mol Cell Cardiol **38**(2): 277-287.

Ma, N., X. Y. Wu, C. S. Ma, N. Liu, R. Bai, X. Du, Y. F. Ruan and J. Z. Dong (2016). "QTc interval predicts outcome of catheter ablation in paroxysmal atrial fibrillation patients with type 2 diabetes mellitus." J Huazhong Univ Sci Technolog Med Sci **36**(5): 646-652.

Mantziari, A. A., V. P. Vassilikos, Y. S. Chatzizisis, G. Dakos, G. Stavropoulos, S. Paraskevaidis and I. H. Styliadis (2011). "Cardiac arrest caused by torsades de pointes tachycardia after successful atrial flutter radiofrequency catheter ablation." Open Cardiovasc Med J **5**: 1-3.

Maury, P., F. Extramiana, P. Sbragia, C. Giustetto, R. Schimpf, A. Duparc, C. Wolpert, I. Denjoy, M. Delay, M. Borggrefe and F. Gaita (2008). "Short QT syndrome. Update on a recent entity." Arch Cardiovasc Dis **101**(11-12): 779-786.

Mazhari, R., J. L. Greenstein, R. L. Winslow, E. Marban and H. B. Nuss (2001). "Molecular interactions between two long-QT syndrome gene products, HERG and KCNE2, rationalized by in vitro and in silico analysis." Circ Res **89**(1): 33-38.

Mazzanti, A., A. Kanthan, N. Monteforte, M. Memmi, R. Bloise, V. Novelli, C. Miceli, S. O'Rourke, G. Borio, A. Zienciuk-Krajka, A. Curcio, A. E. Surducan, M. Colombo, C. Napolitano and S. G. Priori (2014). "Novel Insight Into the Natural History of Short QT Syndrome." J Am Coll Cardiol **63**(13): 1300-1308.

Mazzanti, A., R. Maragna, G. Vacanti, A. Kostopoulou, M. Marino, N. Monteforte, R. Bloise, K. Underwood, V. Tibollo, E. Pagan, C. Napolitano, R. Bellazzi, V. Bagnardi and S. G. Priori (2017a). "Hydroquinidine Prevents Life-Threatening Arrhythmic Events in Patients With Short QT Syndrome." J Am Coll Cardiol **70**(24): 3010-3015.

Mazzanti, A., K. Underwood, D. Nevelev, S. Kofman and S. G. Priori (2017b). "The new kids on the block of arrhythmogenic disorders: Short QT syndrome and early repolarization." J Cardiovasc Electrophysiol **28**(10): 1226-1236.

McDonald, T. V., Z. Yu, Z. Ming, E. Palma, M. B. Meyers, K. W. Wang, S. A. Goldstein and G. I. Fishman (1997). "A minK-HERG complex regulates the cardiac potassium current I(Kr)." Nature **388**(6639): 289-292.

McNally, B. A., Z. D. Pendon and M. C. Trudeau (2017). "hERG1a and hERG1b potassium channel subunits directly interact and preferentially form heteromeric channels." J Biol Chem **292**(52): 21548-21557.

McPate, M. J., R. S. Duncan, J. C. Hancox and H. J. Witchel (2008). "Pharmacology of the short QT syndrome N588K-hERG K(+) channel mutation: differential impact on selected class I and class III antiarrhythmic drugs." Br J Pharmacol **155**(6): 957-966.

McPate, M. J., R. S. Duncan, J. T. Milnes, H. J. Witchel and J. C. Hancox (2005). "The N588K-HERG K+ channel mutation in the 'short QT syndrome': Mechanism of gain-in-function determined at 37°C." Biochemical and Biophysical Research Communications **334**(2): 441-449.

McPate, M. J., R. S. Duncan, H. J. Witchel and J. C. Hancox (2006). "Disopyramide is an effective inhibitor of mutant HERG K+ channels involved in variant 1 short QT syndrome." J Mol Cell Cardiol **41**(3): 563-566.

McPate, M. J., H. Zhang, I. Adeniran, J. M. Cordeiro, H. J. Witchel and J. C. Hancox (2009a). "Comparative effects of the short QT N588K mutation at 37 degrees C on hERG K+ channel current during ventricular, Purkinje fibre and atrial action potentials: an action potential clamp study." J Physiol Pharmacol **60**(1): 23-41.

McPate, M. J., H. Zhang, J. M. Cordeiro, C. E. Dempsey, H. J. Witchel and J. C. Hancox (2009b). "hERG1a/1b heteromeric currents exhibit amplified attenuation of inactivation in variant 1 short QT syndrome." Biochemical and Biophysical Research Communications **386**(1): 111-117.

Melgari, D., C. Du, A. El Harchi, Y. Zhang and J. C. Hancox (2014). "Suppression of the hERG potassium channel response to premature stimulation by reduction in extracellular potassium concentration." Physiol Rep **2**(10).

Melgari, D., Y. Zhang, A. El Harchi, C. E. Dempsey and J. C. Hancox (2015). "Molecular basis of hERG potassium channel blockade by the class Ic antiarrhythmic flecainide." Journal of Molecular and Cellular Cardiology **86**: 42-53.

Milnes, J. T., H. J. Witchel, J. L. Leaney, D. J. Leishman and J. C. Hancox (2010). "Investigating dynamic protocol-dependence of hERG potassium channel inhibition at 37 degrees C: Cisapride versus dofetilide." J Pharmacol Toxicol Methods **61**(2): 178-191.

Mitcheson, J. S., J. Chen, M. Lin, C. Culberson and M. C. Sanguinetti (2000). "A structural basis for drug-induced long QT syndrome." Proceedings of the National Academy of Sciences **97**(22): 12329.

Miyamoto, A., H. Hayashi, T. Yoshino, T. Kawaguchi, A. Taniguchi, H. Itoh, Y. Sugimoto, M. Itoh, T. Makiyama, J. Q. Xue, Y. Murakami and M. Horie (2012). "Clinical and electrocardiographic characteristics of patients with short QT interval in a large hospital-based population." Heart Rhythm **9**(1): 66-74.

Modell, S. M. and M. H. Lehmann (2006). "The long QT syndrome family of cardiac ion channelopathies: A HuGE review*." Genetics In Medicine **8**: 143.

Mondoly, P., C. Cardin, A. Rollin, A. Duparc and P. Maury (2016). "Use of a subcutaneous ICD in a patient with short QT syndrome." Clin Case Rep **4**(1): 35-38.

Moreno, C., A. Macias, A. Prieto, A. de la Cruz, T. Gonzalez and C. Valenzuela (2012). "Effects of n-3 Polyunsaturated Fatty Acids on Cardiac Ion Channels." Front Physiol **3**: 245.

Nerbonne, J. M. and R. S. Kass (2005). "Molecular physiology of cardiac repolarization." Physiol Rev **85**(4): 1205-1253.

Noble, D. and R. W. Tsien (1969). "Outward membrane currents activated in the plateau range of potentials in cardiac Purkinje fibres." J Physiol **200**(1): 205-231.

Noble, D., A. Varghese, P. Kohl and P. Noble (1998). "Improved guinea-pig ventricular cell model incorporating a diadic space, IKr and IKs, and length- and tension-dependent processes." Can J Cardiol **14**(1): 123-134.

Nof, E., H. Barajas-Martinez, M. Eldar, J. Urrutia, G. Caceres, G. Rosenfeld, D. Bar-Lev, M. Feinberg, E. Burashnikov, O. Casis, D. Hu, M. Glikson and C. Antzelevitch (2011). "LQT5 masquerading as LQT2: a dominant negative effect of KCNE1-D85N rare polymorphism on KCNH2 current." Europace **13**(10): 1478-1483.

Numaguchi, H., F. M. Mullins, J. P. Johnson, Jr., D. C. Johns, S. S. Po, I. C. Yang, G. F. Tomaselli and J. R. Balser (2000). "Probing the interaction between inactivation gating and Dd-sotalol block of HERG." Circ Res **87**(11): 1012-1018.

Ohno, S., D. P. Zankov, H. Yoshida, K. Tsuji, T. Makiyama, H. Itoh, M. Akao, J. C. Hancox, T. Kita and M. Horie (2007). "N- and C-terminal KCNE1 mutations cause distinct phenotypes of long QT syndrome." Heart Rhythm **4**(3): 332-340.

Okin, P. M., R. B. Devereux, B. V. Howard, R. R. Fabsitz, E. T. Lee and T. K. Welty (2000). "Assessment of QT interval and QT dispersion for prediction of all-cause and cardiovascular mortality in American Indians: The Strong Heart Study." Circulation **101**(1): 61-66.

Paul, A. A., H. J. Witchel and J. C. Hancox (2001). "Inhibition of HERG potassium channel current by the class 1a antiarrhythmic agent disopyramide." Biochem Biophys Res Commun **280**(5): 1243-1250.

Paul, A. A., H. J. Witchel and J. C. Hancox (2002). "Inhibition of the current of heterologously expressed HERG potassium channels by flecainide and comparison with quinidine, propafenone and lignocaine." Br J Pharmacol **136**(5): 717-729.

Pavão, M., V. C. Ono, E. Arfelli, M. V. Simões, J. A. Marin Neto and A. Schmidt (2014). "Sudden Cardiac Death and Short QT Syndrome." Arq Bras Cardiol **103**(3): e37-40.

Perez Riera, A. R., A. Paixao-Almeida, R. Barbosa-Barros, F. G. Yanowitz, A. Baranchuk, S. Dubner and A. C. Palandri Chagas (2013). "Congenital short QT syndrome: landmarks of the newest arrhythmogenic cardiac channelopathy." Cardiol J **20**(5): 464-471.

Perissinotti, L. L., P. M. De Biase, J. Guo, P. C. Yang, M. C. Lee, C. E. Clancy, H. J. Duff and S. Y. Noskov (2018). "Determinants of Isoform-Specific Gating Kinetics of hERG1 Channel: Combined Experimental and Simulation Study." Front Physiol **9**.

Perrin, M. J., P. W. Kuchel, T. J. Campbell and J. I. Vandenberg (2008). "Drug Binding to the Inactivated State Is Necessary but Not Sufficient for High-Affinity Binding to Human Ether-à-go-go-Related Gene Channels." Molecular Pharmacology **74**(5): 1443.

Perry, M., M. J. de Groot, R. Helliwell, D. Leishman, M. Tristani-Firouzi, M. C. Sanguinetti and J. Mitcheson (2004). "Structural Determinants of HERG Channel Block by Clofilium and Ibutilide." Molecular Pharmacology **66**(2): 240.

Perry, M., M. Sanguinetti and J. Mitcheson (2010). "Revealing the structural basis of action of hERG potassium channel activators and blockers." J Physiol **588**(Pt 17): 3157-3167.

Perry, M. D., C. A. Ng, S. A. Mann, A. Sadrieh, M. Imtiaz, A. P. Hill and J. I. Vandenberg (2015). "Getting to the heart of hERG K(+) channel gating." J Physiol **593**(Pt 12): 2575-2585.

Perry, M. D., C. A. Ng and J. I. Vandenberg (2013a). "Pore Helices Play a Dynamic Role as Integrators of Domain Motion during Kv11.1 Channel Inactivation Gating." J Biol Chem **288**(16): 11482-11491.

Perry, M. D., S. Wong, C. A. Ng and J. I. Vandenberg (2013b). "Hydrophobic interactions between the voltage sensor and pore mediate inactivation in Kv11.1 channels." J Gen Physiol **142**(3): 275-288.

Phan, K., C. A. Ng, E. David, D. Shishmarev, P. W. Kuchel, J. I. Vandenberg and M. D. Perry (2017). "The S1 helix critically regulates the finely tuned gating of Kv11.1 channels." J Biol Chem **292**(18): 7688-7705.

Phartiyal, P., E. M. Jones and G. A. Robertson (2007). "Heteromeric assembly of human ether-a-go-go-related gene (hERG) 1a/1b channels occurs cotranslationally via N-terminal interactions." J Biol Chem **282**(13): 9874-9882.

Phartiyal, P., H. Sale, E. M. Jones and G. A. Robertson (2008). "Endoplasmic reticulum retention and rescue by heteromeric assembly regulate human ERG 1a/1b surface channel composition." J Biol Chem **283**(7): 3702-3707.

Pond, A. L., B. K. Scheve, A. T. Benedict, K. Petrecca, D. R. Van Wagoner, A. Shrier and J. M. Nerbonne (2000). "Expression of distinct ERG proteins in rat, mouse, and human heart. Relation to functional I(Kr) channels." J Biol Chem **275**(8): 5997-6006.

Pourrier, M., S. Zicha, J. Ehrlich, W. Han and S. Nattel (2003). "Canine ventricular KCNE2 expression resides predominantly in Purkinje fibers." Circ Res **93**(3): 189-191.

Priori, S. G., C. Blomstrom-Lundqvist, A. Mazzanti, N. Blom, M. Borggrefe, J. Camm, P. M. Elliott, D. Fitzsimons, R. Hatala, G. Hindricks, P. Kirchhof, K. Kjeldsen, K. H. Kuck, A. Hernandez-Madrid, N. Nikolaou, T. M. Norekval, C. Spaulding and D. J. Van Veldhuisen (2015). "2015 ESC Guidelines for the management of patients with ventricular arrhythmias and the prevention of sudden cardiac death: The Task Force for the Management of Patients with Ventricular Arrhythmias and the Prevention of Sudden Cardiac Death of the European Society of Cardiology (ESC). Endorsed by: Association for European Paediatric and Congenital Cardiology (AEPC)." Eur Heart J **36**(41): 2793-2867.

Priori, S. G., A. A. Wilde, M. Horie, Y. Cho, E. R. Behr, C. Berul, N. Blom, J. Brugada, C.-E. Chiang, H. Huikuri, P. Kannankeril, A. Krahn, A. Leenhardt, A. Moss, P. J. Schwartz, W. Shimizu, G. Tomaselli and C. Tracy (2013). "Executive Summary: HRS/EHRA/APHRS Expert Consensus Statement on the Diagnosis and Management of Patients with Inherited Primary Arrhythmia Syndromes." Heart Rhythm **10**(12): e85-e108.

Redpath, C. J., M. S. Green, D. H. Birnie and M. H. Gollob (2009). "Rapid genetic testing facilitating the diagnosis of short QT syndrome." Can J Cardiol **25**(4): e133-135.

Rudic, B., R. Schimpf and M. Borggrefe (2014). "Short QT Syndrome – Review of Diagnosis and Treatment." Arrhythm Electrophysiol Rev **3**(2): 76-79.

Sale, H., J. Wang, T. J. O'Hara, D. J. Tester, P. Phartiyal, J. Q. He, Y. Rudy, M. J. Ackerman and G. A. Robertson (2008). "Physiological properties of hERG 1a/1b heteromeric currents and a hERG 1b-specific mutation associated with Long-QT syndrome." Circ Res **103**(7): e81-95.

Sanchez-Chapula, J. A., T. Ferrer, R. A. Navarro-Polanco and M. C. Sanguinetti (2003). "Voltage-dependent profile of human ether-a-go-go-related gene channel block is influenced by a single residue in the S6 transmembrane domain." Mol Pharmacol **63**(5): 1051-1058.

Sanguinetti, M. C., M. E. Curran, A. Zou, J. Shen, P. S. Spector, D. L. Atkinson and M. T. Keating (1996). "Coassembly of K(V)LQT1 and minK (IsK) proteins to form cardiac I(Ks) potassium channel." Nature **384**(6604): 80-83.

Sanguinetti, M. C., C. Jiang, M. E. Curran and M. T. Keating (1995). "A mechanistic link between an inherited and an acquired cardiac arrhythmia: HERG encodes the IKr potassium channel." Cell **81**(2): 299-307.

Sanguinetti, M. C. and N. K. Jurkiewicz (1990). "Two components of cardiac delayed rectifier K+ current. Differential sensitivity to block by class III antiarrhythmic agents." J Gen Physiol **96**(1): 195-215.

Sanguinetti, M. C. and N. K. Jurkiewicz (1992). "Role of external Ca2+ and K+ in gating of cardiac delayed rectifier K+ currents." Pflugers Arch **420**(2): 180-186.

Sanguinetti, M. C. and M. Tristani-Firouzi (2006). "hERG potassium channels and cardiac arrhythmia." Nature **440**: 463.

Saxena, P., E. M. Zangerl-Plessl, T. Linder, A. Windisch, A. Hohaus, E. Timin, S. Hering and A. Stary-Weinzinger (2016). "New potential binding determinant for hERG channel inhibitors." Scientific Reports **6**: 24182.

Schimpf, R., C. Veltmann, C. Giustetto, F. Gaita, M. Borggrefe and C. Wolpert (2007). "In vivo effects of mutant HERG K+ channel inhibition by disopyramide in patients with a short QT-1 syndrome: a pilot study." J Cardiovasc Electrophysiol **18**(11): 1157-1160.

Schonherr, R. and S. H. Heinemann (1996). "Molecular determinants for activation and inactivation of HERG, a human inward rectifier potassium channel." J Physiol **493 (Pt 3)**: 635-642.

Schram, G., M. Pourrier, P. Melnyk and S. Nattel (2002). "Differential distribution of cardiac ion channel expression as a basis for regional specialization in electrical function." Circ Res **90**(9): 939-950.

Schwartz, P. J. and M. J. Ackerman (2013). "The long QT syndrome: a transatlantic clinical approach to diagnosis and therapy." Eur Heart J **34**(40): 3109-3116.

Sesti, F., G. W. Abbott, J. Wei, K. T. Murray, S. Saksena, P. J. Schwartz, S. G. Priori, D. M. Roden, A. L. George and S. A. N. Goldstein (2000). "A common polymorphism associated with antibiotic-induced cardiac arrhythmia." Proc Natl Acad Sci U S A **97**(19): 10613-10618.

Shibasaki, T. (1987). "Conductance and kinetics of delayed rectifier potassium channels in nodal cells of the rabbit heart." J Physiol **387**: 227-250.

Sicouri, S., A. Glass, M. Ferreiro and C. Antzelevitch (2010). "Transseptal Dispersion of Repolarization and Its Role in the Development of Torsade de Pointes Arrhythmias." J Cardiovasc Electrophysiol **21**(4): 441-447.

Smith, P. L., T. Baukrowitz and G. Yellen (1996). "The inward rectification mechanism of the HERG cardiac potassium channel." Nature **379**(6568): 833-836.

Spector, P. S., M. E. Curran, A. Zou, M. T. Keating and M. C. Sanguinetti (1996). "Fast inactivation causes rectification of the IKr channel." J Gen Physiol **107**(5): 611-619.

Sun, Y., X. Q. Quan, S. Fromme, R. H. Cox, P. Zhang, L. Zhang, D. Guo, J. Guo, C. Patel, P. R. Kowey and G. X. Yan (2011). "A novel mutation in the KCNH2 gene associated with short QT syndrome." J Mol Cell Cardiol **50**(3): 433-441.

Thomas, D., J. Kiehn, H. A. Katus and C. A. Karle (2003). "Defective protein trafficking in hERG-associated hereditary long QT syndrome (LQT2): molecular mechanisms and restoration of intracellular protein processing." Cardiovascular Research **60**(2): 235-241.

Thorsen, K., V. S. Dam, K. Kjaer-Sorensen, L. N. Pedersen, V. A. Skeberdis, J. Jurevicius, R. Treinys, I. Petersen, M. S. Nielsen, C. Oxvig, J. P. Morth, V. V. Matchkov, C. Aalkjaer, H. Bundgaard and H. K. Jensen (2017). "Loss-of-activity-mutation in the cardiac chloride-bicarbonate exchanger AE3 causes short QT syndrome." Nat Commun **8**(1): 1696.

Trudeau, M. C., L. M. Leung, E. R. Roti and G. A. Robertson (2011). "hERG1a N-terminal eag domain-containing polypeptides regulate homomeric hERG1b and heteromeric hERG1a/hERG1b channels: a possible mechanism for long QT syndrome." J Gen Physiol **138**(6): 581-592.

Trudeau, M. C., J. W. Warmke, B. Ganetzky and G. A. Robertson (1995). "HERG, a human inward rectifier in the voltage-gated potassium channel family." Science **269**(5220): 92-95.

Tse, G., Y. W. F. Chan, W. Keung and B. P. Yan (2017). "Electrophysiological mechanisms of long and short QT syndromes." Int J Cardiol Heart Vasc **14**: 8-13.

Tseng, G. N. (2006). "Linkage between 'disruption of inactivation' and 'reduction of K(+) selectivity' among hERG mutants in the S5-P linker region." J Physiol **577**(Pt 1): 459-460.

Um, S. Y. and T. V. McDonald (2007). "Differential association between HERG and KCNE1 or KCNE2." PLoS One **2**(9): e933.

Vandenberg, J. I., M. D. Perry, M. J. Perrin, S. A. Mann, Y. Ke and A. P. Hill (2012). "hERG K(+) channels: structure, function, and clinical significance." Physiol Rev **92**(3): 1393-1478.

Vandenberg, J. I., A. M. Torres, T. J. Campbell and P. W. Kuchel (2004). "The HERG K+ channel: progress in understanding the molecular basis of its unusual gating kinetics." Eur Biophys J **33**(2): 89-97.

Vandenberg, J. I., A. Varghese, Y. Lu, J. A. Bursill, M. P. Mahaut-Smith and C. L. Huang (2006). "Temperature dependence of human ether-a-go-go-related gene K+ currents." Am J Physiol Cell Physiol **291**(1): C165-175.

Viskin, S., A. A. Wilde, M. E. Guevara-Valdivia, A. Daoulah, A. D. Krahn, D. P. Zipes, A. Halkin, K. Shivkumar, N. G. Boyle, A. Adler, B. Belhassen, E. Schapachnik, F. Asrar and R. Rosso (2013a). "Quinidine, a life-saving medication for Brugada syndrome, is inaccessible in many countries." J Am Coll Cardiol **61**(23): 2383-2387.

Viskin, S., A. A. Wilde, A. D. Krahn and D. P. Zipes (2013b). "Inaccessibility to quinidine therapy is about to get worse." J Am Coll Cardiol **62**(4): 355.

Wang, J., C. D. Myers and G. A. Robertson (2000). "Dynamic Control of Deactivation Gating by a Soluble Amino-Terminal Domain in HERG Channels." The Journal of General Physiology **115**(6): 749.

Wang, J., M. C. Trudeau, A. M. Zappia and G. A. Robertson (1998). "Regulation of Deactivation by an Amino Terminal Domain in Human Ether-à-go-go–related Gene Potassium Channels." J Gen Physiol **112**(5): 637-647.

Wang, W. and R. MacKinnon (2017). "Cryo-EM Structure of the Open Human Ether-a-go-go-Related K(+) Channel hERG." Cell **169**(3): 422-430.e410.

Wang, Y., J. Guo, L. L. Perissinotti, J. Lees-Miller, G. Teng, S. Durdagi, H. J. Duff and S. Y. Noskov (2016). "Role of the pH in state-dependent blockade of hERG currents." Sci Rep **6**: 32536.

Warmke, J., R. Drysdale and B. Ganetzky (1991). "A distinct potassium channel polypeptide encoded by the Drosophila eag locus." Science **252**(5012): 1560-1562.

Warmke, J. W. and B. Ganetzky (1994). "A family of potassium channel genes related to eag in Drosophila and mammals." Proc Natl Acad Sci U S A **91**(8): 3438-3442.

Weerapura, M., T. E. Hebert and S. Nattel (2002a). "Dofetilide block involves interactions with open and inactivated states of HERG channels." Pflugers Arch **443**(4): 520-531.

Weerapura, M., S. Nattel, D. Chartier, R. Caballero and T. E. Hebert (2002b). "A comparison of currents carried by HERG, with and without coexpression of MiRP1, and the native rapid delayed rectifier current. Is MiRP1 the missing link?" J Physiol **540**(Pt 1): 15-27.

Whicher, J. R. and R. MacKinnon (2016). "Structure of the voltage-gated K(+) channel Eag1 reveals an alternative voltage sensing mechanism." Science **353**(6300): 664-669.

Whittaker, D. G., H. Ni, A. P. Benson, J. C. Hancox and H. Zhang (2017). "Computational Analysis of the Mode of Action of Disopyramide and Quinidine on hERG-Linked Short QT Syndrome in Human Ventricles." Frontiers in Physiology **8**(759).

Wilders, R. and A. O. Verkerk (2010). "Role of the R1135H KCNH2 mutation in Brugada syndrome." Int J Cardiol **144**(1): 149-151.

Witchel, H. J. and J. C. Hancox (2000). "Familial and acquired long qt syndrome and the cardiac rapid delayed rectifier potassium current." Clin Exp Pharmacol Physiol **27**(10): 753-766.

Wolpert, C., R. Schimpf, C. Giustetto, C. Antzelevitch, J. Cordeiro, R. Dumaine, R. Brugada, K. U. I. Hong, U. R. S. Bauersfeld, F. Gaita and M. Borggrefe (2005). "Further Insights into the Effect of Quinidine in Short QT Syndrome Caused by a Mutation in HERG." Journal of cardiovascular electrophysiology **16**(1): 54-58.

Wu, W., A. Gardner and M. C. Sanguinetti (2014). "Cooperative subunit interactions mediate fast C-type inactivation of hERG1 K+ channels." J Physiol **592**(20): 4465-4480.

Wu, W., A. Gardner and M. C. Sanguinetti (2015). "The Link between Inactivation and High-Affinity Block of hERG1 Channels." Mol Pharmacol **87**(6): 1042-1050.

Xu, L., M. Xia, J. Guo, X. Sun, H. Li, C. Xu, X. Gu, H. Zhang, J. Yi, Y. Fang, H. Xie, J. Wang, Z. Shen, B. Xue, Y. Sun, T. Meckel, Y. H. Chen, Z. Hu, Z. Li, C. Xu, H. Gong and W. Liu (2016). "Impairment on the lateral mobility induced by structural changes underlies the functional deficiency of the lupus-associated polymorphism FcγRIIB-T232." J Exp Med **213**(12): 2707-2727.

Yang, T., M. S. Wathen, A. Felipe, M. M. Tamkun, D. J. Snyders and D. M. Roden (1994). "K+ currents and K+ channel mRNA in cultured atrial cardiac myocytes (AT-1 cells)." Circ Res **75**(5): 870-878.

Yao, J. A., X. Du, D. Lu, R. L. Baker, E. Daharsh and P. Atterson (2005). "Estimation of potency of HERG channel blockers: impact of voltage protocol and temperature." J Pharmacol Toxicol Methods **52**(1): 146-153.

Yap, Y. G. and A. J. Camm (2003). "Drug induced QT prolongation and torsades de pointes." Heart **89**(11): 1363-1372.

Zhang, M., J. Liu, M. Jiang, D. M. Wu, K. Sonawane, H. R. Guy and G. N. Tseng (2005). "Interactions between charged residues in the transmembrane segments of the voltage-sensing domain in the hERG channel." J Membr Biol **207**(3): 169-181.

Zhang, M., Y. Wang, M. Jiang, D. P. Zankov, S. Chowdhury, V. Kasirajan and G. N. Tseng (2012). "KCNE2 protein is more abundant in ventricles than in atria and can accelerate hERG protein degradation in a phosphorylation-dependent manner." Am J Physiol Heart Circ Physiol **302**(4): H910-922.

Zhang, Y., C. K. Colenso, A. El Harchi, H. Cheng, H. J. Witchel, C. E. Dempsey and J. C. Hancox (2016). "Interactions between amiodarone and the hERG potassium channel pore determined with mutagenesis and in silico docking." Biochem Pharmacol **113**: 24-35.

Zhang, Y. H., C. K. Colenso, R. B. Sessions, C. E. Dempsey and J. C. Hancox (2011). "The hERG K(+) channel S4 domain L532P mutation: Characterization at 37 °C." Biochim Biophys Acta **1808**(10): 2477-2487.

Zhou, Z., Q. Gong, B. Ye, Z. Fan, J. C. Makielski, G. A. Robertson and C. T. January (1998). "Properties of HERG channels stably expressed in HEK 293 cells studied at physiological temperature." Biophys J **74**(1): 230-241.

Zou, A., Q. P. Xu and M. C. Sanguinetti (1998). "A mutation in the pore region of HERG K+ channels expressed in Xenopus oocytes reduces rectification by shifting the voltage dependence of inactivation." J Physiol **509 (Pt 1)**: 129-137.